

INFORMATION TO USERS

This manuscript has been reproduced from the microfilm master. UMI films the text directly from the original or copy submitted. Thus, some thesis and dissertation copies are in typewriter face, while others may be from any type of computer printer.

The quality of this reproduction is dependent upon the quality of the copy submitted. Broken or indistinct print, colored or poor quality illustrations and photographs, print bleedthrough, substandard margins, and improper alignment can adversely affect reproduction.

In the unlikely event that the author did not send UMI a complete manuscript and there are missing pages, these will be noted. Also, if unauthorized copyright material had to be removed, a note will indicate the deletion.

Oversize materials (e.g., maps, drawings, charts) are reproduced by sectioning the original, beginning at the upper left-hand corner and continuing from left to right in equal sections with small overlaps.

ProQuest Information and Learning
300 North Zeeb Road, Ann Arbor, MI 48106-1346 USA
800-521-0600

UMI[®]

University of Alberta

Design of Low Noise Amplifiers for the DRAO
Synthesis Telescope

by

Alma Angela Risma Garcia



A thesis submitted to the Faculty of Graduate Studies and Research in
partial fulfillment of the

requirements for the degree of *Master of Science*

Department of *Electrical and Computer Engineering*

Edmonton, Alberta
Spring 2005



Library and
Archives Canada

Bibliothèque et
Archives Canada

0-494-08057-4

Published Heritage
Branch

Direction du
Patrimoine de l'édition

395 Wellington Street
Ottawa ON K1A 0N4
Canada

395, rue Wellington
Ottawa ON K1A 0N4
Canada

Your file *Votre référence*

ISBN:

Our file *Notre référence*

ISBN:

NOTICE:

The author has granted a non-exclusive license allowing Library and Archives Canada to reproduce, publish, archive, preserve, conserve, communicate to the public by telecommunication or on the Internet, loan, distribute and sell theses worldwide, for commercial or non-commercial purposes, in microform, paper, electronic and/or any other formats.

The author retains copyright ownership and moral rights in this thesis. Neither the thesis nor substantial extracts from it may be printed or otherwise reproduced without the author's permission.

AVIS:

L'auteur a accordé une licence non exclusive permettant à la Bibliothèque et Archives Canada de reproduire, publier, archiver, sauvegarder, conserver, transmettre au public par télécommunication ou par l'Internet, prêter, distribuer et vendre des thèses partout dans le monde, à des fins commerciales ou autres, sur support microforme, papier, électronique et/ou autres formats.

L'auteur conserve la propriété du droit d'auteur et des droits moraux qui protègent cette thèse. Ni la thèse ni des extraits substantiels de celle-ci ne doivent être imprimés ou autrement reproduits sans son autorisation.

In compliance with the Canadian Privacy Act some supporting forms may have been removed from this thesis.

Conformément à la loi canadienne sur la protection de la vie privée, quelques formulaires secondaires ont été enlevés de cette thèse.

While these forms may be included in the document page count, their removal does not represent any loss of content from the thesis.

Bien que ces formulaires aient inclus dans la pagination, il n'y aura aucun contenu manquant.


Canada

University of Alberta

Library Release Form

Name of Author: *Alma Angela Risma Garcia*

Title of Thesis: *Design of Low Noise Amplifiers for the DRAO Synthesis Telescope*

Degree: *Master of Science*

Year this Degree Granted: *2005*

Permission is hereby granted to the University of Alberta Library to reproduce single copies of this thesis and to lend or sell such copies for private, scholarly or scientific research purposes only.

The author reserves all other publication and other rights in association with the copyright in the thesis, and except as herein before provided, neither the thesis nor any substantial portion thereof may be printed or otherwise reproduced in any material form whatsoever without the author's prior written permission.

Signature

Dedicated to my dad Serafin, my mom Sabrina and my lil sis Bim.

Abstract

This thesis documents the design of low noise amplifiers (LNAs) with coaxial connectors and probe LNAs for the Dominion Radio Astrophysical Observatory (DRAO) Synthesis radio telescope. Both designs use Agilent ATF-34143 pseudomorphic high electron mobility transistors (pHEMTs). The design process included measurement of the ATF-34143's scattering parameters (S-parameters) for circuit and noise modelling. ATF-34143 S-parameters were obtained from 0.5 - 10 GHz and a LNA with coaxial connectors and 30 K noise temperature was designed and constructed. The LNA has a noise performance 5 K better than the noise performance of the LNAs currently operating on the Synthesis Telescope. The probe LNA design is a fairly new and promising concept, integrating the waveguide probe directly into the circuit board and eliminating coaxial connection losses. Currently, the probe LNA has the same noise performance as the LNA with coaxial connectors when placed in a waveguide.

Acknowledgement

First and foremost, I would like to thank my two “official” supervisors Tom Landecker and Dave Routlege and my “non-official” supervisor Bruce Veidt for their extensive help and support. Also, many thanks to the people at DRAO, who not only helped me with different aspects of my project, but made my stay there a very memorable and pleasant one. In particular, I would like to thank the following people:

- Tom Burgess, for teaching me how to solder (and unsolder) such tiny things.
- Ron Casorso, for debugging the FET supply.
- Ev Sheehan, for installation of the LNAs and all the help in the machine shop.
- Dean Chalmers, for machining the probe LNA cases.
- Ed Reid, for help with EM simulations.
- Rick Smegal, for helping me hunt for oscillations.
- Peter Cimbaro, for all the computer help.

Contents

1	The Synthesis Telescope and the Signals it Receives	1
1.1	The Synthesis Telescope	1
1.2	Aperture Synthesis	5
1.2.1	The Two-Element Interferometer	6
1.2.2	The Visibility Function	7
1.2.3	The Fringe Washing Function and Delay Compensation. .	9
1.3	Synthesis Telescope Observations at 1420 MHz	11
1.4	Basic Components of the Synthesis Telescope at 1420 MHz ...	12
1.5	Noise and Temperature	15
1.6	Doubling Sensitivity	19
1.7	Reducing Receiver Front-End Noise	21
1.8	Previous Work	23
1.9	Project Goals	24
2	Low Noise Amplifier (LNA) Design	28
2.1	How Field Effect Transistors (FETs) Work	29
2.1.1	Metal-Semiconductor Field Effect Transistors (MESFETs)	30

2.1.2	High Electron Mobility Transistors (HEMTs)	31
2.1.3	Pseudomorphic High Electron Mobility Transistors (pHEMTs)	32
2.2	S-Parameters and the Smith Chart	33
2.2.1	Reflection Coefficients and Impedance	37
2.2.2	The Smith Chart	38
2.3	Transistor S-Parameter Measurement	45
2.4	FET Modelling and Noise Parameter Calculation	45
2.5	Noise Analysis and Design	47
3	Transistor S-Parameter Measurement	49
3.1	Measuring S-parameters of a FET: Thru-Reflect-Line (TRL) Calibration	49
3.2	Thru-Reflect-Line (TRL) Standards	53
3.2.1	THRU	54
3.2.2	REFLECT	55
3.2.3	LINE	55
3.3	Connectors for Fixtures	57
4	Field Effect Transistor (FET) Modelling Using S- Parameters and FET Noise Parameter Calculation	62
4.1	Noise Power	63
4.2	Noise Temperature and Noise Figure	66

4.3	Noise Parameters	68
4.4	Using a FET Equivalent Circuit Model to Find Noise Parameters: the Pospieszalski Method	72
4.5	Adding Extrinsic to Pospieszalski's Model: the Total FET Chip Equivalent Circuit	75
4.6	Determination of FET Equivalent Circuit Element Initial Values	76
4.6.1	Previous FET Circuit Models	77
4.6.2	Various DC-biased S-Parameters - the Cold FET Method	78
4.6.3	Agilent ATF-34143 Specification Circuit Model	84
4.6.4	Initial Values	84
4.7	Sequential Fitting of Simulated S-Parameters to Measured Sparameters	86
4.7.1	Calculation of FET Equivalent Circuit Element Values Using <i>nodal</i>	87
4.8	Obtaining Noise Parameters from the FET Equivalent Circuit . .	91
4.8.1	Estimation of T_d	92
4.8.2	Intrinsic Noise Parameter Calculation	93
4.8.3	Total FET Equivalent Circuit Noise Parameter Calculation	94

5 Design of Low Noise Amplifiers (LNAs) With Coaxial Connectors and Probe LNAs for the Synthesis Telescope 98

5.1	LNA Design Concepts	99
5.1.1	Impedance Matching for Lowest Noise	99
5.1.2	Stability	104
5.1.3	Gain	110
5.1.4	Input Return Loss	110
5.1.5	DC Biasing	112
5.2	LNA Design With Coaxial Connectors	115
5.2.1	Initial LNA Configuration	115
5.2.2	Final LNA Configuration	117
5.2.3	Dealing With Low Frequency Oscillations	120
5.2.4	Better Circuit Simulation	121
5.2.5	Low Loss Components	123
5.3	Probe LNA Design - the Mark 1	127
5.3.1	Measured Impedance of the Probe	128
5.3.2	Mark 1 LNA Design	128
5.3.3	Varying Probe Impedance and the Mark 2 Design	131
5.3.4	Improvement of the Mark 1 and Noise Measurements. .	131
5.3.5	Suggested Further Improvements	135

6 Conclusion

137

List of Tables

1.1 The types of CGPS data being collected and data sources.	4
1.2 Present and targeted system temperatures.	20
4.1 Sequence of steps for optimizing FET circuit model elements.	86
4.2 Discrepancy between measured and simulated S-parameters.	90
4.3 Comparison between specified and calculated noise parameters.	96
5.1 List of components for the LNA biasing circuit.	115
5.2 Components used for the LNA with coaxial connectors.	125
5.3 Varying the impedance of the waveguide probe.	131

List of Figures

1.1 A parabolic reflector.	2
1.2 Waveguide-to-coaxial transition.	2
1.3 a) A Synthesis Telescope parabolic antenna. b) The Synthesis Telescope at DRAO.	3
1.4 A simple two-element multiplying interferometer.	6
1.5 The fringe washing function when the interferometer frequency response is a rectangular passband.	10
1.6 Allocation of frequency bands for 1420 MHz observations.	12
1.7 How polarization products are formed in the C21 correlator.	14
1.8 Basic block diagram of the 1420 MHz signal path from antenna to correlator in the Synthesis Telescope.	14
1.9 Blackbody radiation curves as a function of temperature and frequency.	16
1.10 The power pattern of an antenna.	17
1.11 The Mark 1 probe LNA.	25
2.1 Symbolic representation of a FET.	29
2.2 MESFET cross-section.	31
2.3 HEMT cross-section.	32
2.4 a) Packaging of the Agilent ATF 34143 pHEMT. b) Relative	

physical size of the ATF 34143.	34
2.5 Dependence of reflection and transmission on Z_L and Z_O	35
2.6 Incident and reflected waves in a two-port network.	36
2.7 Generalized analytical form of the low noise amplifier.	38
2.8 Normalized resistance circles on the Smith Chart.	39
2.9 Normalized reactance curves on the Smith Chart.	40
2.10 Normalized conductance circles on the Smith Chart.	41
2.11 Normalized susceptance circles on the Smith Chart.	41
2.12 The Smith Chart displaying admittance or impedance.	43
2.13 The Smith Chart displaying both normalized impedance and admittance.	44
2.14 Procedure for calculating pHEMT noise parameters.	47
3.1 S_{11} data provided by Agilent.	50
3.2 Microstrip geometry.	51
3.3 Microstrip insertion loss.	52
3.4 Measured S_{11} of ATF 34143 pHEMT plotted on the Smith Chart. . .	53
3.5 S-parameter measurement of a non-coaxial device in fixture.	54
3.6 a) Low quality TRL fixtures. b) Measurement attempt above 6 GHz with low quality fixtures.	58
3.7 Southwest Microwave microstrip-to-coax transitions.	59
3.8 Better quality TRL fixtures.	60
3.9 S-parameter measurement from 500 MHz to 10 GHz.	61
4.1 Equivalent models of a noisy resistor R.	64

4.2 Voltage generator driving a load.	64
4.3 Noisy network modelled as a noisy resistor.	65
4.4 a) Noisy two-port network. b) Noiseless two-port network model of noisy two-port network.	66
4.5 Noise representation of noisy two-port used to define noise parameter R_n and g_n	69
4.6 a) Noise figure F as a function of source reflection coefficient. b) Example of noise figure circles on the Smith Chart.	71
4.7 Intrinsic noise equivalent circuit of a FET.	72
4.8 Extrinsic FET circuit representing chip package parasitics.	75
4.9 Total FET equivalent circuit model including extrinsic parasitics.	76
4.11 Equivalent FET circuit at zero drain bias voltage and gate voltage below pinchoff.	80
4.10 Cold FET method for deriving the intrinsic circuit.	81
4.12 Equivalent FET circuit at zero drain bias voltage and gate voltage above pinchoff value.	81
4.13 FET equivalent circuit optimization flowchart.	89
4.14 Smith Chart displaying measured reflection S-parameters.	90
4.15 Polar plot displaying measured transmission S-parameters.	91
4.16 Measured and simulated noise figure from 0.5 GHz to 3 GHz used to estimate equivalent drain temperature T_d	93
4.17 <i>Nodal's</i> MESFET model.	94
4.18 Calculated and specified Γ_{opt} values displayed on the Smith Chart.	96

5.1 a) A matching network consisting of series inductor L. b) Movement of Z_S on Smith Chart with increasing L.	102
5.2 a) Initial configuration of the input matching network design for the LNA with coaxial connectors. b) Smith Chart interpretation of the input matching network design.	103
5.3 A better input matching network.	104
5.4 Two port network and associated reflection coefficients.	105
5.5 Stability circles and unstable regions in the Smith Chart. a) The output stability circle in the Γ_L -plane. b) The input stability circle in the Γ_S -plane.	108
5.6 Stability circles of the ATF-34143 at 1.42 GHz. a) The input stability circle. b) The output stability circle.	109
5.7 The dependency of Z_{in} on increasing values of source inductance L_S for the NEC 34018 FET.	113
5.8 Biasing circuit schematic.	114
5.9 Matching networks for a two-stage LNA.	116
5.10 Schematic for LNA.	119
5.11 Impedance Z_S seen by the input of the first transistor in the LNA using the schematic in Figure 5.10.	120
5.12 Input matching network with stabilizing resistor.	121
5.13 a) Simulated and measured noise figure of the LNA with coaxial connectors. b) Simulated and measured input return loss of the LNA with coaxial connectors. c) Simulated and measured	

output return loss of the LNA with coaxial connectors. d) Simulated and measured gain of the LNA with coaxial connectors.	122
5.14 LNA with coaxial connectors.	126
5.15 Dimensions of the probe for Mark 1.	128
5.16 Input impedance of the probe inside the waveguide.	129
5.17 Mark 1 LNA schematic.	130
5.18 Impedance presented to the input of the ATF- 34143 transistor. .	130
5.19 Measured impedances of different lengths of probes on the Smith Chart.	132
5.20 a) Improved Mark 1 probe LNA. b) The Mark 1 with biasing circuit removed.	133
5.21 Noise measurement of LNA with coaxial connectors in waveguide.	134
5.22 Noise measurement of probe LNA in waveguide.	134

Chapter 1

The Synthesis Telescope and the Signals it Receives

This chapter offers some background on the Synthesis radio telescope and noise concepts such as the use of noise temperatures and the importance of first stage receiver noise. The main goals of this project and the degree to which they were accomplished are stated at the end of this chapter.

1.1 The Synthesis Telescope

The Synthesis Telescope is a radio telescope that operates simultaneously at 408 and 1420 MHz. It is located at the Dominion Radio Astrophysical Observatory (DRAO) near Penticton, British Columbia. DRAO operates under the National Research Council of Canada's Herzberg Institute of Astrophysics (NRC-HIA). Composed of an array of seven 9-m parabolic antennas, the Synthesis Telescope runs in a 600 m straight line from east to west as shown in Figure 1.3. The array of parabolic antennas collects radio signals at 408 and 1420 MHz and uses the method of aperture synthesis to create radio images of the sky. Aperture Synthesis is described in Section 1.2.

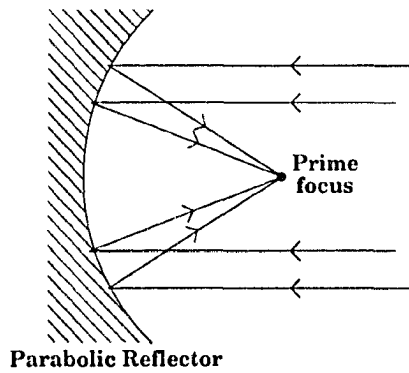


Figure 1.1: A parabolic reflector.

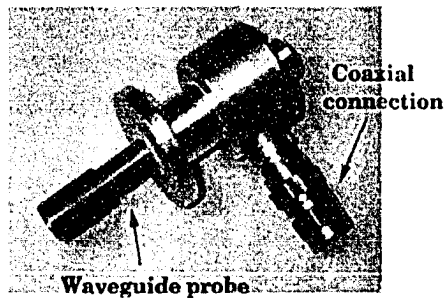
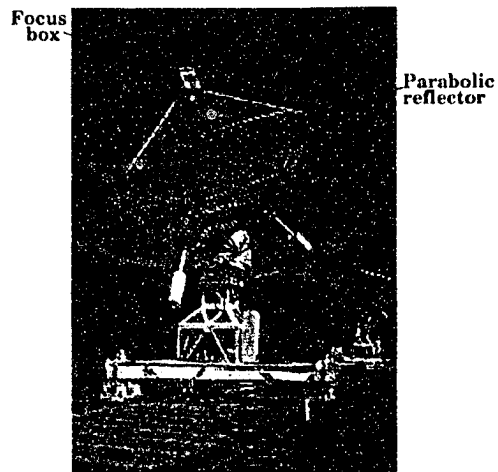


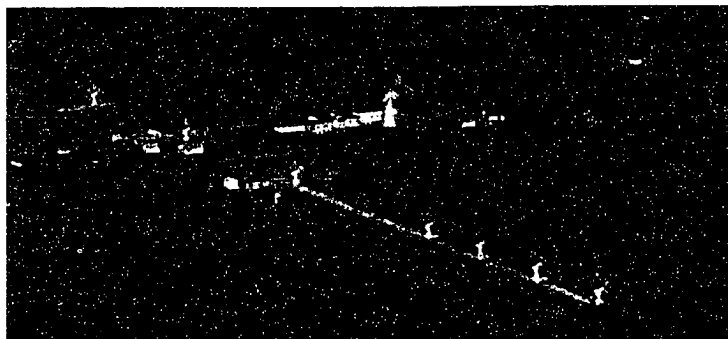
Figure 1.2: Waveguide-to-coaxial transition.

Each parabolic antenna has a parabolic reflector (refer to Figure 1.1) and a focus box, located at the prime focus of the reflector. Signals bounce off the reflector and into the focus box, which contains a dual frequency waveguide feed connected to receivers. Each antenna of the Synthesis Telescope collects circular polarization at the two operating frequencies. Both left and right-hand circular polarizations are collected at 1420 MHz, and right-hand circular polarization at 408 MHz. At 1420 MHz, left and right-hand circular polarizations (LHCP and RHCP) are collected by means of two waveguide probes (refer to Figure 1.2) oriented perpendicular to each other in each waveguide feed. Each of the waveguide probes is connected to a low noise amplifier, which is followed by further amplification and frequency conversion components that are

all located in the focus box. The outputs from the focus box, at the intermediate frequency (IF) of 30 MHz, travel by coaxial cable to the central receiver building where further amplification and frequency conversion occur. Cross correlators form products from all antenna pairs. The correlator outputs are the basic data, which flow to image formation routines. For further discussion of the Synthesis Telescope components at 1420 MHz, refer to Section 1.4.



(a)



(b)

Figure 1.3: a) A Synthesis Telescope parabolic antenna [2]. b) The Synthesis Telescope at DRAO. It is the array of 7 smaller parabolic antennas from the top left to the bottom right [3].

A major portion of the Synthesis Telescope's observing time is set aside for the Canadian Galactic Plane Survey (CGPS). The CGPS is an international collaboration devoted to surveying the interstellar medium (ISM) in the Milky Way with unsurpassed spatial resolution - better than the resolution of previous studies by more than a factor of 10 [18]. Table 1.1 lists the institutions that make CGPS observations and the different types of data collected. All the 408 and 1420 MHz CGPS data is collected at DRAO, which permits mapping of gases, magnetic fields and relativistic plasma. The 1420 MHz DRAO observations of continuum radiation (including polarization) and HI spectroscopic images are the primary data produced by the CGPS. Continuum and spectral observations are further described in Section 1.3.

Frequency	Wavelength	Observation	ISM Component	Source
151 MHz	199 cm	Continuum	Ionized Gas and Relativistic Plasma	MRAO (UK)
408 MHz	74 cm	Continuum		DRAO (Canada)
1420 MHz	21 cm	(Polarization)	Magnetic Fields	
		HI Spectral Line	Atomic Gas	
115 GHz	2.6 mm	CO Spectral Line	Molecular Gas	FCRAO (US)
3 THz	100 μ m	Continuum	Dust Grains	Caltech (US)
5 THz	60 μ m		Very Small Dust Grains & PAHs*	CITA (Canada)
12 THz	25 μ m			
25 THz	12 μ m			

*PAHs=polycyclic aromatic hydrocarbons

Table 1.1: The types of CGPS data being collected and data sources [1]. The Mullard Radio Astronomy Observatory (MRAO) is located in Cambridge, UK. Two of the data sources are American: the Five College Radio Astronomy Observatory (FCRAO) in Massachusetts and the California Institute of Technology (Caltech). The Canadian Institute for Theoretical Astrophysics (CITA) is a research centre hosted by the University of Toronto. Data at 12, 25, 60 and 100 μ m were collected from Earth orbit by the Infrared Astronomical Satellite (IRAS).

The CGPS began almost a decade ago and upon completion of its first phase inspired the creation of the International Galactic Plane Survey (IGPS), which will combine other surveys with CGPS data to map more than 90% of the galactic stellar disk at the frequency of 1420 MHz and at resolution similar that of the CGPS - the first ever high resolution map of neutral hydrogen throughout the whole Galactic plane [19].

1.2 Aperture Synthesis

The Synthesis Telescope collects data using aperture synthesis - an interferometry method that uses several smaller antennas to obtain an angular resolution equivalent to that of one large antenna. This is why the Synthesis Telescope is composed of seven dishes instead of just one. The beamwidth of a parabolic antenna is inversely proportional to its collecting diameter, meaning that angular resolution gets better with an increase in collecting diameter [20]. The diffraction limit for the angular resolution of a telescope is equivalent to approximately $\frac{\lambda}{D}$ in radians, where λ is the observing wavelength and D is the collecting diameter [21]. For a one-antenna radio telescope to obtain the same angular resolution as the Synthesis array, ideally it would require an aperture equivalent to the length between the dishes furthest apart from each other, which is 600 m. Such a large single collecting area would be extremely difficult to physically realize. Even the largest single telescope in the world, the Arecibo Radio Telescope in Puerto Rico, has a diameter of roughly only half the size at 305 m [22].

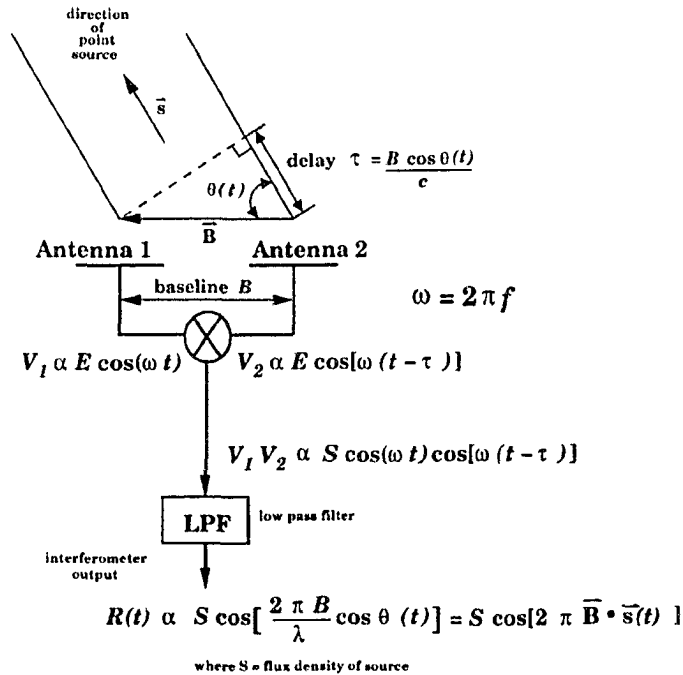


Figure 1.4: A simple two-element multiplying interferometer.

1.2.1 The Two-Element Interferometer

In order to understand how aperture synthesis works, one must take into account its basic building block — the two-element interferometer. Consider an interferometer which consists of two antennas separated by distance B and a point source in space, as depicted in Figure 1.4. The length B is oriented in the east-west direction and is referred to as the baseline. The voltage generated at each antenna is proportional to the electric field generated by the source. Antenna #1 can be considered as the reference antenna. The point source is located at angle $\theta(t)$ with respect to the baseline. Because of the baseline B , signals from the source arrive at antenna #2 with delay $\tau = \frac{B \cos \theta(t)}{c}$ relative to antenna #1. The voltage outputs of antennas #1 and #2 are multiplied together and higher frequencies are filtered out to produce the output $R(t)$ [21]:

$$R(t) \propto S \cos\left(\frac{2\pi B}{\lambda} \cos \theta(t)\right) \quad (1.1)$$

where S is the flux density ($\text{W m}^{-2} \text{ Hz}^{-1}$) of the source. As the Earth rotates, $\theta(t)$ varies with time and signals from the point source arrive at antennas #1 and #2 in and out of phase alternately, producing interference fringes in the interferometer output $R(t)$. Fringes are spaced approximately $\frac{\lambda}{B}$ radians (or $\frac{1}{B_\lambda}$ where B_λ is the baseline in wavelengths) apart. The interferometer output can also be thought of as

$$R(t) \propto S \cos\left(2\pi \vec{B} \cdot \vec{s}(t)\right) \quad (1.2)$$

where \vec{B} is a vector parallel to the baseline and \vec{s} is a vector in the direction of the source [21].

1.2.2 The Visibility Function

Now consider a source that has a finite angular width, with \vec{s} pointing in the direction of its phase center. This extended source can be considered as a collection of point sources where any point can be denoted by $\vec{s} + \vec{\sigma}$ with brightness distribution $I(\vec{\sigma})$. $\vec{\sigma}$ can be considered as a vector that has two components in a plane which is perpendicular to \vec{s} (“the plane of the sky”). The response of the interferometer is then the sum of its own individual responses to each point source [21]:

$$R(t) \propto \int_{-\infty}^{\infty} I(\vec{\sigma}) \cos\left[2\pi \vec{B} \cdot (\vec{s}(t) + \vec{\sigma})\right] d\vec{\sigma}. \quad (1.3)$$

Because $\vec{\sigma}$ is perpendicular to $\vec{s}(t)$,

$$\vec{B} \cdot (\vec{s} + \vec{\sigma}) = \vec{B} \cdot \vec{s} + \vec{b} \cdot \vec{\sigma} \quad (1.4)$$

where \vec{b} is the projected baseline (i.e. the component of \vec{B}) in the direction perpendicular to \vec{s} :

$$\vec{b} = \vec{B} - (\vec{B} \bullet \vec{s})\vec{s}. \quad (1.5)$$

The interferometer output can then be expressed in the complex form

$$R(t) \propto V \exp\{j2\pi\vec{B} \bullet s(t)\} \quad (1.6)$$

where V is the complex visibility function and is expressed as

$$V = \int_{-\infty}^{\infty} I(\vec{\sigma}) \exp\{j2\pi\vec{b} \bullet \vec{\sigma}\} d\vec{\sigma}. \quad (1.7)$$

The amplitude of V is proportional to the amplitude of the output fringe pattern while the argument of V gives the phase shift in the fringe pattern with respect to the phase of the interferometer response to a point source at the phase center (see Equation 1.2). The visibility function V is the two-dimensional Fourier transform of the source brightness distribution. To recover the source brightness distribution, the inverse two-dimensional Fourier transform is performed [21]:

$$I(\vec{\sigma}) = \int_{-\infty}^{\infty} V(\vec{b}) \exp\{-j2\pi\vec{b} \bullet \vec{\sigma}\} d\vec{b}. \quad (1.8)$$

The central point here is that an interferometer pair of antennas whose effective detection beam is pointing at a source can measure a Fourier component in the brightness distribution of the source, which means an image of the source can be generated by performing inverse Fourier transforms.

Recall that the projected baseline \vec{b} is in the direction perpendicular to \vec{s} . The projected baseline \vec{b} is generally resolved into u , an East component, and

v , a North component. In aperture synthesis, pairs of antennas form interferometer pairs called baselines, with each instantaneous baseline sampling a point in the (u, v) plane. As the Earth rotates, samples are taken along an elliptical locus in the (u, v) plane for each pair of antennas. Movable pairs of antennas form even more possible baseline lengths, allowing sampling of more points in the (u, v) plane. Coupled with the Earth's rotation, these baselines effectively sample the radio sky in the Fourier transform domain with the same resolution as an antenna with an aperture diameter as large as the longest baseline. Because each antenna pair is interchangeable, full sampling of an elliptical locus in the (u, v) plane can be achieved in 12 hours instead of 24. Powerful computers are used to calculate Fourier transforms of the Fourier components produced by the baselines and generate radio images of the sky.

1.2.3 The Fringe Washing Function and Delay Compensation

For continuum observations, wide frequency bandwidth is desirable in order to increase sensitivity (see Section 1.6). For an observing bandwidth Δf , a two-element interferometer with frequency response $\alpha(f)$ will have the following response:

$$R(t) \propto \int \alpha(f) \cos\left(\frac{2\pi B}{\lambda} \cos\theta(t)\right) df. \quad (1.9)$$

and since delay $\tau = \frac{B \cos\theta(t)}{c}$ (refer to Section 1.2.1), the interferometer response can be written as

$$R(t) \propto \int \alpha(f) \cos(2\pi f\tau) df. \quad (1.10)$$

If the observing bandwidth Δf is greater than $\frac{1}{\tau}$, the correlation between signals is lost. To compensate, additional time delay τ_D that is approxi-

mately equal to τ can be inserted in one of the interferometer arms so that the equalized phase delay between the signals allows for a greater observing bandwidth. If additional time delay τ_D is added, the total time delay becomes $\Delta\tau = \tau(t) - \tau_D$. Now correlation between signals will be lost if observing bandwidth Δf is greater than $\frac{1}{\Delta\tau}$. To illustrate the $\Delta f > \frac{1}{\Delta\tau}$ rule, consider the complex Fourier transform of $\alpha(f)$, which is called the fringe washing function $\beta(\Delta\tau)$. The interferometer response involves integration over the finite bandwidth, which corresponds to multiplication of the visibility function amplitude by the fringe washing function in the $\Delta\tau$ domain. It is therefore important that the fringe washing function be as close to unity as possible. If $\alpha(f)$ is a rectangular passband, the fringe washing function is the sinc function $\frac{\sin(\pi\Delta f\Delta\tau)}{(\pi\Delta f\Delta\tau)}$, which falls to zero at $\Delta\tau = \frac{1}{\Delta f}$. To keep the fringe washing function close to unity,

$$\Delta\tau \ll \frac{1}{\Delta f} \text{ or } \Delta f \ll \frac{1}{\Delta\tau}$$

as is shown in Figure 1.5.

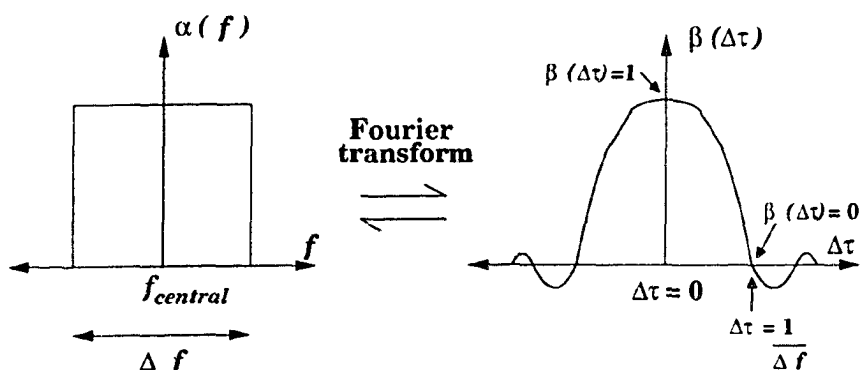


Figure 1.5: The fringe washing function when the interferometer frequency response is a rectangular passband.

1.3 Synthesis Telescope Observations at 1420 MHz

At 1420 MHz, continuum maps are generated in four sub-bands of 7.5 MHz each, adding up to a total bandwidth of 30 MHz. The four continuum sub-bands exist in order to keep the fringe-washing function close to 1 in value (refer to Section 1.2.3) in order to prevent bandwidth smearing in images. This continuum band, along with another continuum band at 408 MHz, allows detection of synchrotron radiation as well thermal emission such as that of ionized hydrogen (HII). Synchrotron radiation is emitted by electrons spiraling in magnetic fields at relativistic velocities. Sources such as pulsars and supernova remnants emit synchrotron radiation.

The narrower bandwidth of spectral line observations is centered on the frequency at which neutral hydrogen (HI) atoms radiate electromagnetic energy. Spectral line emissions are caused by electron transitions from one energy level to another and the frequency of radiation is unique to every element. Hydrogen emission occurs near 1420.406 MHz [18]. Spectral line observations are made using a central band of 5 MHz at 1420 MHz. Located at each side of the central band are two continuum sub-bands, making up five observation bands that total 35 MHz, as shown in Figure 1.6.

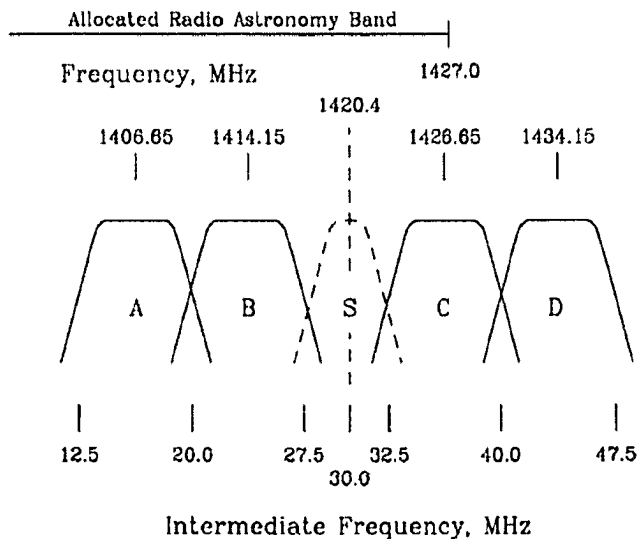


Figure 1.6: Allocation of frequency bands for 1420 MHz observations [4].

1.4 Basic Components of the Synthesis Telescope at 1420 MHz

The simplest radio telescope can be broken down into an antenna and a receiver followed by some sort of data-recording system. The Synthesis Telescope, however, is composed of an array of parabolic antennas. Signals are collected by the antennas, amplified, undergo frequency conversion and more amplification, and then end up being multiplied together in a correlator. The following describes the path of a 1420 MHz signal after it is collected by a Synthesis Telescope antenna.

- Radio Frequency (RF) low noise amplifier (LNA): Amplifies the weak 1420 MHz signal from the antenna with gain on the order of 40 dB.
- Band Pass Filter (BPF): Filters out parts of the signal at unwanted frequencies.

- **Intermediate Frequency (IF) Signal Path:** The band-pass-filtered signal is mixed with a local-oscillator (LO) signal. This results in an intermediate frequency (IF) signal whose power is proportional to the RF signal power. Here, the BPF signal is converted to an IF band of 12.5 - 47.5 MHz (refer to Figure 1.6). The four continuum sub-bands are defined by IF bandpass filters and are converted to baseband using fixed second LOs, where a quadrature replica of each band is created using a phase-shifted second LO. The spectral (H) band is converted to a lower frequency in a single-sideband mixer. The IF signals are conveyed by coaxial transmission line to the control room and then digitized before being correlated. Delay compensation is inserted in the IF signal path to equalize signal path lengths (refer to Section 1.2.3). Before digitizing, the spectral band is sharply defined by a bandpass filter (the overall spectrometer band can be varied from 0.125 MHz to 4 MHz) [4].
- **Digital Correlator System:** Takes the digitized IF signals from all the antennas and multiplies them together in pairs. The continuum sub-bands are processed by the C21 correlator and the spectral band is processed by the S21 correlator spectrometer, which has 256 channels. Each continuum sub-band is digitized to 14 levels and products are formed in one of four identical correlators. The C21 correlator forms all four polarization products from the LHCP and RHCP inputs of each antenna pair (see Figure 1.8). The spectral band is digitized to 3 levels by the S21 system and two identical correlators form products from LHCP and RHCP signals. Unlike the C21 system, however, cross-correlation between the two hands of polarization is not currently available in the S21 [4].

Figure 1.7 is a basic block diagram of how the Synthesis Telescope collects, filters and processes 1420 MHz signals.

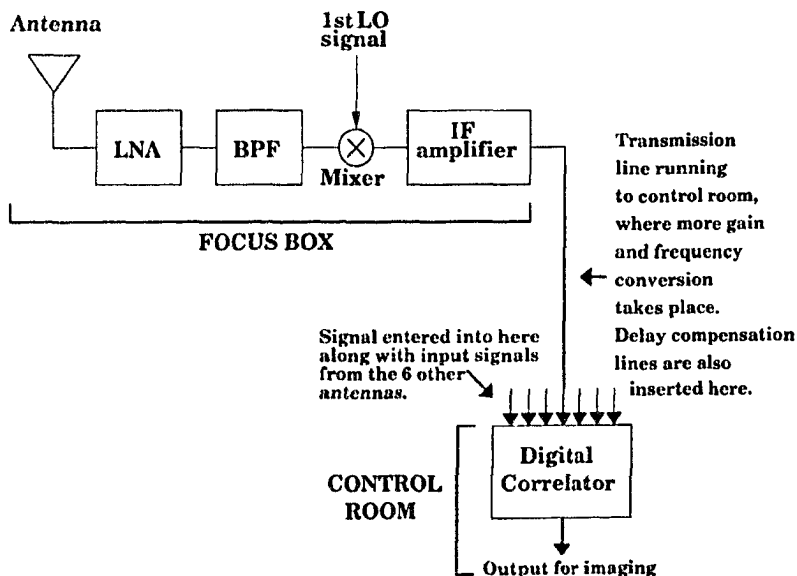


Figure 1.7: Basic block diagram of the 1420 MHz signal path from antenna to correlator in the Synthesis Telescope.

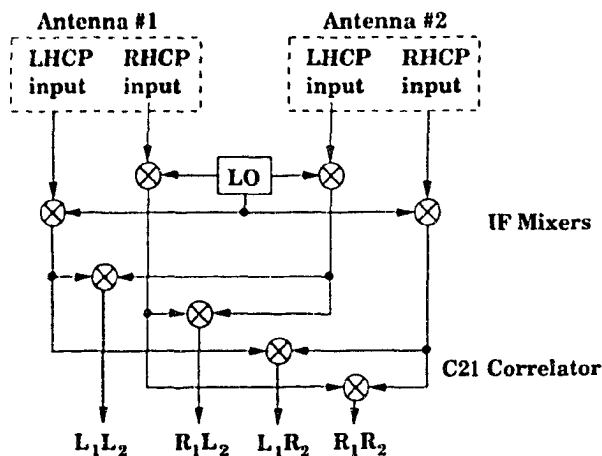


Figure 1.8: How polarization products are formed in the C21 correlator [5].

This project deals with designing the RF LNA, which is commonly known as the receiver front-end. The input of the RF amplifier is where extremely weak signals from thousands of light years away are encountered. The design of the RF amplifier must prioritize noise first and gain second. Noise should be reduced sufficiently to avoid drowning out the weak signals, while gain

should be high enough so that the noise from subsequent components becomes insignificant (further explanation in Section 1.7).

1.5 Noise and Temperature

In general, noise is something indistinct, undesirable or even loud. In the world of electronics however, it is something that will always exist and must be dealt with. Even when an amplifier has no input signal, a small randomly fluctuating output signal can still be detected and is referred to as noise. Noise in electronic components is caused by random thermal fluctuations of electrons. Therefore any device operating above absolute zero will generate noise.

As commonly practised in radio astronomy, noise is expressed in terms of noise temperature. The noise temperature of an antenna is defined as the thermal temperature of a resistor whose terminals, over a specified frequency bandwidth, have a mean available noise power due to thermal agitation equal to the available power at the antenna's terminals [23]. Using temperature units allows direct comparison with celestial "source temperatures." Any object will emit electromagnetic waves if its temperature is above absolute zero. Ideally, the noise temperature of an antenna's radiation resistance will be equal to the temperature of the particular source the antenna is "looking at" if the angular extent of the source "fills" the antenna beam. This statement excludes non-thermal mechanisms that generate electromagnetic waves such as synchrotron radiation. In such cases, the noise temperature of the antenna's radiation resistance will not equal the thermal temperature of the source but instead would be equivalent to the thermal temperature of an ideal blackbody emitting the same radiation at the observing frequency.

An ideal blackbody is defined as a perfect absorber and radiator: it ab-

sorbs radiation at all frequencies and its own radiation is a function of only temperature and frequency. The brightness of radiation from a blackbody at temperature T and frequency ν can be expressed with Planck's Law [20]:

$$B = \frac{2hf^3}{c^2} \frac{1}{e^{\frac{hf}{kT}} - 1} \quad (1.11)$$

where c is the velocity of light and h and k are respectively Planck's constant and Boltzmann's constant. Figure 1.9 illustrates the dependence of blackbody radiation on temperature and wavelength.

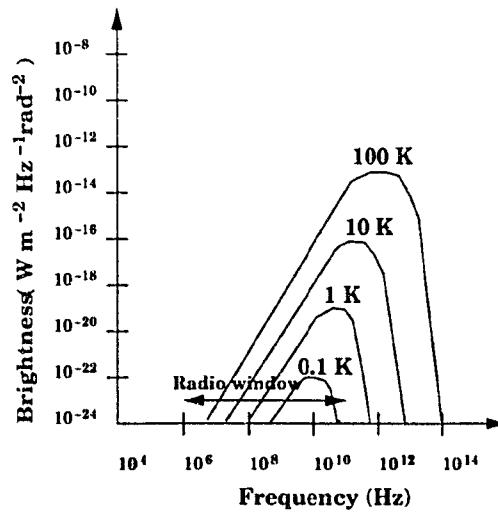


Figure 1.9: Blackbody radiation curves as a function of temperature and frequency.

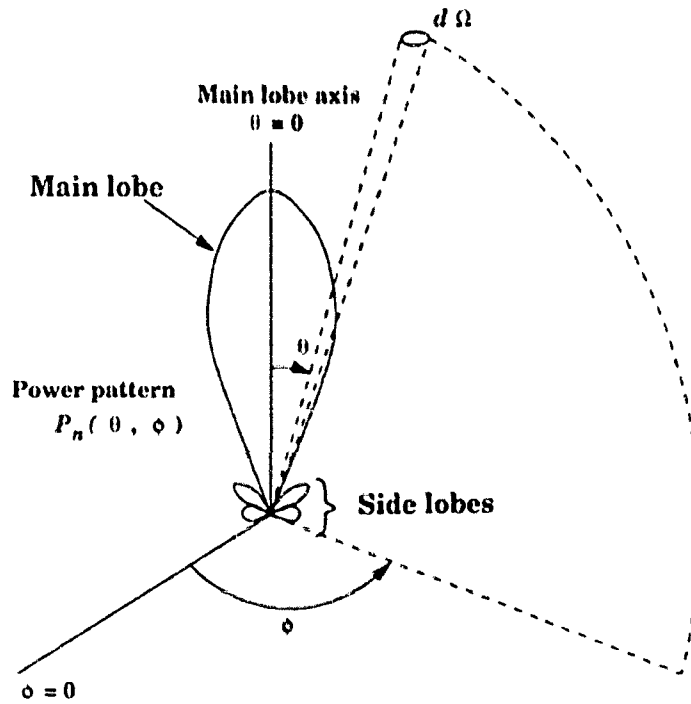


Figure 1.10: The power pattern of an antenna. $d\Omega$ is an element of solid angle equivalent to $\sin\theta d\theta d\phi$.

The pattern of an antenna represents the antenna's response as a function of direction, and can be expressed in terms of field intensity (field pattern) or radiation intensity (power pattern). An example of an antenna power pattern is shown in Figure 1.10. The antenna is a channel for the flow of energy from sources seen in the main beam and sidelobes. When observing a source with temperature $T_S(\theta, \phi)$, the antenna temperature T_A will be a function composed of the source temperature distribution and the antenna power pattern $P_n(\theta, \phi)$ [20]:

$$T_A = \frac{1}{\Omega_A} \iint T_S(\theta, \phi) P_n(\theta, \phi) d\Omega \quad (1.12)$$

where Ω_A is the antenna beam area (in rad^2 or steradians) and is defined as

$$\Omega_A = \int P_n(\theta, \phi) d\Omega \quad (1.13)$$

and

$$P_n(0, 0) = 1. \quad (1.14)$$

Noise and temperature are related in the following manner. For a resistor R at temperature T , the relation between noise power W and temperature T is expressed as follows [20]:

$$W = kT\Delta f \quad (1.15)$$

W = noise power available from resistor (watts)

k = Boltzmann's constant (J/K)

T = temperature of resistor in Kelvin

Δf = operating bandwidth (Hz)

Ideally, Equation 1.15 also applies to an antenna with radiation resistance R which is receiving signal from a blackbody at temperature T whose angular extent fills the antenna beam. Realistically, however, the noise temperature referred to the antenna's terminals will consist not only of the source temperature but the noise temperature of the receiver it is connected to, not to mention additional noise from the thermal radiation of the ground (which gets "picked up" by antenna sidelobes) and the sky (at 1420 MHz there will always be cosmic background radiation of approximately 3 K left over from the Big Bang). The total sum of noise temperatures can then be grouped into a single term: "system noise temperature." When observing at the HI line, system temperature is higher due to signals from additional HI clouds, especially at low galactic latitude.

Radio telescope system noise temperatures can vary from tens of degrees Kelvin to tens of thousands of degrees Kelvin depending on the frequency

of operation. The radio frequency window itself extends from a few MHz to hundreds of GHz. The lower system temperatures apply to microwave (centimetre wavelength) frequencies while the higher system temperatures apply to receivers in the millimetre, sub-millimetre wavelength bands and also decametric wavelengths (due to the brightness of the Galaxy at a few MHz).

1.6 Doubling Sensitivity

Signals from distant celestial sources are weak — to put things in perspective, the basic unit of power flux in radio astronomy is the Jansky. The Jansky is equivalent to only $10^{-26} \text{ W m}^{-2} \text{ Hz}^{-1}$. It has been estimated that the energy from all the radio signals ever collected by all the radio telescopes on Earth amounts to no more than the kinetic energy of a falling snowflake. Receiver and antenna noise is an obstacle to detecting such small signals and must be minimized to maximize the sensitivity of a radio telescope. For the Synthesis Telescope, sensitivity in imaging can be thought of as the minimum detectable r.m.s. fluctuation ΔS whose units are $\text{W m}^{-2} \text{ Hz}^{-1}$ [4]:

$$\Delta S = W \frac{\sqrt{2}kT_{sys}}{\eta_c \eta_A A \sqrt{N_b N_{IF}} \Delta f \tau} \quad (1.16)$$

W = factor depending on weighting scheme used in imaging

k = Boltzmann's constant

T_{sys} = system temperature

η_c = correlator efficiency

η_A = aperture efficiency of the antennas

A = area of each antenna aperture in m^2

N_b = number of baselines

N_{IF} = number of IF channels

Δf = bandwidth of each IF channel

τ = integration time constant

Relation 1.16 demonstrates the dependence of sensitivity on T_{sys} and operating bandwidth. Currently at 1420 MHz, continuum observations are made over a bandwidth of 30 MHz. Spectral observations use a bandwidth of $\frac{B}{160}$, where B is the overall spectrometer band in MHz (variable from 0.125 to 4 MHz). Inevitably, continuum observations have higher sensitivity than spectral line observations due to wider bandwidth. Sensitivity could be further improved by increasing observing bandwidth, but to do so would require a huge effort: there would be a required increase in not only receiver electronics, but computing, data processing and data storage as well. The only other options for improving sensitivity are increasing observation time and decreasing T_{sys} . Increasing observation time is not a viable option, which leaves the option of decreasing T_{sys} . As well, sensitivity ΔS is proportional to the square root of both bandwidth and observing time. Sensitivity ΔS and T_{sys} are directly proportional, which means decreasing T_{sys} would have a greater impact on sensitivity.

The present noise performances along with target noise performances of the Synthesis telescope at 1420 MHz are listed in Table 1.2 [24]:

Noise Temperature Source	Present (K)	Target (K)
Receivers	35 (mean)	20
Losses (due to Antenna-Receiver connection)	5	0
Ground Noise	15	5
Sky (zenith)	5	5
TOTAL	60	30

Table 1.2: Present and targeted system temperatures of the Synthesis Telescope.

Meeting the target performance would roughly cut noise in half, doubling sensitivity of the telescope for 1420 MHz continuum observations. 30 K is a very ambitious target - currently the lowest achievable system temperature is around 15 K, which is what the American National Aeronautics and Space Administration's (NASA) Deep Space Network (DSN) 2.3 GHz receivers operate at [25],[26]. This accomplishment by NASA required the use of cryogenically cooled maser LNAs, which are extremely expensive. At 1420 MHz, the Westerbork Synthesis Radio Telescope (WSRT) in the Netherlands has a system temperature of approximately 30 K, which is accomplished with cryogenically cooled receivers [27]. At 1400 MHz, the Arecibo Radio Telescope in Puerto Rico has a system temperature of approximately 27 K and also uses cryogenic cooling [22]. The goal of this project, however, is to meet the target system temperature of 30 K using uncooled receiver front-ends by taking advantage of recent advances in low noise transistor technology. As shown in Table 1.2, receiver noise is a major factor - it is accountable for more than half of the system noise temperature.

The ground noise component of antenna noise is also a large contributor to system noise temperature and can be reduced by improving antenna design (e.g. reducing spillover and mesh leakage). An MSc thesis project that ran parallel with this one was finished by Teresia Ng, who managed to show that the current system noise temperature may be reduced by 6 K through improvement in antenna design [5].

1.7 Reducing Receiver Front-End Noise

By the time radio signals reach Earth from thousands of light years away, they are greatly attenuated and very weak. To detect these signals, receiver

front-ends are required to have high gain and most importantly, very low noise. Noise and gain are important due to a particular property of amplifiers: first stage amplifier noise typically dominates the noise of the stages after it. For a chain of n amplifiers, the total noise temperature can be generalized [7]:

$$T = T_1 + \frac{T_2}{G_{A1}} + \frac{T_3}{G_{A1}G_{A2}} + \frac{T_4}{G_{A1}G_{A2}G_{A3}} + \dots \quad (1.17)$$

T = total noise temperature

T_n = noise temperature of n th amplifier

G_{An} = available power gain of n th amplifier

Therefore the noise performance of the first stage of the receiving system is the primary determining factor in the total noise performance of the system because it is only T_1 that does not get reduced by power gain of other stages. A stage that contributes loss to the system and has physical temperature $T_{attenuator}$ will introduce a gain ϵ of less than unity as well as the following noise temperature T [20]:

$$T = \left(\frac{1}{\epsilon} - 1\right)T_{attenuator}.$$

The key to obtaining low noise in an amplifier is the type of transistor that is used in the design. The most common types of transistors used in LNAs at microwave frequencies are gallium arsenide field-effect transistors (GaAs FETs) and high electron mobility transistors (HEMTs). Gallium arsenide is preferred over silicon due to its superior performance at microwave frequencies. GaAs FETs and HEMTs are further discussed in Chapter 2. Such new technology has made it possible for a 1420 MHz amplifier to have excellent noise performance without the need for cryogenic cooling. Cryogenic cooling of receivers is commonly used to achieve low system noise temperatures in

radio astronomy. However, the aim of this project is to meet target performance of the Synthesis telescope without cooling. Although highly effective, cryogenic cooling is an expensive and high-maintenance method of reducing receiver noise.

1.8 Previous Work

Each of the Synthesis Telescope's seven parabolic antennas has a dual-frequency feed at its prime focus to collect signals. To collect signals at 1420 MHz, multi-mode waveguide feeds are used. These feeds are connected by coaxial cables to the existing front-end LNAs. Before this project began, a matched waveguide probe was designed by Bruce Veidt using software simulating the waveguide-to-coaxial transition. Using a matched probe reduces connection loss because the waveguide probe is directly integrated with the amplifier, eliminating the need for a coaxial cable connection and accompanying losses. As shown in Table 1.2, the coaxial antenna-receiver connection is also a significant factor in system temperature. The term "matched" refers to the impedance of the probe, which was designed to be closer to the value required for lowest noise temperature performance of the transistor in the amplifier. Transistor noise temperature and dependence on impedance will be further discussed in Chapter 4.

Using Agilent ATF-34143 transistors, a single-stage low noise amplifier with matched probe was designed and built by Bruce Veidt and Annie-Claude Lachappelle - the Mark 1, as shown in Figure 1.11 [28]. Unfortunately, it was shown by Bruce Veidt that the Agilent transistor data-sheet scattering parameters (*S*-parameters) are not correct (refer to Section 3.1). Also, the Mark 1's bias lines did not work as well as expected — there was a need for better

decoupling between the bias lines and the amplifier circuit [29]. Despite these obstacles, the work that has been done on Mark 1 is encouraging. The Mark 1 can be thought of as an active integrated antenna (AIA) since it consists of a microstrip antenna that is connected to an active device, resulting in the active device having an input impedance that is different from conventional $50\ \Omega$ [30]. AIAs are a fairly new concept and offer much opportunity in receiver front-end design due to the elimination of losses present in connectors. Since this probe has been designed to match the transistor's optimum impedance, there is elimination of losses due to input matching components such as capacitors and resistors as well (see Section 5.2.5).

1.9 Project Goals

Initially there were three main goals for this project: obtaining the correct S-parameters of the Agilent ATF-34143 transistor, obtaining the noise parameters of the transistor, and improving on the Mark 1 matched probe LNA design. Since the Agilent transistor data-sheet S-parameters were not believed to be correct, it became necessary that S-parameters be measured for verification. S-parameters are useful because they directly reveal the impedance and gain of the transistor at a particular frequency. Furthermore, when obtained over a wide range of frequencies, S-parameters also provide a means to calculate the equivalent circuit model of a field-effect transistor (FET), which in turn allows calculation of transistor noise parameters. For an accurate circuit model, S-parameters needed to be measured over as wide a frequency range as possible (refer to Chapter 4). S-parameter measurement required the design and construction of test fixtures so that the transistors could be connected to a network analyzer for measurement. Calibration fixtures were also needed

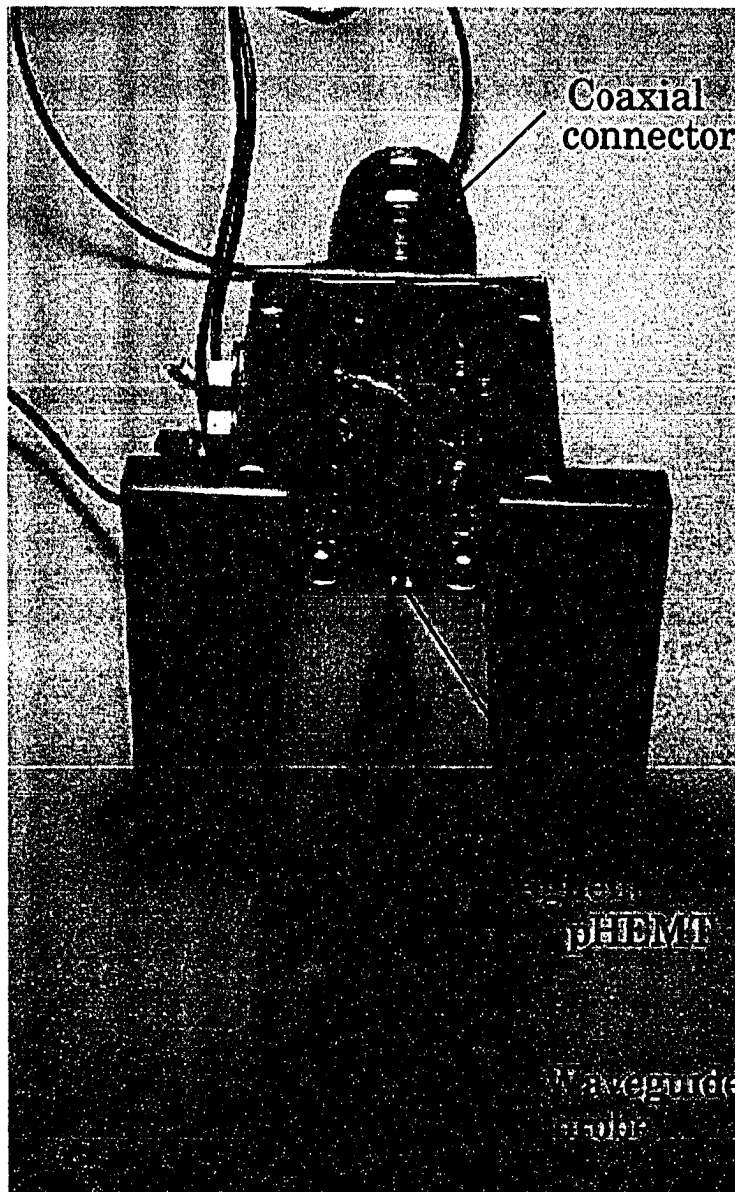


Figure 1.11: The Mark 1 probe LNA. The wires connect the pHEMT to a separate FET biasing power supply. This project resulted in the addition of a new biasing circuit to the Mark 1 (see Chapter 5). The waveguide probe replaces the waveguide-coaxial transition needed for an LNA with coaxial connectors (see Figure 1.2).

so that the effects of the test fixture could be removed from each transistor measurement.

Upon determination of the correct S-parameter values, transistor noise pa-

rameters can be calculated. A new single-stage amplifier probe was proposed to be designed and built - Mark 2. The purpose of Mark 2 is to resolve issues that previously plagued Mark 1, such as problems with decoupling the biasing circuit from the LNA circuit. Better knowledge of actual transistor parameter values could have resulted in the probe design of Mark 2 being an altered version of Mark 1's probe design. As well, the Mark 1 had a gain of only 15 dB which is not sufficient for a Synthesis Telescope receiver front-end. Recall that not only is first stage noise the dominating factor in a cascade of amplifiers, but that first stage gain is also what the noise of the subsequent stages is reduced by. Approximately 30 dB is sufficient for noise reduction of the subsequent stages (about 100 K for the Synthesis Telescope). The single-stage Mark 2 would not have been able to produce more than 15 or 20 dB gain (refer to Section 5.1.3). A gain-enhancing option would have been the design and construction of a multi-stage LNA - the Mark 3.

After successful measurement of S-parameters, however, the option of building an LNA with coaxial connectors using the ATF-34143 was added as an intermediate goal. An LNA with coaxial connectors would not only provide a stepping stone towards a probe LNA, but would also allow for easier integration into the Synthesis Telescope as well as straightforward testing and measurement. The four main goals of this project can then be summarized as follows:

1. S-parameter measurement of the ATF-34143 over as wide a range as possible.
 - (a) Design and construction of test fixtures for transistor S-parameter measurement.
 - (b) Accurate S-parameter measurements using TRL calibration.

2. Circuit and noise modelling of transistor using successful S-parameter measurements.
3. Design and construction of 1420 MHz coaxial LNA.
 - (a) Noise lower than 35 K (mean noise temperature of Synthesis LNAs).
 - (b) Gain of 30 dB or greater, necessitating a 2-stage design since each transistor contributes approximately 15 dB of gain.
4. Improvement of Mark 1 probe LNA design.
 - (a) Probe impedance sufficiently close to transistor's optimum impedance for lowest noise, so that a noise figure of 20 K can be achieved.
 - (b) Improvement of transistor DC biasing.
 - (c) Design and construction of 2-stage LNA to meet the 30 dB gain requirement.

By the end of this project, S-parameters were successfully measured up to 10 GHz and an LNA with coaxial connectors was designed and built with a noise temperature of approximately 30 K and 30 dB gain at 1420 MHz. The Mark 1's bias lines were improved and its noise performance is now similar to that of the LNA with coaxial connectors. Progress is currently still at the 1-stage version. A 2-stage version of Mark 1 was attempted but there were problems encountered with oscillations.

Chapter 2

Low Noise Amplifier (LNA)

Design

This chapter describes derivation of a circuit model for a field effect transistor (FET) from S-parameter measurements and one noise measurement. The derived model will form the basis for amplifier design, described in Chapter 5. Given an equivalent circuit for a FET, simulation software can calculate expected S-parameters, and values of circuit elements within the model can be adjusted until simulated S-parameters match measured values. For high accuracy, this procedure can be repeated for a wide frequency range. *Nodal*, a high frequency circuit simulation package for *Mathematica* (further discussion in Section 2.4), was used to simulate the FET equivalent circuit, and least-squares fitting over the frequency range 0.5 GHz to 10 GHz successfully established values of the circuit elements of the Agilent ATF-34143 pHEMT. The method of Pospieszalski [12], together with the *nodal* simulation, was then used to determine the noise parameters.

The transistor equivalent circuit should be able to reproduce the transistor measured S-parameters and predict the transistor noise parameters. Design-

ing an LNA for lowest noise temperature requires knowing transistor noise parameters. Noise parameters can be obtained through a process that begins with measuring the S-Parameters of a FET and ends with using the circuit parameters of a FET model to calculate noise parameters. The final stage of LNA design involves building matching networks around the transistor which optimize the transistor for best noise performance. The main steps are summarized as following:

- S-Parameter Measurement
- Circuit Modelling
- Noise Parameter Calculation
- Noise Analysis and Design of Matching Networks

2.1 How Field Effect Transistors (FETs) Work

The FET is a three-terminal semiconductor device, represented by Figure 2.1. The voltage between two terminals of a FET controls the current flow in the third terminal, enabling the device to function as an amplifier. These three terminals are referred to as source, gate and drain. It is the voltage between gate and source that controls the current in the drain.

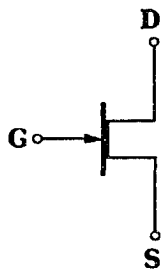


Figure 2.1: Symbolic representation of a FET.

The late 1970's brought into existence different types of FETs starting with the MOSFET (metal-oxide semiconductor FET). The MOSFET as well as numerous other types of FETs are silicon-based. Of interest here, however, are the more newly developed gallium arsenide (GaAs) based devices. GaAs FETs are also commonly referred to as MESFETs (metal-semiconductor FETs). MESFETs became commercially available in the 1980's [26]. At higher frequencies (on the order of GHz), gallium arsenide has superior performance compared with that of silicon, due to the high electron drift mobility of GaAs, which is five to ten times higher than that of silicon [31]. At the time work began on this thesis, there were two main types of GaAs devices available: MESFETs and HEMTs (high electron mobility transistors). HEMTs were even more recently developed than MESFETs and have come to exceed MESFETs in noise performance [26].

2.1.1 Metal-Semiconductor Field Effect Transistors (MESFETs)

A MESFET is fabricated on undoped GaAs substrate (undoped GaAs has very low conductivity and isolates devices on a chip from each other as well as ensuring small capacitances between the devices and ground [31]). The source and drain terminals are heavily n-doped GaAs regions with metal contacts. The gate terminal, however, consists of a Schottky-barrier junction, which is a metal-semiconductor junction that behaves like a diode (conducts current when voltage is applied in a particular direction and acts like an open circuit when the voltage is reversed). Current flows from drain to source by means of a conducting channel consisting of n-type GaAs which is not as heavily doped as the source and drain contact regions. Applying a small negative gate voltage creates an electron depletion region in the channel. The thickness of

the depletion region (which in turn determines the physical dimensions of the channel) is determined by the value of the voltage applied, thus allowing the gate voltage to control drain-to-source current [31]. Channel length is defined by the length of the gate electrode and is typically 0.2-2 μm [31]. Channel width (the dimension of the gate electrode into the page) is determined by the designer. Refer to Figure 2.2 for a typical MESFET cross-section.

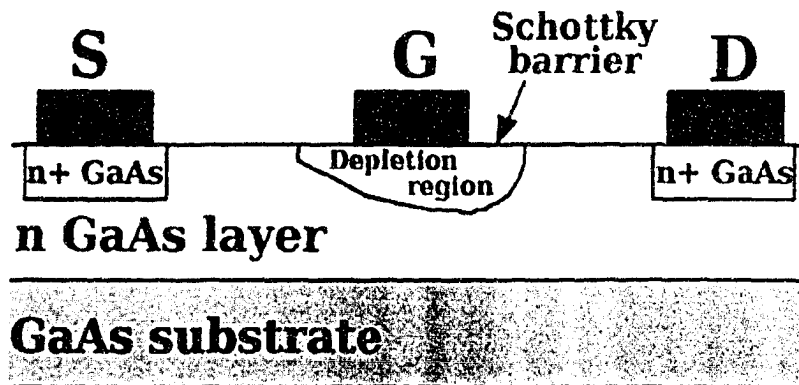


Figure 2.2: MESFET cross-section.

2.1.2 High Electron Mobility Transistors (HEMTs)

A HEMT can be thought of as a MESFET with a heterojunction. A heterojunction is the boundary between two layers composed of materials with different band gaps, a band gap being the energy difference between the valence band and the conduction band of a semiconductor. The layers are commonly composed of GaAs and n-type gallium aluminum arsenide (AlGaAs) [7] as shown in Figure 2.3. The heterojunction provides a very low resistance channel almost free of impurities for electron carriers. This high electron mobility channel is also commonly referred to as a 2D (two-dimensional) electron gas. The high mobility and the freedom from impurities allow electrons to move with relatively few lattice collisions, with the result that noise generated in the

transistor is very low.

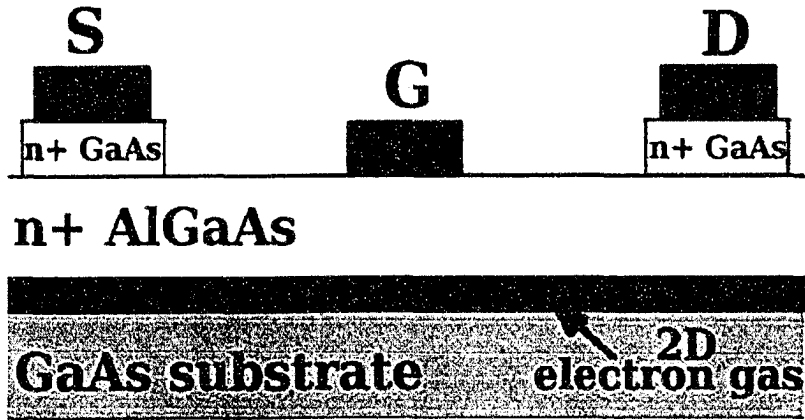


Figure 2.3: HEMT cross-section.

2.1.3 Pseudomorphic High Electron Mobility Transistors (pHEMTs)

The transistor chosen for the project is an Agilent pHEMT (pseudomorphic HEMT), shown in Figure 2.4. Essentially, pHEMTs are HEMTs in which different layers have not only different band gaps but different lattice constants (spacing between the atoms) as well. A greater number of different types of layers to choose from allows for an even bigger bandgap difference between layers, further improving electron mobility in the channel. pHEMTs are currently the fastest operating transistors available - the frequency of operation reaches hundreds of GHz. Of interest here, however, is noise performance at 1.42 GHz. At the time commercial transistors were being investigated for this project, the Agilent ATF-34143 pHEMT became the prime candidate due primarily to its noise temperature. Agilent specifications state a noise temperature of 36 K when operated at 2 GHz for the ATF-34143 when DC biased at 3 V and 20 mA [6], which was one of the best commercial transistor noise performances

at the time of investigation. As mentioned in Section 2.1.1, FET gate width is determined by the designer: the ATF-34143 pHEMT has a gate width of $800\ \mu\text{m}$ [6]. The wider gate width of the ATF-34143 provides impedances that are easier to match to as well as high linearity [32]. Linearity is important in amplifiers: non-linearity leads to intermodulation, the generation of in-band signals by out-of-band interference.

2.2 S-Parameters and the Smith Chart

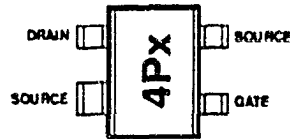
At microwave frequencies, wavelengths become comparable in size to the circuit. In such a case, simple circuit analysis does not suffice because the phase of electrical signals will change significantly as the signals travel the length the circuit. Instead, voltages have to be modelled as travelling waves - complete with reflection coefficients and transmission coefficients. As shown in Figure 2.5, the most basic picture consists of a voltage wave leaving source impedance Z_S , travelling along a transmission line with characteristic impedance Z_O , and then reaching load impedance Z_L . If the load impedance is equal to the characteristic impedance of the transmission line ($Z_L = Z_O$), the wave is fully absorbed by the load and none of it is reflected back towards the source Z_S . If there is a mismatch between the load impedance and the characteristic impedance of the line ($Z_L \neq Z_O$), a portion of the wave is reflected back towards the source Z_S .

Terminating a port with a load equivalent to the characteristic impedance of the transmission line eliminates any reflected waves due to mismatch in transmission line and load. Characteristic impedance of a transmission line can therefore be defined as the value of impedance that, when attached to the end of a line, eliminates any reflection. A real value of 50 Ohms is the industry

Surface Mount Package
SOT-343



Pin Connections and
Package Marking



(a)



(b)

Figure 2.4: a) Packaging of the Agilent ATF 34143 pHEMT [6]. b) Relative physical size of the ATF 34143.

standard value for characteristic impedance.

To represent a two-port network at microwave frequencies, scattering parameters (S-parameters) can be used. S-parameters themselves (S_{11} , S_{12} , S_{21} ,

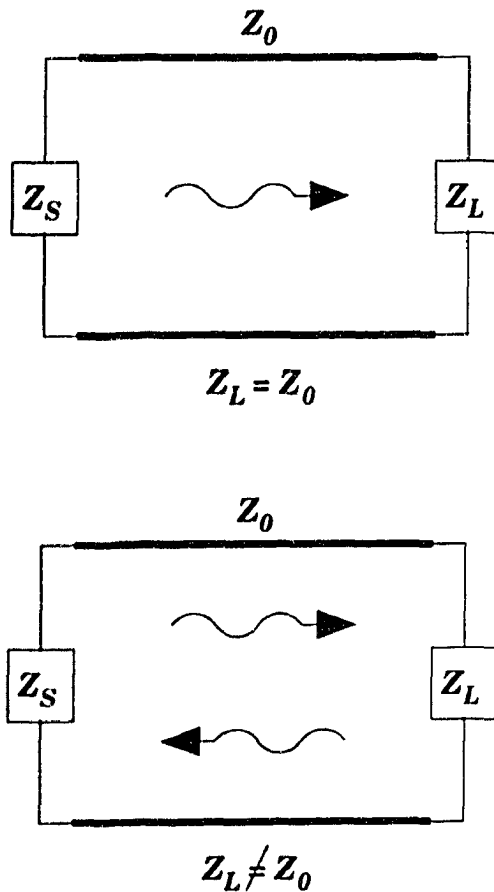


Figure 2.5: Dependence of reflection and transmission on Z_L and Z_0 .

S_{22}) represent reflection and transmission coefficients of the two-port under certain "matched" conditions. S_{11} is the reflection coefficient and S_{21} is the transmission coefficient at port 1 when port 2 is terminated in a load whose impedance is equal to that of the transmission line characteristic impedance. Likewise S_{22} is the reflection coefficient and S_{12} is the transmission coefficient at port 2 when port 1 is terminated in a matched load.

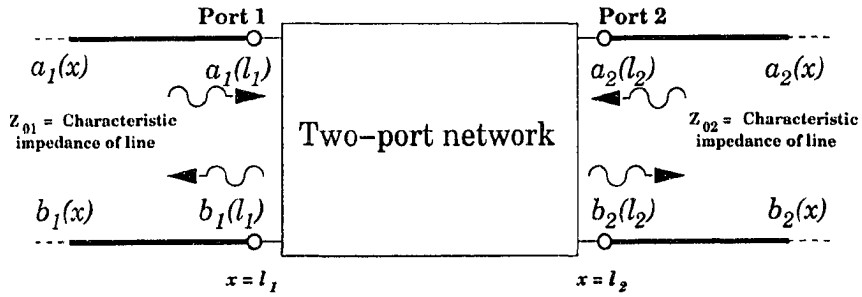


Figure 2.6: Incident and reflected waves in a two-port network [7].

In matrix form,

$$\begin{bmatrix} b_1(l_1) \\ b_2(l_2) \end{bmatrix} = \begin{bmatrix} S_{11} & S_{12} \\ S_{21} & S_{22} \end{bmatrix} \begin{bmatrix} a_1(l_1) \\ a_2(l_2) \end{bmatrix} \quad (2.1)$$

where $a_1(l_1)$ and $a_2(l_2)$ represent incident waves and $b_1(l_1)$ and $b_2(l_2)$ represent reflected waves. Note that when the output port is terminated with $Z_L = Z_{O2}$, $a_2(l_2) = 0$ (no reflection occurs at Z_L). Therefore S_{11} and S_{21} can be defined as the following:

$$S_{11} = \left. \frac{b_1(l_1)}{a_1(l_1)} \right|_{a_2(l_2)=0} \quad (\text{input reflection coefficient; output port matched})$$

$$S_{21} = \left. \frac{b_2(l_2)}{a_1(l_1)} \right|_{a_2(l_2)=0} \quad (\text{forward transmission coefficient: output port matched})$$

Similarly, when the input is terminated with $Z_S = Z_{O1}$, $a_1(l_1) = 0$ (no reflection occurs at Z_S) and S_{22} and S_{12} are defined as follows:

$$S_{22} = \left. \frac{b_2(l_2)}{a_2(l_2)} \right|_{a_1(l_1)=0} \quad (\text{input reflection coefficient; input port matched})$$

$$S_{12} = \left. \frac{b_1(l_1)}{a_2(l_2)} \right|_{a_1(l_1)=0} \quad (\text{reverse transmission coefficient; input port matched})$$

2.2.1 Reflection Coefficients and Impedance

At a particular node, the voltage reflection coefficient Γ is related to the complex impedance Z seen at that point by means of the following equation where Z_0 is the characteristic impedance of the line (usually a real value of 50Ω) [7]:

$$\Gamma = \frac{Z - Z_0}{Z + Z_0}. \quad (2.2)$$

Inversely,

$$Z = \frac{Z_0(1 + \Gamma)}{1 - \Gamma} \quad (2.3)$$

Associated with the two-port are input and output reflection coefficients Γ_{IN} and Γ_{OUT} . Source and load reflection coefficients Γ_S and Γ_L are respectively associated with input and output matching networks as shown in the following.

When the two-port is a transistor, its performance is optimized by inserting a matching network at each port. The input matching network presents reflection coefficient Γ_S at the “source” side of the two-port and the output matching network presents Γ_L at the “load” side. Each matching network is designed so that each port sees a desired impedance. For example, when de-

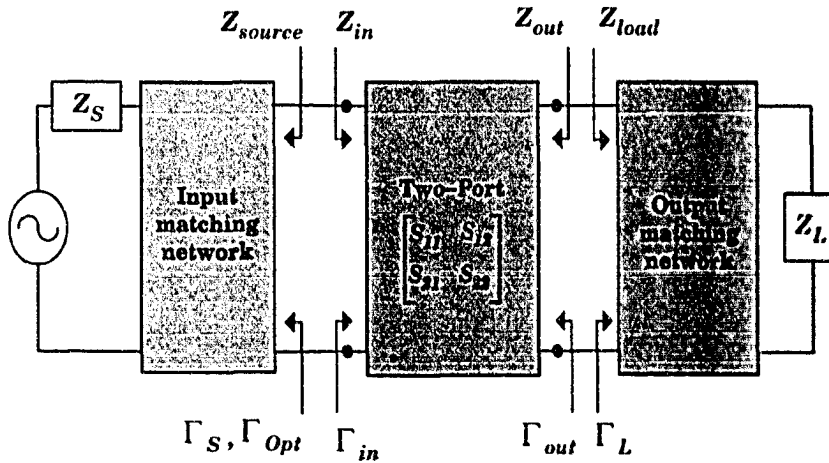


Figure 2.7: Generalized analytical form of the low noise amplifier [8].

significance for noise figure requires transfer analysis, which is beyond the scope of this document. conjugate. With reference to Figure 2.7, Z_S should see Z_S^* when looking at the conjugate. With reference to Figure 2.7, Z_S should see Z_S^* when looking at the input matching network. In turn, the two-port should see Γ_{in}^* when looking at the input matching network. Similarly at the output of the two-port, Z_L should see Z_L^* when looking at the output matching network and $\Gamma_L = \Gamma_{out}^*$. Designing for minimum noise however, has only one requirement: the input port of the transistor needs to see the optimum reflection coefficient. To achieve minimum noise, $\Gamma_S = \Gamma_{opt}$ [7].

2.2.2 The Smith Chart

The Smith Chart is a straightforward way of displaying reflection coefficients and corresponding impedances at the same time. The Smith Chart is a plot of impedances (and/or admittances) mapped onto the Γ -plane. Since the Smith Chart is in Γ -plane format, Γ can be plotted in polar form. $|\Gamma| = 1$ implies 100% reflection or fully reflected voltage waves while $|\Gamma| = 0$ (the center of the Smith Chart) implies zero reflection and fully transmitted waves. Each polar point on the Smith Chart corresponds to a particular impedance.

On the Smith Chart, impedance is normalized by the characteristic impedance value Z_o (usually a real value of 50 Ω):

$$z = \frac{Z}{Z_o} = \frac{R + jX}{Z_o} = r + jx \quad (2.4)$$

z = normalized impedance

Z_o = characteristic impedance

Z = impedance

R = resistance (real part of impedance)

X = reactance (imaginary part of impedance)

r = normalized resistance

x = normalized reactance

The relationship between z and Γ (Equation 2.5) forms constant resistance r circles on the Smith Chart as shown in Figure 2.8.

$$z = \frac{Z}{Z_o} = \frac{1 + \Gamma}{1 - \Gamma} = \frac{R + jX}{Z_o} = r + jx \quad (2.5)$$

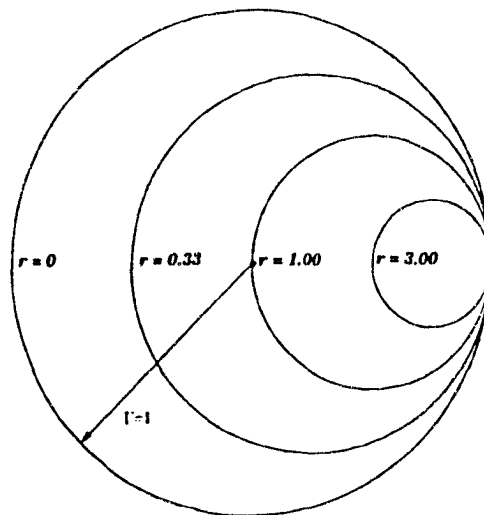


Figure 2.8: Normalized resistance circles on the Smith Chart.

Normalized reactance x forms curves on the Smith Chart which are orthogonal to the resistance circles as shown in Figure 2.9

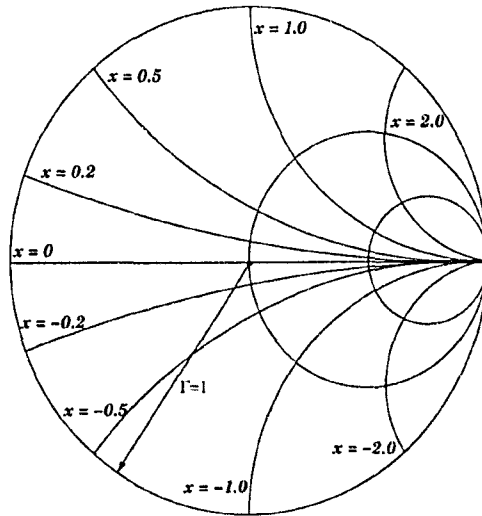


Figure 2.9: Normalized reactance curves on the Smith Chart.

Similarly for normalized admittance y ,

$$y = YZ_o = (G + jB)Z_o = g + jb$$

y = normalized admittance

Z_o = characteristic impedance

Y = admittance

G = conductance (real part of admittance)

B = susceptance (imaginary part of admittance)

g = normalized conductance

b = normalized susceptance

In accordance with r and x respectively, g forms constant conductance circles on the Smith Chart while b forms constant susceptance curves (refer to Figures 2.10 and 2.11).

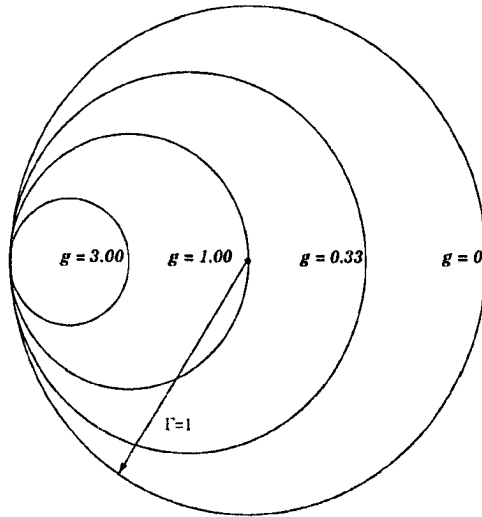


Figure 2.10: Normalized conductance circles on the Smith Chart.

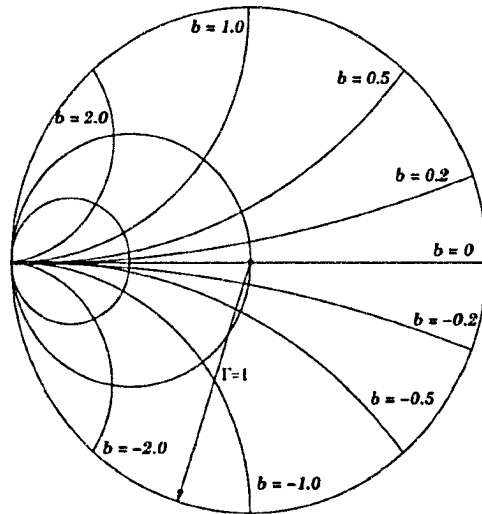


Figure 2.11: Normalized susceptance circles on the Smith Chart.

The circumference of the Smith Chart is marked with degrees and corresponding fractions of a wavelength. Rotation along a constant radius in the Smith Chart corresponds to motion along the transmission line, where the center of the circular motion corresponds to the normalized characteristic impedance of the line. Clockwise motion corresponds to motion away from the

source and towards the load. One full 360° rotation around the Smith Chart is equivalent to a displacement of half a wavelength along the transmission line. This is because we are measuring reflection coefficients, which means the path of a travelling wave includes “forward” and “backward” motion. If the point of reflection is half a wavelength away, the wave would have still undergone a 360° phase shift going there and then back to the point of measurement.

In Figure 2.12, a standard Smith Chart displaying impedance is shown. A standard Smith Chart displaying both impedance and admittance can be quite intimidating when seen for the first time (Figure 2.13). Once understood however, the Smith Chart becomes a useful visual tool in designing matching networks.

Smith Chart

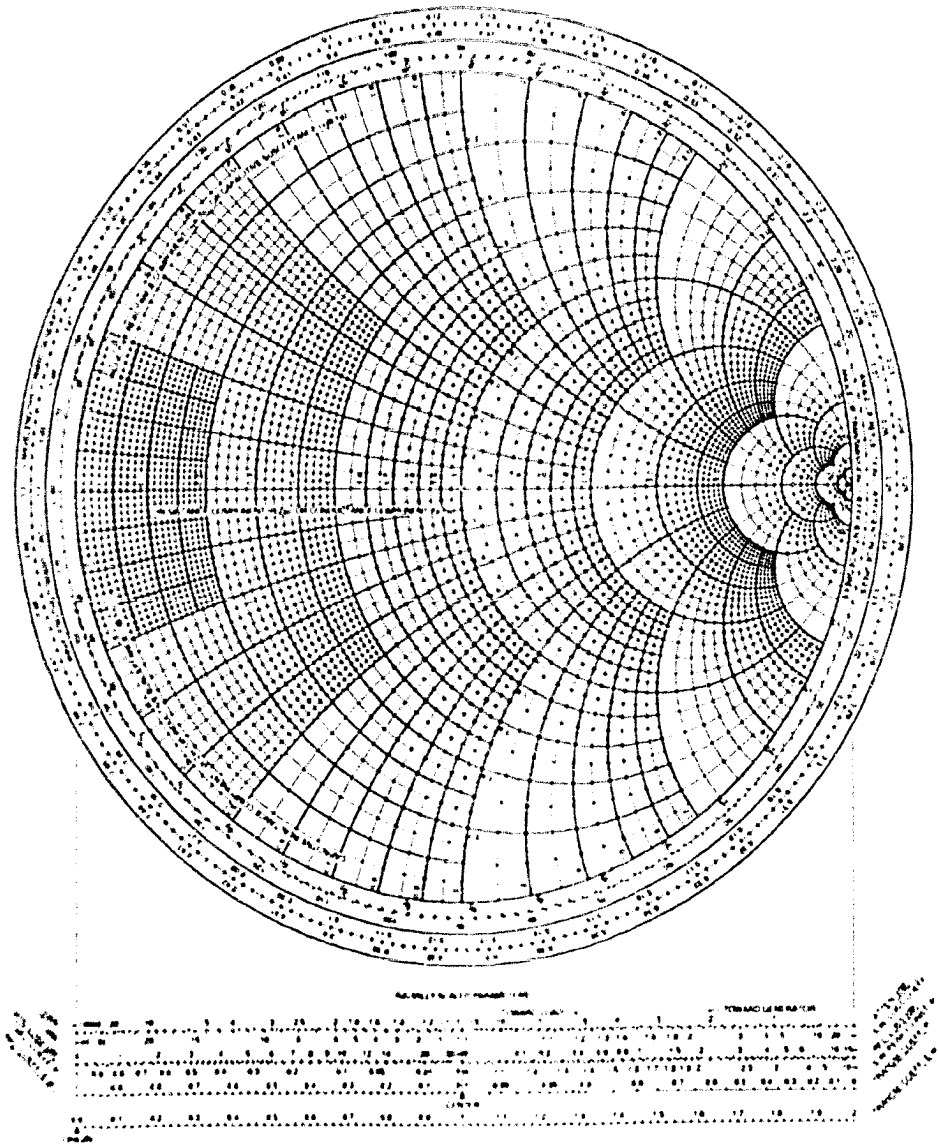


Figure 2.12: The Smith Chart displaying admittance or impedance.

The Complete Smith Chart (ZY)

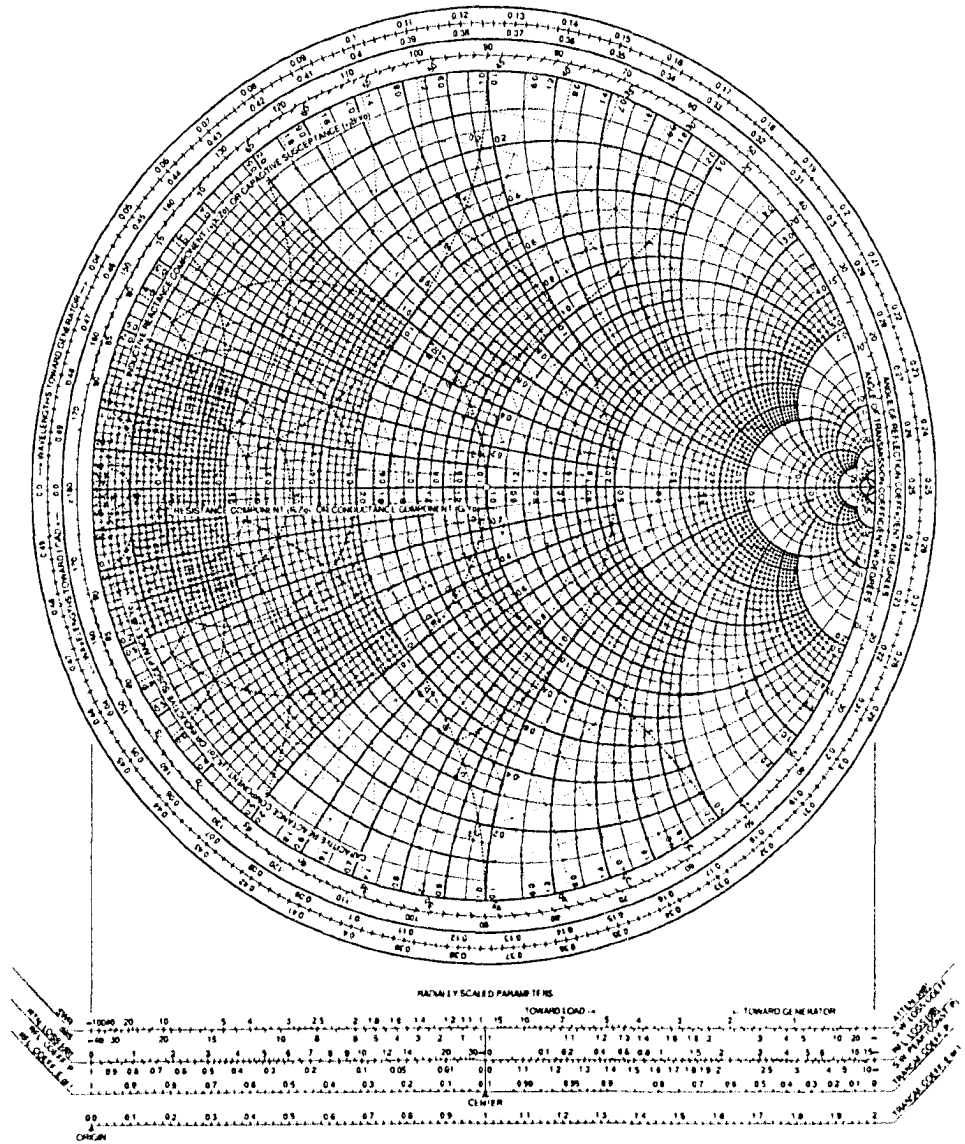


Figure 2.13: The Smith Chart displaying both normalized impedance and admittance.

2.3 Transistor S-Parameter Measurement

Transistor S-parameters are an essential part of the transistor model used in amplifier design. Even if an amplifier is being designed for a single particular frequency, acquiring transistor S-parameters over a large range of frequencies is valuable for modelling purposes. Using high frequency circuit simulation software, the circuit model of a transistor can be calculated by fitting simulated S-parameters to measured S-parameters. A larger number of frequency points results in a more accurate transistor model.

Because wavelengths are short at high frequencies, transistors must be very small. Coupling transistors to laboratory instruments becomes very difficult, and test fixtures are needed to provide the interface. Chapter 3 describes the process of measuring S-parameters of the Agilent ATF-34143 pHEMT with a network analyzer using test fixtures. Thru-Reflect-Line (TRL) calibration, a method of in-fixture calibration, was performed in order to remove the effects of the test fixtures and obtain the S-parameters of the ATF-34143.

2.4 FET Modelling and Noise Parameter Calculation

The noise parameters of a FET can be calculated upon obtaining its equivalent circuit noise model. Theoretically, the noise parameters depend on certain parameters of the circuit model. The circuit model of the transistor is obtained by iteratively fitting the model S-parameters to the actual measured S-parameters of the device. There are various methods of doing this. Here, the chosen method is centered around least-squares fitting of the simulated output of a circuit model to measured S-parameters. After convergence, reliable values

for various circuit elements such as package capacitances and inductances are obtained.

During this project, *nodal* was used for circuit simulation. *Nodal* is a *Mathematica* package that performs high frequency circuit analysis - it even contains FET equivalent circuit models and well as noise models. Since *nodal* performs computations with *Mathematica*, it can be a powerful simulation tool. *Mathematica* was released in 1988 and combines numerical, algebraic and graphical tasks [33]. *Mathematica*'s powerful abilities lie in its use of symbolic language - it can perform not just numerical analysis, but symbolic analysis as well. Variables can be manipulated and their effects on computations can be monitored. *Nodal* takes full advantage of these capabilities while calculating voltages, currents, S-parameters and noise parameters.

The circuit model used here is Marian Pospieszalski's FET noise model [12]. Chapter 4 discusses the use of Pospieszalski's method to obtain transistor noise parameters. The Pospieszalski circuit model is one of the simpler ones to obtain because only one noise measurement of the transistor at a single frequency point, combined with the transistor circuit model, allows for calculation of all four transistor noise parameters. The procedure used for calculating noise parameters is summarized in Figure 2.14.

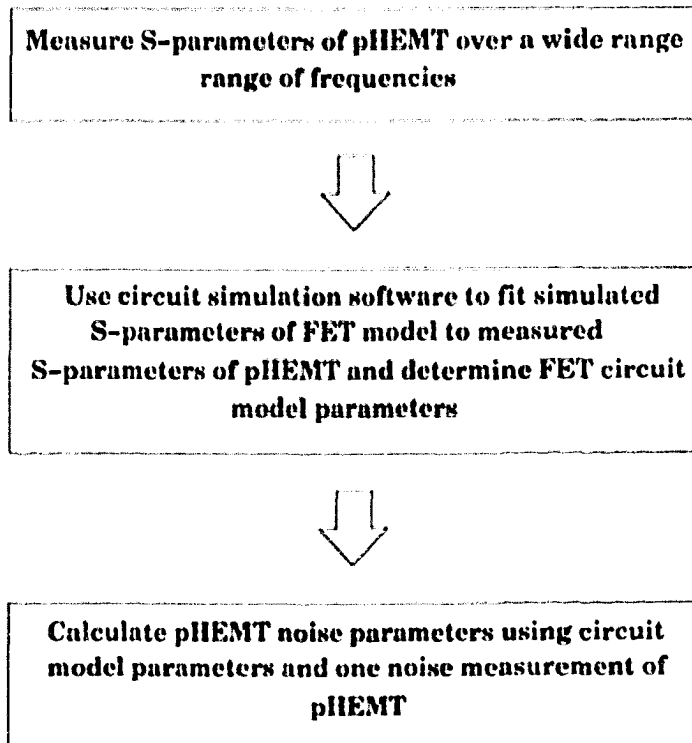


Figure 2.14: Procedure for calculating pHEMT noise parameters.

2.5 Noise Analysis and Design

After the FET modelling described in the previous section, a good knowledge of S-parameters and the noise parameters can be obtained. There are four noise parameters:

- T_{min}
- the real part of Z_{opt}
- the imaginary part of Z_{opt}
- R_n

The most important are T_{min} and the real and imaginary parts of Z_{opt} . T_{min} is a value that specifies the lowest noise temperature the FET can have. Z_{opt}

is the impedance the FET's input should "see" in order to achieve T_{min} (recall for minimum noise $\Gamma_S = \Gamma_{opt}$). The fourth parameter R_n is referred to as the equivalent noise resistance and is a sensitivity parameter for mismatches between Z_{opt} and Z_S .

Knowledge of a FET's S-parameters and noise parameters allows for the design of the required input matching network in the LNA circuit. Once Z_{opt} is obtained, an input matching network can be designed to present the desired impedance to the transistor input. Noise analysis and the design process are further documented respectively in Chapters 4 and 5.

Chapter 3

Transistor S-Parameter Measurement

Successful S-parameter measurement of the Agilent ATF-34143 pHEMT was achieved up to 10 GHz using TRL calibration. This chapter covers the method of calibration used as well as the components used to construct the test and calibration fixtures for the ATF-34143.

3.1 Measuring S-parameters of a FET: Thru-Reflect-Line (TRL) Calibration

Agilent specification sheets for the ATF-34143 provide S-parameters from 0.5 GHz to 18 GHz. However, displaying them on the Smith Chart shows that the S11 curve does a full 360° rotation (as shown in Figure 3.1). Using high frequency circuit simulation software such as *nodal* to simulate pHEMT S-parameters, Bruce Veidt was able to conclude that this behavior is impossible to simulate with a FET unless something additional is connected to its input — for example, a long transmission line. Agilent's given S-parameters were clearly

incorrect. Transistor S-parameters would have to be measured manually.

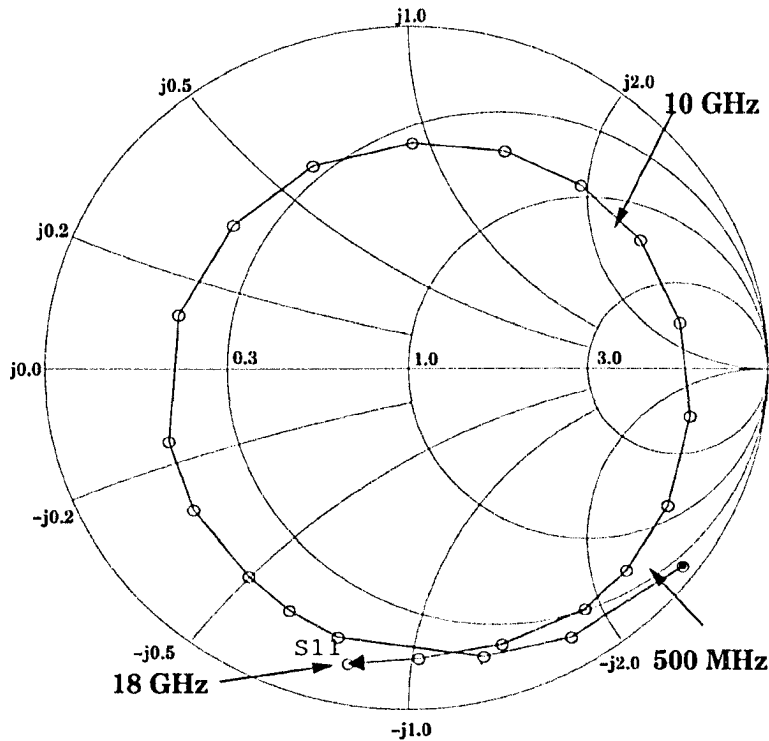


Figure 3.1: S_{11} data provided by Agilent.

Accurate transistor S-parameters were obtained using TRL calibration with an Agilent 8720 ES network analyzer. The network analyzer's coaxial cables cannot be directly attached to the transistor due to the mismatch in physical size. Therefore a fixture is needed to provide an interface between the coaxial cable and the transistor, and TRL calibration is a means of eliminating fixture and cable effects on S-Parameter measurement of a non-coaxial device. TRL was chosen because it requires calibration standards that are easier to realize with microstrip (see following paragraph) at high frequencies. Short-Open-Load-Thru (SOLT) is another common way of calibrating non-coaxial devices but the required standards are not as easy to build. In particular, the load standard introduces a challenge because a purely resistive load is difficult to realize over a large bandwidth in microstrip [9].

Calibration fixtures were constructed using microstrip, the transmission medium of choice in building the LNA. Microstrip is a type of transmission line used in the construction of PCBs (printed circuit boards). It is commonly used in the construction of high frequency circuits due to its high bandwidth, excellent miniaturization, easy integration with chip devices, and low radiation losses[34]. Signals are transmitted by a conducting trace on a dielectric (non-conducting) substrate. The substrate rests on a conducting sheet that acts as the ground plane. Convenience lies in the simple geometry of microstrip (see Figure 3.2), which allows for easy mounting of circuit components.

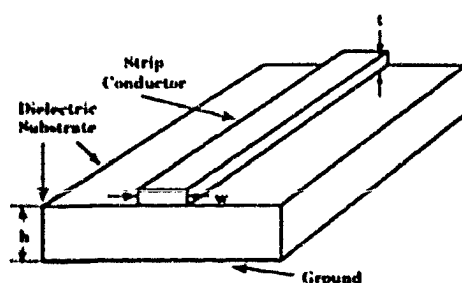


Figure 3.2: Microstrip geometry [9].

The fixture is ideally lossless or “invisible.” Therefore in order to keep losses at a minimum, Rogers RO4003 microstrip was selected. RO4003 is composed of a very low loss substrate, as demonstrated in Figure 3.3. The chart displays insertion loss, which is obtained by measuring the gain (also known as scattering parameter S_{21}) of the microstrip. If the microstrip were perfectly lossless, the gain would be unity (0 dB). In actuality, however, microstrip has some loss, which introduces negative gain. RO4003 is inferior to only two types of laminate on the chart: RO3003 and PTFE/woven glass. RO3003 was not chosen because it is not as rigid as RO4003, making its sturdiness questionable. PTFE is more expensive due to special high-cost fabrication processes [35].

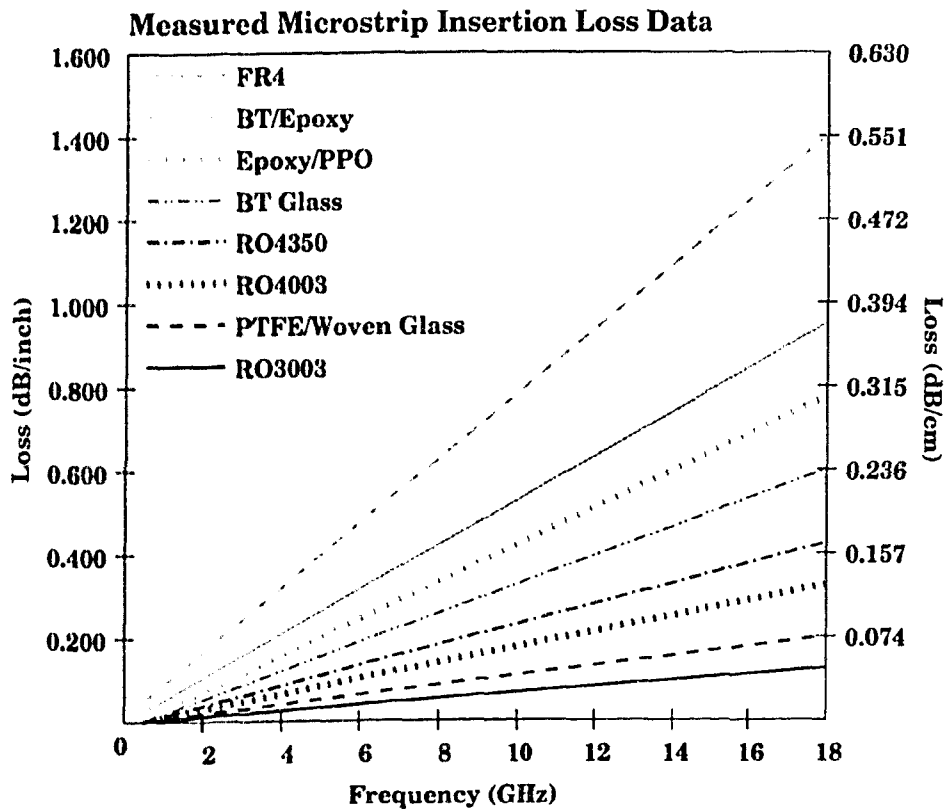


Figure 3.3: Microstrip insertion loss [10].

Care should be taken when selecting connectors as well. Connectors should provide a good transition from the network analyzer cables (coaxial) to the fixture (microstrip). Further detail on the type of connectors used for the fixtures is discussed in section 3.3. TRL calibration was successfully performed over the frequency range 500 MHz - 10 GHz as shown in the following.

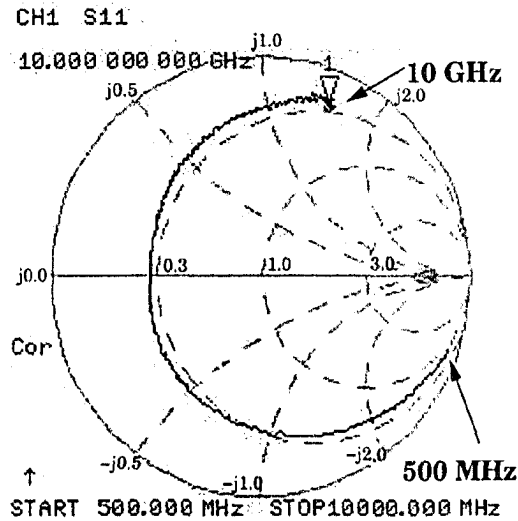


Figure 3.4: Measured S_{11} of ATF 34143 pHEMT from 500 MHz to 10 GHz plotted on the Smith Chart.

3.2 Thru-Reflect-Line (TRL) Standards

The fixtures used in these measurements are shown in Figures 3.6 and 3.8. During S-Parameter measurement, the device under test (DUT) is sandwiched between two fixture-halves. Each fixture-half terminates in a coaxial connector, acting as an interface to the coaxial cables of the network analyzer. To maximize the transparency of the fixture to the network analyzer, fixtured calibration standards are required so that the fixture itself may be calibrated out of the measurement. These standards consist of a THRU, a REFLECT and at least one LINE (depending on the range of frequencies used). The following are guidelines for building TRL standards.

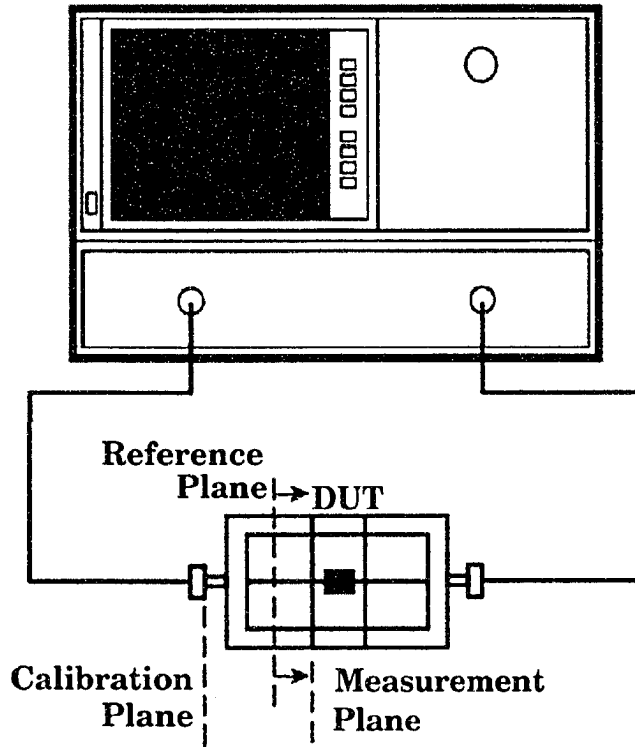


Figure 3.5: S-parameter measurement of a non-coaxial device in fixture based on [9].

3.2.1 THRU

The THRU standard is simply the fixture by itself (i.e. the fixture-halves joined together). It consists of a 1" (2.54 cm) length of microstrip with two coaxial connectors soldered at each end. The middle of the THRU standard sets the reference plane for measurement. Recall that impedances displayed on a Smith Chart require a normalizing value. The THRU standard provides the characteristic impedance for measurements to be referenced to. In this case the standard 50 Ohms was used. The characteristic impedance of microstrip transmission line depends on not only the width of the conducting trace, but the thickness and dielectric constant of the substrate as well. The dependence

of characteristic impedance on these factors can be quite complex and requires substantial computational efforts [36]. However, there are software tools that prove to be useful. *Nodal* has a Z_0 function and Rogers Corporation offers a free program on its website to calculate characteristic impedance of microstrip lines [37]. Using these two tools, it was calculated that RO4003, which has a dielectric constant of 3.38 [10], should have a line width of approximately 0.080" (0.20 cm) in order to have a characteristic impedance of 50 Ohms.

3.2.2 REFLECT

The REFLECT standard can be either an open circuit or a short circuit. A perfect open or short causes 100% of an incoming voltage wave to be reflected back, which is equivalent to a 0-degree (open) or 180-degree (short) phase shift in the wave. The point of reflection establishes the reference plane (the point where each fixture-half meets the device). Because the reflection needs to occur at the reference plane, the REFLECT standard is constructed using a fixture-half that terminates in an open or a short.

Due to the fringing capacitance of an open circuit created in microstrip [38], a short circuit was chosen for the reflect standard (fringing capacitance brings the impedance of a microstrip open circuit further away from that of an ideal open circuit). The short was constructed using vias (holes that are plated through with conductor so that they are connected to the ground plane of the microstrip).

3.2.3 LINE

Although its characteristic impedance should be equal to that of the THRU standard, each LINE standard must not have the same insertion phase as the THRU. Insertion phase is the phase of the signal at the output port relative to

the input port. In other words, the LINE standard has to be a certain length longer than the THRU but not long enough that insertion phase is duplicated. The difference in insertion phase between the THRU and LINE standard must remain between $(20^\circ \text{ and } 160^\circ) \pm n \times 180^\circ$ to avoid ambiguity. Optimal line length is 90° , which is one quarter-wavelength. The usable bandwidth of a single LINE has an 8:1 ratio, meaning the upper frequency limit is 8 times that of the lowest frequency being used [9]. Because of this bandwidth limitation, more than one line standard may be needed if the usable frequency span of a single line standard is not wide enough.

For example, the Agilent datasheet gives S-Parameter data from 500 MHz to 18 GHz. TRL calibration would require more than one LINE standard to cover this entire range. Due to the 8:1 bandwidth limitation, the upper frequency limit for LINE 1 would be 8×500 MHz, or 4 GHz. LINE 2 would be usable from 4 GHz to 18 GHz. The lengths of the excess transmission line (relative to the length of the THRU standard) for use within frequency range f_1 to f_2 are calculated as follows [38].

$$length(cm) = \frac{15000 \cdot VF}{f1(MHz) + f2(MHz)} \quad (3.1)$$

VF is velocity factor, or the amount the speed of electromagnetic propagation in a medium is reduced relative to that of propagation in free space. In the case of microstrip, the velocity factor depends on the effective dielectric constant of the substrate.

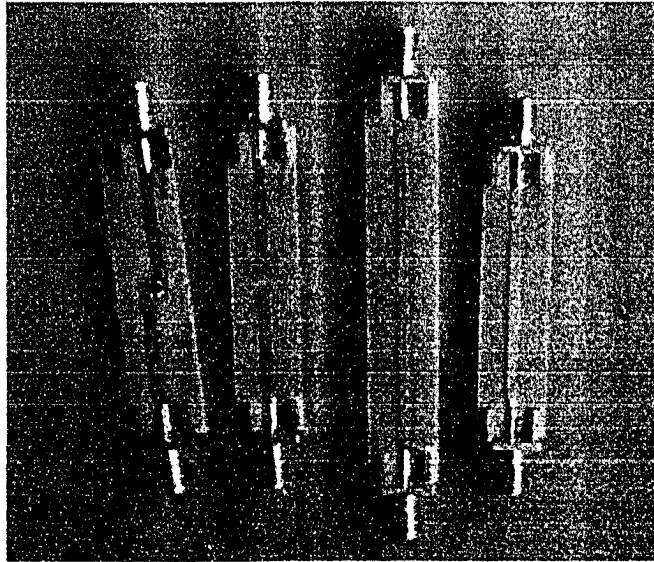
$$VF = \frac{1}{\sqrt{\epsilon_{eff}}} \quad (3.2)$$

Microstrip effective dielectric constant is a function of the relative dielectric constant of the microstrip substrate and microstrip geometry. It accounts for

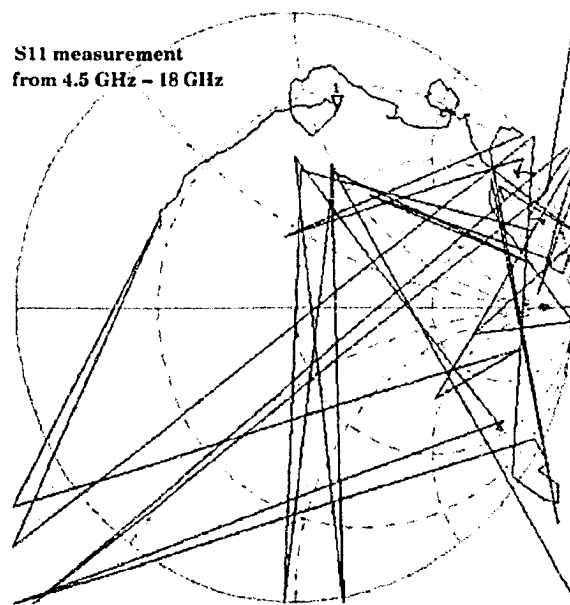
electric fields not being fully constrained within the substrate: they “leak” into the air. RO4003 has a dielectric constant (ϵ_r) of 3.38, which means its effective dielectric constant is 2.68 (calculated with *nodal's DielectricConstant* function). As a result, the excess lengths of LINE 1 and LINE 2 relative to the length of the THRU standard were calculated respectively to be 0.74” (1.88 cm) and 0.15” (0.38 cm).

3.3 Connectors for Fixtures

SMA (Sub-miniature version A type of coaxial connector) connectors are required for the test fixtures so as to interface to the network analyzer cables. Special care needs to be taken when choosing SMA connectors for TRL calibration fixtures because these connectors provide the transition from coaxial cable to microstrip over a wide frequency range. It is extremely important that the microstrip-coaxial transition is high quality and works well at higher frequencies. Mounting the fixture on something solid will ensure consistency by keeping the microstrip board fixed in place. Unfortunately, the first set of test fixtures were constructed without mounting blocks and with typical off-the-shelf SMA connectors. S-parameter measurement was successful up to only 6 GHz (see Figure 3.6).



(a)



(b)

Figure 3.6: a) Low quality microstrip TRL fixtures. b) Measurement attempt above 6 GHz with low quality fixtures.

Finally, high quality SMA connectors were purchased from Southwest Mi-

crowave because of their specially designed microstrip-to-coax transitions and used to construct new test fixtures (refer to Figure 3.8). The target upper frequency for S-Parameter measurements was 18 GHz but measurements were successful only up to 10 GHz (see Figure 3.9). However, 10 GHz is still a significant improvement over 6 GHz - nearly double the measurement bandwidth. Southwest Microwave provides a variety of coax-microstrip transitions to accommodate different microstrip conducting trace widths and substrate thicknesses. For this particular application, 290-36G panel mount connectors with launch pin and dielectric transitions were used, as shown in Figure 3.7.

LAUNCH PIN & DIELECTRIC TRANSITION

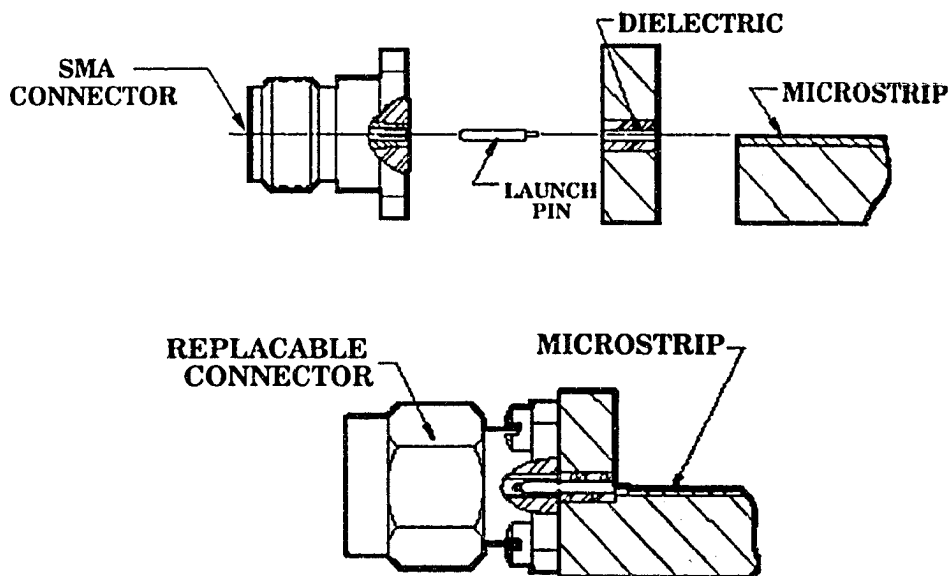


Figure 3.7: Southwest Microwave microstrip-to-coax transitions [11].

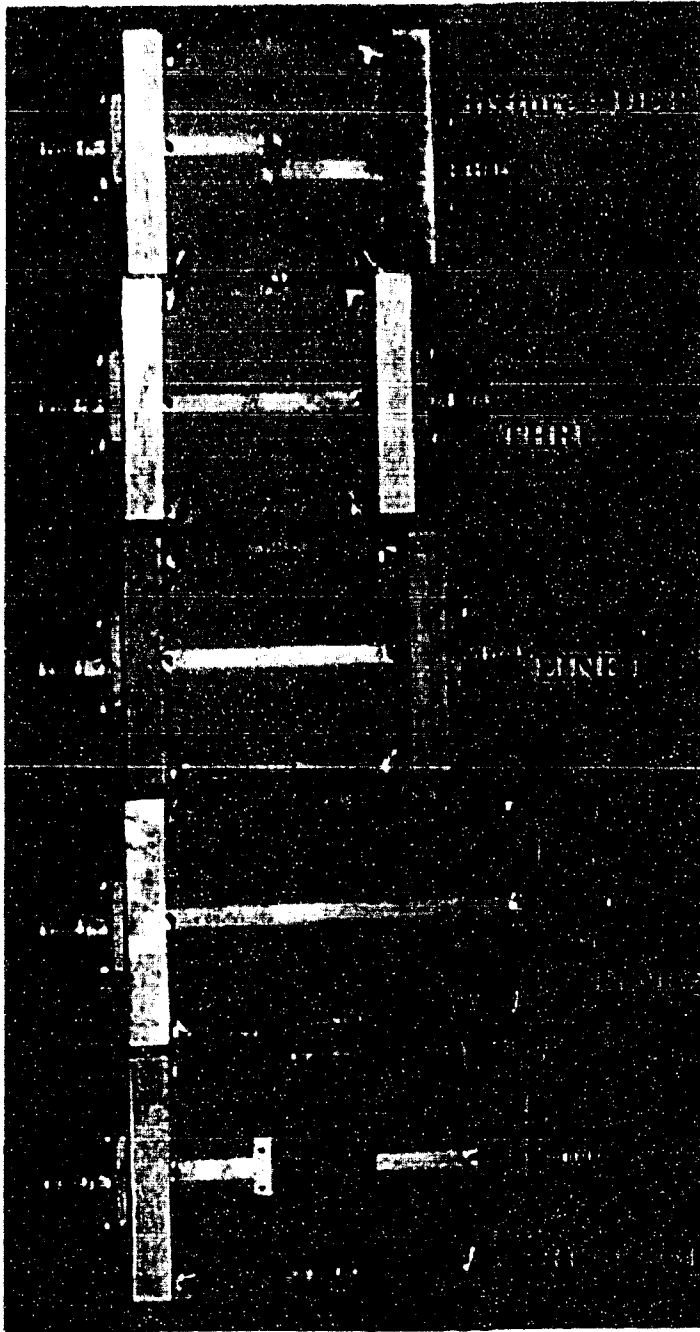


Figure 3.8: Better quality microstrip TRL fixtures.

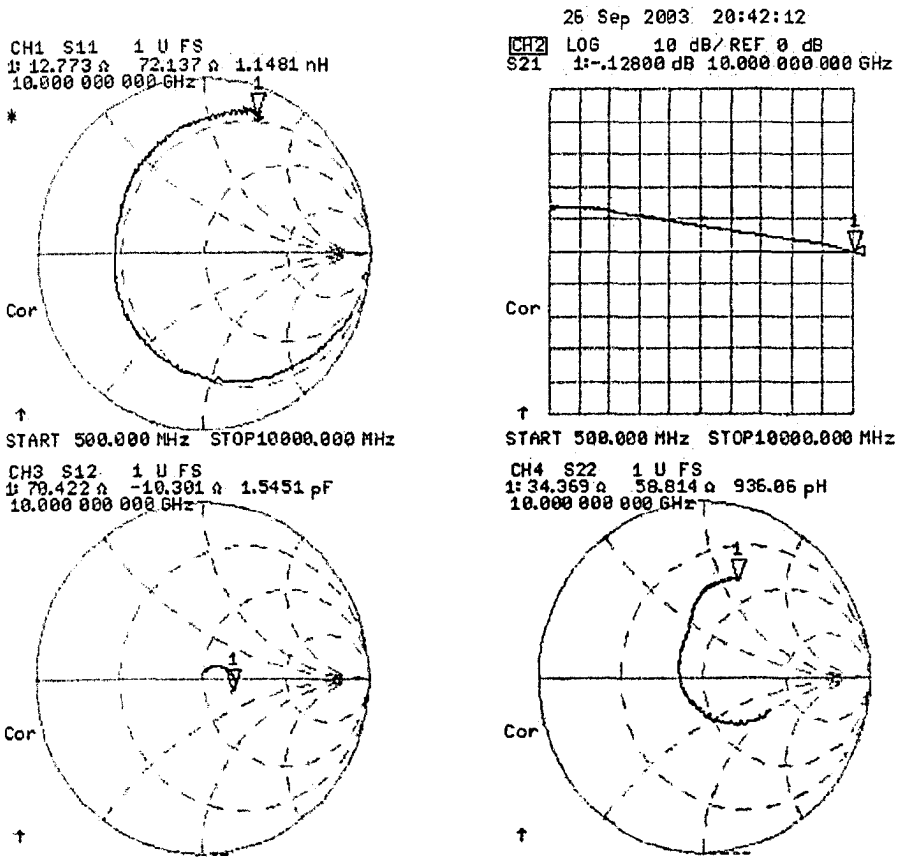


Figure 3.9: S-parameter measurement with the Agilent 8720 ES network analyzer from 500 MHz to 10 GHz. The pointer marked "1" in the graphs lies on 10 GHz. Graph S21 (top right) is on the scale of 10 dB per grid division.

Chapter 4

Field Effect Transistor (FET)

Modelling Using S-Parameters

and FET Noise Parameter

Calculation

How the equivalent circuit model of the Agilent ATF-34143 pHEMT was obtained from its measured S-parameters is documented in this chapter. Theoretically, the equivalent circuit of a FET can be determined using the FET's measured S-parameters and simulated S-parameters over a wide frequency range. The equivalent FET circuit can then be used to calculate the FET noise parameters, which are necessary for LNA design. Simulated S-parameters can be generated from a FET equivalent circuit model using high frequency circuit simulation software. For this project, *nodal* was used to simulate the S-parameters of the FET equivalent circuit. Optimization of the equivalent circuit element values was performed iteratively by least-squares fitting of simulated S-parameters to measured S-parameters of the ATF-34143 over the

frequency range 0.5 - 10 GHz. To obtain initial values for the optimization process, I used a variety of sources, including values specified by Agilent for the ATF-34143 as well as already-documented values for other FETs. I also attempted to obtain rough estimates of FET circuit model parameters with a method commonly known as the cold FET method, which involves taking S-parameter measurements of the ATF-34143 at different bias conditions. Finally, noise parameters were determined using Pospieszalski's method, which will be discussed in this chapter, as well as circuit noise modelling performed by *nodul*.

4.1 Noise Power

Recall from Section 1.5 that noise in electronic devices is generated by thermal fluctuations in electrons. Equation 1.15, which states the maximum power obtainable from a noisy resistor within bandwidth Δf , comes from Nyquist's derivation in 1928 of the following relation between the rms voltage of thermal noise $v_{n,rms}$ appearing across a resistor R [39]:

$$v_{n,rms} = \sqrt{v_n^2} = \sqrt{4kTR\Delta f} \quad (4.1)$$

Equation 4.1 can be used to model the physical resistor R as a noise-free resistor in series with a voltage source of rms voltage $\sqrt{4kTR\Delta f}$. Derived from Norton's theorem, an equivalent current source model consisting of a current source with rms current $\sqrt{4kTG\Delta f}$ in parallel with noise-free conductance $G = \frac{1}{R}$ can also be used to represent a noisy resistor. The equivalent models are shown in Figure 4.1 [39].

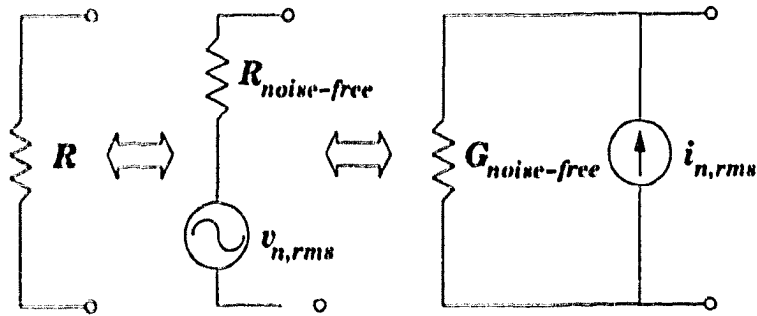


Figure 4.1: Equivalent models of a noisy resistor R .

As stated previously, Equation 1.15 gives the maximum power obtainable from noisy resistor R . With respect to $v_{n,rms}$ and R , Equation 1.15 also translates into the following:

$$P_N = kT\Delta f = \frac{v_{n,rms}^2}{4R} \quad (4.2)$$

Maximum power transfer occurs when the load impedance is the complex conjugate of the source impedance. This can be explained by a simple network with a source generator and a load.

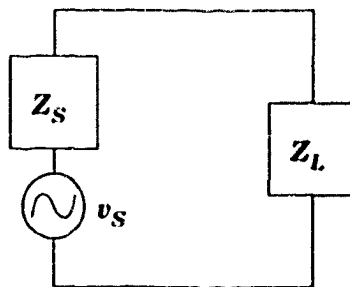


Figure 4.2: Voltage generator driving a load.

The power dissipated in the load can be found using the following relation:

$$P = \frac{1}{2} |I|^2 \operatorname{Re}\{Z_L\}$$

where

$$|I| = \left| \frac{v_s}{Z_S + Z_L} \right|$$

Putting everything together,

$$P = \frac{1}{2} \left| \frac{v_s}{Z_S + Z_L} \right|^2 \operatorname{Re}[Z_L]$$

Letting $Z = R + jX$,

$$P = \frac{1}{2} \frac{|v_s|^2 R_L}{(R_S + R_L)^2 + (X_S + X_L)^2}$$

From the above equation, P is maximized when $Z_L = R_S - jX_S = Z_S^*$.

And when $Z_L = Z_S^*$,

$$P = \frac{1}{2} \frac{|v_s|^2}{4R_L} = \frac{v_{s,rms}^2}{4R_L}$$

which is equivalent to Equation 4.2 if $v_{n,rms}$ and R comprise the noisy resistor with R as the load.

Similarly, a noisy network with available output power P_a within bandwidth Δf can be modelled as a noisy resistor at temperature T_s producing available power P_a , as shown in Figure 4.3 [7].

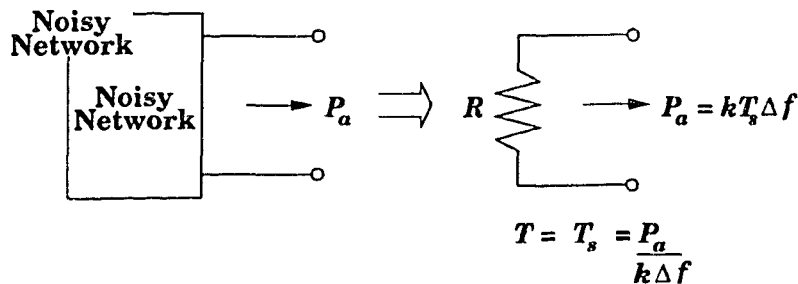


Figure 4.3: Noisy network modelled as a noisy resistor.

4.2 Noise Temperature and Noise Figure

A noisy two-port network can be modelled as a noiseless two-port network with additional noise power at its input (refer to Figure 4.4). Consider a noisy two-port with noise power $P_{Ni} = kT_s\Delta f$ entering at its input. Input noise power P_{Ni} is amplified by the available gain of the two-port G_A , resulting in output noise power $P_{No} = G_A P_{Ni}$. If the two-port is to be modelled as noiseless, then in the model, additional noise power $kT_e\Delta f$ is added at the input, symbolizing the noisy two-port's noise power contribution referred to the input of the network. Therefore, the noisy two-port is defined as having an effective input noise temperature of T_e . The noisy two-port's input noise power contribution is amplified by the two-port's available gain G_A and shows up at the output as $(kT_e\Delta f)G_A$.

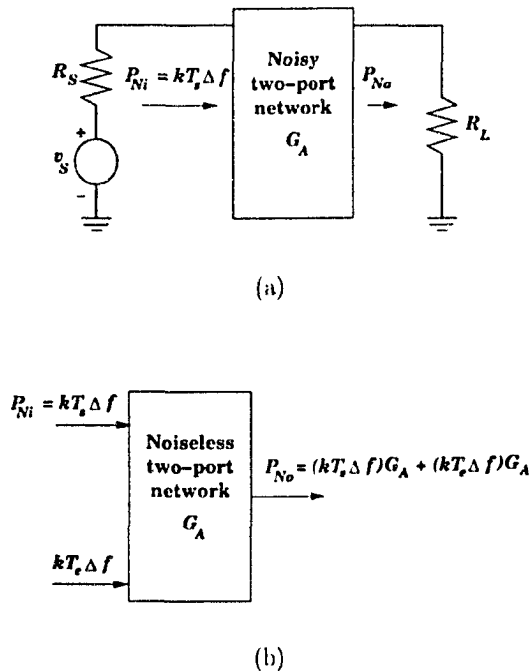


Figure 4.4: a) Noisy two-port network. b) Noiseless two-port network model of noisy two-port network [7].

Because of the additional input noise power $kT_e\Delta f$, the total output noise power P_{No} becomes a sum of two terms:

$$P_{No} = G_A P_{Ni} + G_A kT_e \Delta f \quad (4.3)$$

$$= kT_s \Delta f G_A + kT_e \Delta f G_A$$

$$= kT_s \left(1 + \frac{T_e}{T_s}\right) \Delta f G_A$$

The available gain G_A is defined as the ratio of available signal power at the output P_{So} to available signal power at the input P_{Si} :

$$G_A = \frac{P_{So}}{P_{Si}}. \quad (4.4)$$

The ratio of signal-to-noise power ratio at the input to signal-to-noise ratio at the output defines the noise figure F of the two-port. In other words, noise figure is a measure of how much a signal degrades as it passes through the two-port as a result of the two-port's own noise. Substitution of Equation 4.4 into Equation 4.3 results in an expression for the noise figure of the two-port in terms of input noise temperature T_s and additional effective input noise temperature T_e :

$$\frac{P_{Si}/P_{Ni}}{P_{So}/P_{No}} = F = 1 + \frac{T_e}{T_s}$$

T_e has already been defined as the noise temperature of the noisy two-port. T_s , also known as T_0 , is a reference input noise temperature required to obtain the noise figure of the two-port. The standard value has been set at 290 K. The term “noise figure” has been commonly used since the 1940's, when it was

defined as above by Harold Friis [14]. In modern usage, however, the quantity F has often come to be known as “noise factor,” while the same quantity in dB units, NF , is known as noise figure.

$$NF = 10 \log F.$$

For simplicity however, in this thesis F and NF will both be referred to as noise figure — NF being noise figure in terms of dB.

4.3 Noise Parameters

Noise figure is a convenient way of quantitatively describing the noise performance of an amplifier. Recall from Section 2.5 that a major part of this project involves obtaining the noise parameters of a FET and that there are four noise parameters in total:

- T_{min} or F_{min}
- the real part of Z_{opt} or Γ_{opt}
- the imaginary part of Z_{opt} or Γ_{opt}
- equivalent noise resistance R_n or equivalent noise conductance g_n .

T_{min} and F_{min} specify the lowest noise an amplifier can have. Z_{opt} and Γ_{opt} specify what impedance the input port of the amplifier needs to see in order to achieve lowest noise. R_n and g_n are measures of the sensitivity of amplifier noise temperature T or noise figure F as Z_S deviates from Z_{opt} . Noise resistance R_n and noise conductance g_n arise from the noise representation of the two-port as shown in Fig 4.5.

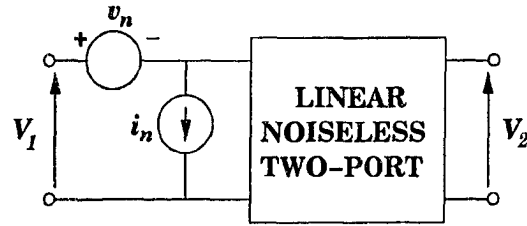


Figure 4.5: Noise representation of noisy two-port used to define noise parameter R_n and g_n [12].

R_n and g_n are defined as the following [12]:

$$R_n = \frac{\overline{|v_n|^2}}{4kT_0\Delta f} \quad (4.5)$$

$$g_n = \frac{\overline{|i_n|^2}}{4kT_0\Delta f} \quad (4.6)$$

R_n = noise resistance (Ω)

g_n = noise conductance (siemens)

$|v_n|$ = noise voltage source amplitude (volts)

$|i_n|$ = noise current source amplitude (amperes)

k = Boltzmann's constant = 1.3807×10^{-23} J/K

T_0 = standard reference noise temperature of 290 K

Δf = bandwidth (Hz)

The noise temperature T of a two-port amplifier can be expressed as a function of the four noise parameters [12]:

$$T = T_{min} + T_0 \frac{g_n}{R_g} |Z_g - Z_{opt}|^2 \quad (4.7)$$

T = noise temperature of amplifier (K)

T_{min} = minimum obtainable noise temperature of amplifier(K)

T_0 = standard reference noise temperature value of 290 K

g_n = noise conductance (siemens)

R_g = real part of source impedance

Z_g = source impedance

Z_{opt} = source impedance seen by amplifier input which achieves T_{min} (Ω)

Since F is related to T , the noise figure F of a two-port amplifier can be expressed as a function of the four noise parameters as well [7]:

$$F = F_{min} + \frac{4r_n |\Gamma_S - \Gamma_{opt}|^2}{(1 - |\Gamma_S|^2) |1 + \Gamma_{opt}|^2} \quad (4.8)$$

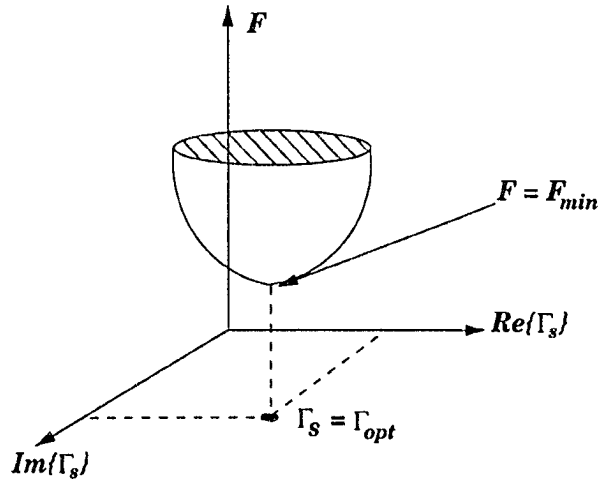
$r_n = \frac{R_n}{50\Omega}$ = equivalent normalized noise resistance of two-port

Γ_S = source reflection coefficient

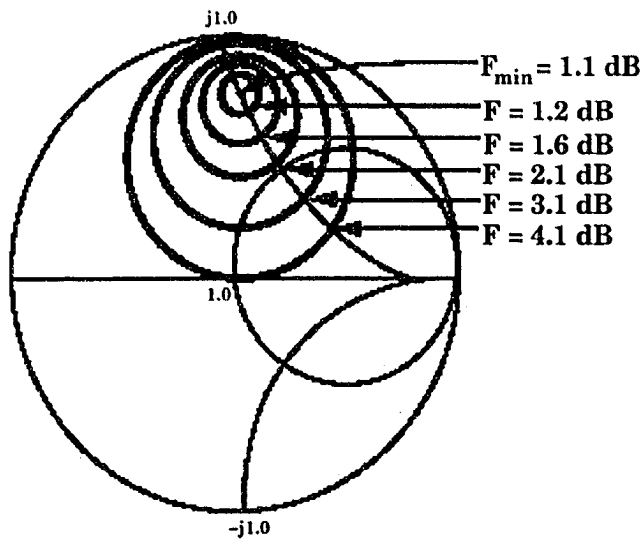
Γ_{opt} = optimum source reflection coefficient for minimum noise

F_{min} = minimum noise figure

Constant noise figure (F) values form circles in the Γ_S -plane except for the single point F_{min} , which corresponds to $\Gamma_S = \Gamma_{opt}$ (refer to Figure 4.6).



(a)



(b)

Figure 4.6: a) Noise figure F as a function of source reflection coefficient Γ_S [13]. b) Example of noise figure circles on the Smith Chart (Γ_S -plane) [14].

4.4 Using a FET Equivalent Circuit Model to Find Noise Parameters: the Pospieszalski Method

If the small-signal equivalent circuit of a FET and two particular frequency-independent constants are known, then theoretically all four noise parameters (F_{min} , r_n , $Re[\Gamma_{opt}]$, $Im[\Gamma_{opt}]$) can be predicted over a broad frequency range. This way of obtaining noise parameters can be attributed to Marian Pospieszalski [12]. According to Pospieszalski [12], Pucel [40] provides the most comprehensive FET noise model. However, Pucel's model requires three frequency-independent noise coefficients to be known in addition to a FET equivalent circuit model. Taking advantage of more recent work by Gupta *et al.* [13], Pospieszalski has been able to show that accurate noise parameters may be calculated from knowledge of a FET equivalent circuit and only one frequency-independent constant [12]. The equivalent circuit model is shown in Figure 4.7.

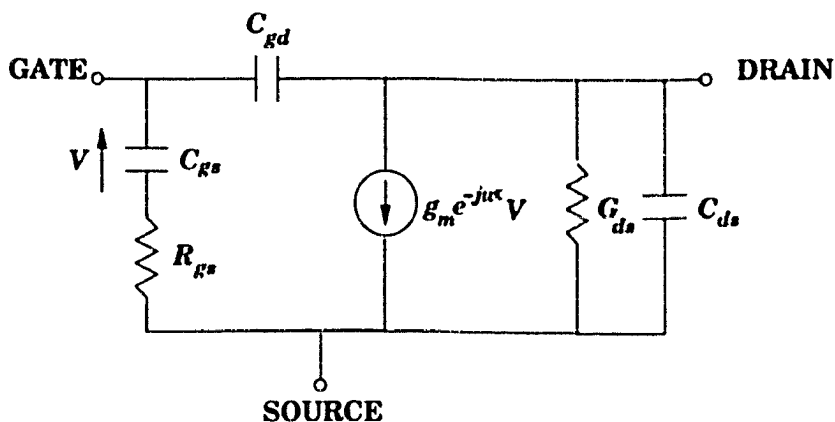


Figure 4.7: Intrinsic noise equivalent circuit of a FET. Delay τ represents the transit time of electrons through the FET channel.

Initially, Pospieszalski's model requires two frequency-independent con-

stants: the gate equivalent temperature T_g and drain equivalent temperature T_d . T_g represents the equivalent noise temperature of the gate resistance R_{gs} while T_d represents the equivalent noise temperature of the drain conductance G_{ds} . However, only one of the frequency-independent constants needs to be determined - T_d . It has been shown experimentally by Gupta *et al.* [13] that T_g can be approximated as the ambient temperature of the device. Upon obtaining an equivalent FET model and T_d , each of the four noise parameters can be expressed in terms of T_g , T_d and FET equivalent circuit parameters [12]:

$$X_{opt} = Im[Z_{opt}] = \frac{1}{2\pi f C_{gs}} \quad (4.9)$$

$$R_{opt} = Re[Z_{opt}] = \sqrt{\left(\frac{f_f}{f}\right)^2 \frac{R_{gs} T_g}{G_{ds} T_d} + R_{gs}^2} \quad (4.10)$$

$$T_{min} = 2\frac{f}{f_f} \sqrt{G_{ds} R_{gs} T_g T_d + \left(\frac{f}{f_f}\right)^2 R_{gs}^2 G_{ds}^2 T_d^2} + 2\left(\frac{f}{f_f}\right)^2 R_{gs} G_{ds} T_d \quad (4.11)$$

$$g_n = \left(\frac{f}{f_f}\right)^2 \frac{G_{ds} T_d}{T_0} \quad (4.12)$$

X_{opt} = imaginary part of optimum impedance for lowest noise (Ω)

R_{opt} = real part of optimum impedance for lowest noise (Ω)

T_{min} = minimum noise temperature (K)

g_n = noise conductance (siemens)

f = frequency (Hz)

f_f = cutoff frequency (Hz)

C_{gs} = gate-to-source capacitance (F)

R_{gs} = gate-to-source resistance (Ω)

R_{ds} = drain-to-source resistance (Ω)

$G_{ds} = \frac{1}{R_{ds}}$ = drain-to-source conductance (siemens)

T_g = equivalent gate temperature (K)

T_d = equivalent drain temperature (K)

where

$$f_T = \frac{g_m}{2\pi C_{gs}} \quad (4.13)$$

g_m = transconductance of FET (siemens)

The transconductance of a FET is the ratio of the change in drain current to a change in gate voltage and has units of siemens. The cutoff frequency is defined as the frequency at which FET current gain drops to unity [31].

This FET noise model is restricted to the following condition:

$$T_{min} \leq 4NT_0$$

where

$$N = R_{opt}g_n$$

Values of N and T_{min} that satisfy this relation allow the model to represent a physical two-port [12]. As will be shown later for the ATF-34143 pHEMT (biased at a drain voltage of 3 V and a drain current of 20 mA), $R_{opt} = 66\Omega$, $R_{ds} = 77.9\Omega$, $g_m = 0.106$ Siemens, $T_d = 927$ K, $T_0 = 290$ and $T_{min} = 7.5$ K (calculated using the Pospieszalski method), which makes $4NT_0$ equivalent to 14 K - therefore Pospieszalski's noise model is applicable. As well, the Pospieszalski noise model is valid for high frequencies where $1/f$ or "flicker noise," is insignificant.

4.5 Adding Extrinsic to Pospieszalski's Model: the Total FET Chip Equivalent Circuit

The model provided by Pospieszalski is only an intrinsic one. Because the ATF-34143 is a packaged chip, an extrinsic circuit needs to be added to the model used by Pospieszalski in order to account for the parasitics introduced by the transistor's chip packaging. The chip packaging of the transistor introduces resistances, inductances and capacitances as shown in Figure 4.8.

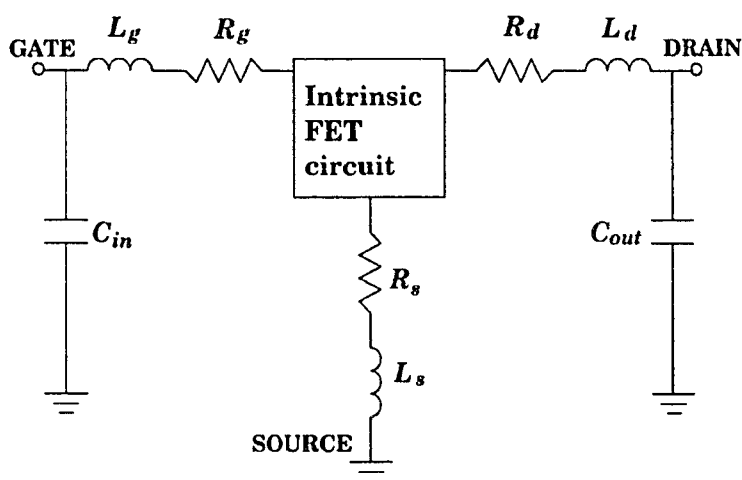


Figure 4.8: Extrinsic FET circuit representing chip package parasitics [15].

Altogether, the intrinsic and extrinsic FET circuit models combine to form a total FET equivalent circuit model consisting of 15 circuit elements that need to be determined (see Figure 4.9). The intrinsic circuit model is obtained from Pospieszalski's work while the extrinsic circuit model is obtained from work done by Brockerhoff *et al* [15]. The next section describes how these circuit parameters are determined.

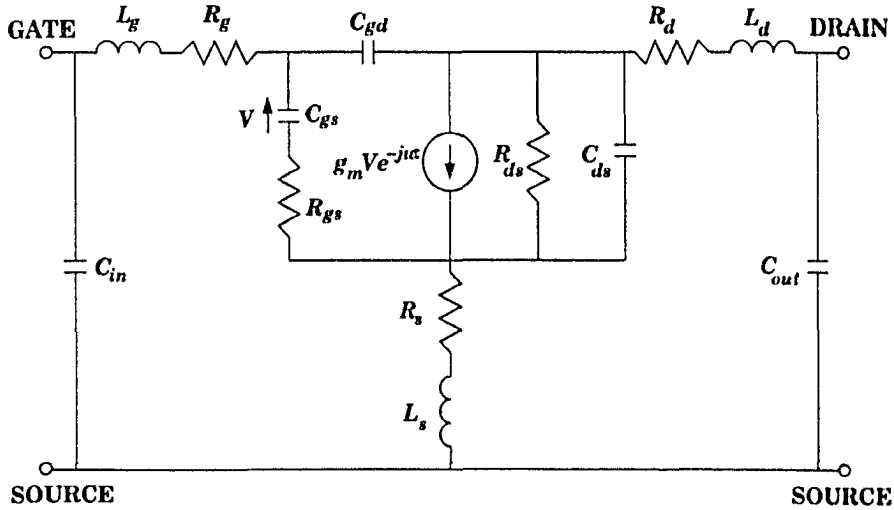


Figure 4.9: Total FET equivalent circuit model including extrinsic parasitics [15].

4.6 Determination of FET Equivalent Circuit Element Initial Values

The FET equivalent circuit model used in work by Brockerhoff *et al.* was chosen because of an accompanying method of circuit element extraction which includes optimization [15]. As will be discussed later, other methods such as the work done by Dambrine *et al.* involve direct extraction from the measured S-parameters themselves [16]. However, extraction of parasitic resistances directly from measured S-parameters has proven to be quite difficult. The work by Brockerhoff *et al.* at least allows for an initial rough estimation of FET circuit elements. The method consists of iteratively fitting simulated S-parameters based on the FET equivalent circuit to actual measured S-parameters in a specific sequence. To begin the process, a FET equivalent circuit with circuit element initial values is needed to start the iteration. This poses a challenge because there are 15 parameters for which initial values are

needed. It is important that these initial values are within reasonable range of typical FET equivalent circuit element values so that the iteration converges to a realistic solution.

Fortunately, many circuit models of FETs have been documented and provide a good estimate of each circuit element's order of magnitude. As well, there are ways to extract certain circuit elements from various DC-biased S-parameter measurements. Thirdly, Agilent provides its own equivalent circuit *model of the ATF-34143*. One does not have to start from scratch when searching for initial values to use in the circuit element extraction iteration. The following is a discussion of these three different sources of circuit element initial values.

4.6.1 Previous FET Circuit Models

Numerous papers on FET modelling provide examples of FET equivalent circuits. These circuit models provide a good estimate of extrinsic parasitics. Although the intrinsic FET itself may vary a large amount from model to model due to the variation in different types of FET chips, the chip packaging parasitics do not hold as much room for variation. For example, source, gate and drain inductances commonly range from the order of tenths of a nanohenry to a nanohenry while corresponding resistances commonly range from the order of a tenth of an ohm to an ohm. Parallel capacitances commonly range from the order of hundredths of a picoFarad to tenths of a picoFarad.

4.6.2 Various DC-biased S-Parameters - the Cold FET Method

According to Dambrine *et al.* [16], S-parameter measurements at different bias voltages can be used to extract the parameters of a FET equivalent circuit. This is because, unlike the intrinsic elements, the extrinsic elements are independent of the biasing conditions. While keeping the drain voltage at zero, S-parameters are measured at a gate voltage above its pinchoff value and a gate voltage lower than its pinchoff value. (The pinchoff value specifies at which gate voltage the FET “turns off.” No current flows through the FET if the gate voltage is lower than its pinchoff value.) The equivalent intrinsic circuit of a FET at these particular voltage biases is simplified, allowing the investigation of extrinsic elements. This method of extracting extrinsic circuit element values is commonly referred to as the cold FET method.

It should be noted that conversions can be made between S-parameters and other network representations such as Z-parameters and Y-parameters. Z-parameters are represented by an impedance matrix. For the Z-parameters of a two-port, the complex matrix elements are defined as follows:

$$Z_{11} = \left. \frac{V_1}{I_1} \right|_{I_2=0} \quad (\text{impedance of port 1; port 2 open-circuited})$$

$$Z_{12} = \left. \frac{V_1}{I_2} \right|_{I_1=0} \quad (\text{port 1 voltage / port 2 current; port 1 open-circuited})$$

$$Z_{21} = \left. \frac{V_2}{I_1} \right|_{I_2=0} \quad (\text{port 2 voltage/port 1 current; port 2 open-circuited})$$

$$Z_{22} = \left. \frac{V_2}{I_2} \right|_{I_1=0} \quad (\text{impedance of port 2; port 1 open-circuited})$$

The Y-parameter matrix is the complementary admittance matrix of the Z-parameter matrix. Y-parameter matrix elements are functions of the Z-parameter matrix elements as follows:

$$\begin{bmatrix} Y_{11} & Y_{12} \\ Y_{21} & Y_{22} \end{bmatrix} = \begin{bmatrix} \frac{Z_{22}}{|Z|} & \frac{-Z_{12}}{|Z|} \\ \frac{-Z_{21}}{|Z|} & \frac{Z_{11}}{|Z|} \end{bmatrix}.$$

where

$$|Z| = Z_{11}Z_{22} - Z_{12}Z_{21}$$

Z-parameters and Y-parameters are convenient for representation of impedances and admittances respectively. Equations that allow conversion between S-parameters, Z-parameters and Y-parameters may be found in numerous electrical engineering texts. Conversion between S-parameters, Z-parameters and Y-parameters are required when de-embedding the FET equivalent circuit elements until only the intrinsic circuit is left. Figure 4.10 summarizes the steps required for de-embedding.

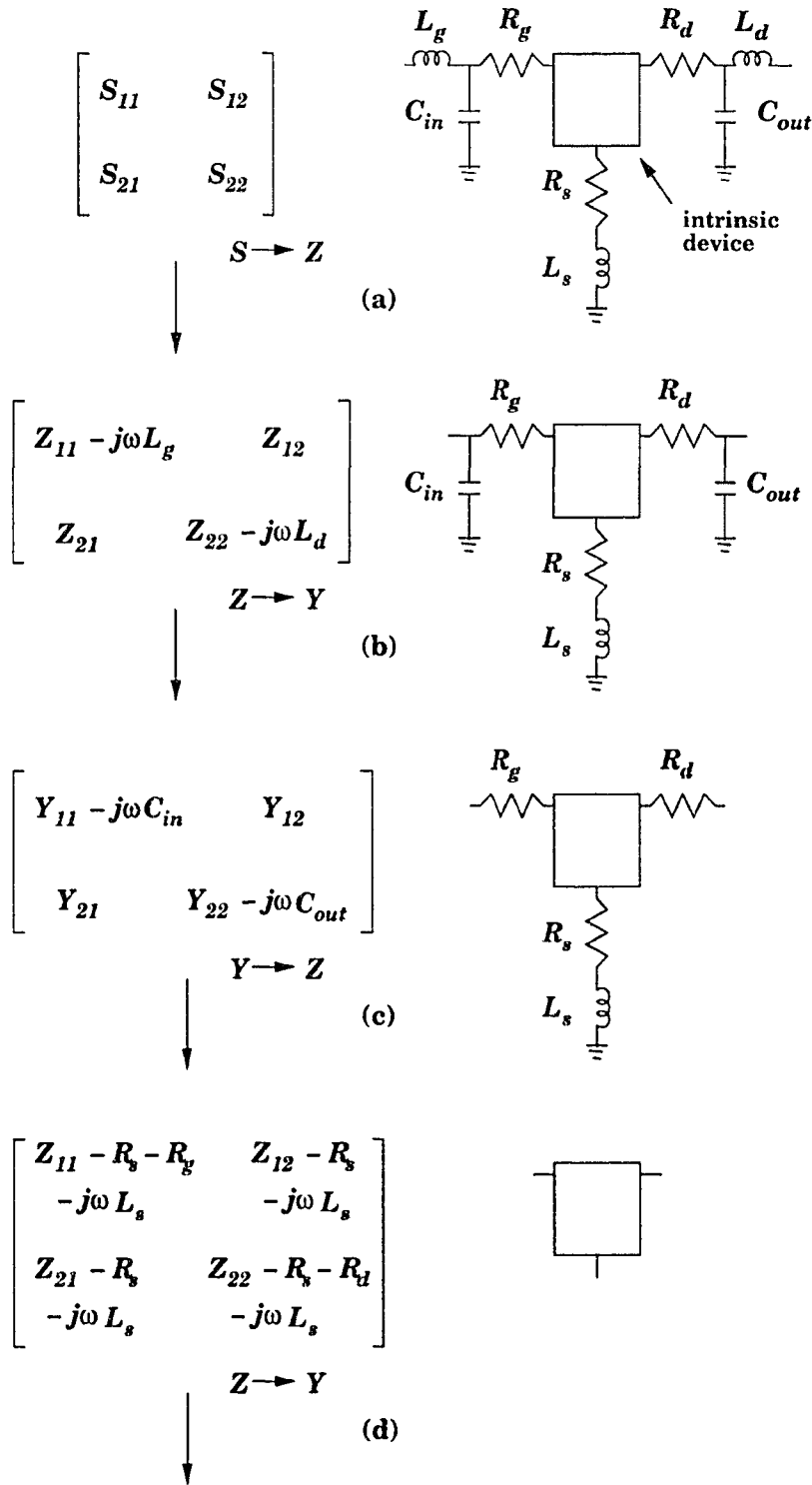


Figure 4.10: Cold FET method for de-embedding to derive the intrinsic circuit based on [16].

How are extrinsic values obtained so that they can be subtracted from the equivalent circuit? This is where the cold FET method comes in. At zero drain voltage and lower-than-pinchoff gate voltage, the equivalent FET circuit is simplified as follows where C_b represents the fringing capacitance at each side of the gate [16]:

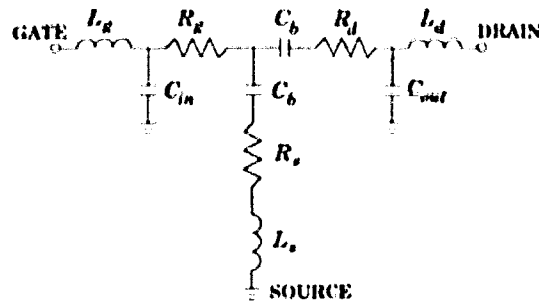


Figure 4.11: Equivalent FET circuit at zero drain bias voltage and gate voltage below pinchoff value [16].

When the gate voltage is above pinchoff value, capacitances become negligible, reducing the equivalent circuit to resistances and inductances as shown in the following, where R_{qq} is the diode resistance of the forward-biased Schottky junction (see Section 2.1.1) and r_{ch} is the channel resistance:

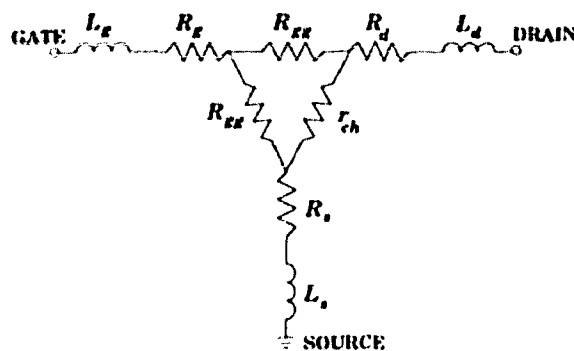


Figure 4.12: Equivalent FET circuit at zero drain bias voltage and gate voltage above pinchoff value [17].

Since the first elements to remove in the de-embedding process are induc-

tances, cold FET S-parameters at gate voltage above pinchoff value are needed in order to determine the extrinsic inductances (see Figure 4.12). The cold FET S-parameters above pinchoff can be converted to Z-parameters, which yield the following approximations [17]:

$$Z_{11} = R_g + (2R_{gg})/(2R_{gg} + r_{ch}) + R_s + j\omega(L_g + L_s)$$

$$Z_{22} = R_d + r_{ch}/4R_{gg} + R_s + j\omega L_s$$

$$Z_{21} = Z_{12} = \frac{1}{2}r_{ch}/4R_{gg} + R_s + j\omega(L_d + L_s)$$

Extracting values for parasitic inductances L_g , L_d and L_s is relatively simple using the imaginary parts of the cold FET Z-parameters above pinchoff. When the imaginary parts of the Z-parameters are plotted with frequency, there is a linear relation between inductive reactance and frequency:

$$\text{Im}(Z_{11}) = j\omega(L_g + L_s)$$

$$\text{Im}(Z_{22}) = j\omega L_s$$

$$\text{Im}(Z_{21}) = \text{Im}(Z_{12}) = j\omega(L_d + L_s)$$

After subtracting the effects of the extrinsic inductance parasitic effects from the equivalent circuit Z-parameters, the new Z-parameters are then converted to Y-parameters so that the effects of extrinsic capacitances C_{in} and

C_{out} can be subtracted (Figure 4.10b and Figure 4.10c). Like the extrinsic inductance values, extrinsic capacitance values are also relatively easy to extract. When the S-parameters below pinchoff are converted to Y-parameters, the following approximations can be used for analysis:

$$Im(Y_{11}) = j\omega(C_{in} + 2C_b)$$

$$Im(Y_{12}) = Im(Y_{21}) = -j\omega C_b$$

$$Im(Y_{22}) = j\omega(C_b + C_{out})$$

At this point, an obstacle was encountered. Extrinsic resistances R_g , R_d and R_s proved to be quite difficult to extract using cold FET parameters at above pinchoff. Aside from the work by Dambrine *et al.*, work by Costa *et al.* [17] provides a detailed explanation on extracting the extrinsic resistance values by using multiple biases of the gate. However, extraction by this method led to the calculation of negative resistance values, which are physically unrealistic. The failure of this method may be attributed to several causes: (a) the small physical values of the resistances, overwhelmed by the effects of other parasitics, or (b) the need for higher accuracy in S-parameter measurements or wider frequency coverage of these measurements. How extrinsic resistance values were obtained for the FET equivalent model is further explained in the next section.

When all that is left is to evaluate the intrinsic circuit, measured S-parameters below 5 GHz of the FET under operating bias conditions are needed for the following equations. At frequencies below 5 GHz, the Y-parameters of the intrinsic circuit can be approximated in a set of equations [16]:

$$Y_{11} = R_{gs}C_{gs}^2\omega^2 + j\omega(C_{gs} + C_{gd})$$

$$Y_{12} = -j\omega C_{gd}$$

$$Y_{21} = g_m - j\omega(C_{gd} + g_m(R_{gs}C_{gs} + \tau))$$

$$Y_{22} = G_{ds} + j\omega(C_{ds} + C_{gd})$$

Unfortunately the inability to obtain extrinsic resistance values prevents further thorough analysis past this point (refer to Figure 4.10 d).

4.6.3 Agilent ATF-34143 Specification Circuit Model

Agilent specifications provide an equivalent model of the ATF-34143. This is valuable especially regarding the extrinsic resistances R_g , R_d and R_s as they are quite difficult to extract using cold FET methods as previously discussed. Other extrinsic values are provided but they are valid only up to 6 GHz [6]. As for the intrinsic equivalent circuit provided, it is different from that used by Pospieszalski, but serves as a useful guide for intrinsic capacitance initial values C_{gd} , C_{gs} and C_{ds} .

4.6.4 Initial Values

As a result of the above analyses, initial values for extrinsic capacitances and inductances were obtained using cold FET methods. Extrinsic resistances proved to be difficult to obtain, so the values specified by Agilent were chosen. Agilent also provides values for the intrinsic capacitances, leaving only initial

values for intrinsics R_{gs} , R_{ds} , g_m and τ to be determined. However, these values can be estimated from the documentation of numerous other already-determined FET equivalent circuit models such as HEMT circuit models provided by Pospieszalski *et al.* [12], Brockerhoff *et al.* [15] and Agilent specifications [6]. The following initial element values for the FET equivalent circuit of the ATF-34143 pHEMT (biased at a drain voltage of 3V and a drain current of 20 mA) were chosen:

$$C_m = 0.01 \text{ pF}$$

$$C_{out} = 0.02 \text{ pF}$$

$$L_g = 1.67 \text{ nH}$$

$$R_g = 1.0 \text{ } \Omega$$

$$L_d = 1.39 \text{ nH}$$

$$R_d = 0.25 \text{ } \Omega$$

$$L_s = 0.42 \text{ nH}$$

$$R_s = 0.125 \text{ } \Omega$$

$$C_{gs} = 0.80 \text{ pF}$$

$$R_{gs} = 5 \text{ } \Omega$$

$$C_{ds} = 0.04 \text{ pF}$$

$$R_{ds} = 100 \text{ } \Omega$$

$$C_{gd} = 0.16 \text{ pF}$$

$$g_m = 0.1 \text{ siemens}$$

$$\tau = 10 \text{ picoseconds}$$

4.7 Sequential Fitting of Simulated S-Parameters to Measured S-Parameters

After performing sensitivity analysis on the effect of different circuit elements on various S-parameters, Brockerhoff *et al.* [15] decided on an optimization procedure. Starting with a certain S-parameter over a wide frequency range, one to three corresponding circuit elements are set as variables. These circuit elements were chosen based on the degree of high sensitivity to the particular S-parameter. Simulated S-parameter values are fitted to the measured S-parameter values by the method of least squares. The solutions for the corresponding circuit element variables are chosen on the basis of minimizing the difference between simulated and fitted S-parameter values. The next step consists of the same process with another S-parameter and a corresponding set of variables. The overall method consists of 8 steps, starting with S-parameter S_{11} (see Table 4.1) [15].

Step	Elements Varied	S-Parameter
1	C_{gs}, R_{gs}	S_{11}
2	C_{ds}, R_{ds}	S_{22}
3	C_{gd}, R_s	S_{12}
4	g_m, τ	S_{21}
5	L_g, R_g, C_{in}	S_{11}
6	L_d, R_d, C_{out}	S_{22}
7	L_s	S_{12}
8	g_m, τ	S_{21}

Table 4.1: Sequence of steps required for optimizing FET circuit model elements.

4.7.1 Calculation of FET Equivalent Circuit Element Values Using *nodal*

Circuit element optimization was performed using *nodal*. As previously mentioned, *nodal* is a valuable circuit simulation tool because it takes advantage of *Mathematica*'s symbolic representation capabilities. To perform least-squares fitting of simulated S-parameters to measured S-parameters, the following error function ε was used:

$$\varepsilon = \sum_{k=1}^K \frac{1}{K} \left| \frac{S_{ijk(\text{measured})} - S_{ijk(\text{simulated})}}{S_{ijk(\text{measured})}} \right|^2 \quad (4.14)$$

k =frequency point

K =total number of frequency points

S_{ij} =S-parameter value where i and j are the port designations

Simulated circuit S-parameters were obtained using *nodal*'s *SParameters* function. Measured S-parameters were obtained using the HP 8720ES network analyzer. The HP 8720ES outputs S-parameter data into .s2p file format, which can be read using *nodal*'s *ReadSParameters* function. Optimization is done by minimizing ε with *Mathematica*'s *FindMinimum* function. The *FindMinimum* function, given an equation and variables, attempts to find values for the variables that will minimize the equation. It has the capability of finding a minimum if *Mathematica* does not have a way to find the derivative of the equation, as is the case with using output from *nodal*'s *SParameters* function. When finding local minima without derivatives, *FindMinimum* uses Brent's principal axis method, which consists of using searching vectors to find minima. The principal axis method requires two starting initial values and uses these values to define the magnitudes of the searching vectors [41]. This method of finding minima is not as reliable as those that use derivatives,

further stressing the importance of obtaining initial values that are close to a realistic solution.

Again, similar difficulties were encountered when dealing with extrinsic resistances R_g , R_d and R_s . When set as variables, the iteration would converge to negative values for the smaller resistances. Because of this, the smallest extrinsic resistance R_d was set fixed at the value given by Agilent, which is 0.1 Ω [6]. As well, all intrinsic capacitances were set fixed at Agilent specification values. These restrictions allowed the optimization procedure to converge upon the following solution for the ATF-34143 equivalent circuit:

$$C_{in} = 0.004 \text{ pF}$$

$$C_{out} = 0.01 \text{ pF}$$

$$L_g = 1.26 \text{ nH}$$

$$R_g = 1.99 \text{ } \Omega$$

$$L_d = 0.56 \text{ nH}$$

$$R_d = 0.1 \text{ } \Omega$$

$$L_s = 0.21 \text{ nH}$$

$$R_s = 0.44 \text{ } \Omega$$

$$C_{gs} = 0.80 \text{ pF}$$

$$R_{gs} = 0.90 \text{ } \Omega$$

$$C_{ds} = 0.04 \text{ pF}$$

$$R_{ds} = 77.9 \text{ } \Omega$$

$$C_{gd} = 0.16 \text{ pF}$$

$$g_m = 0.106 \text{ siemens}$$

$$\tau = 22.4 \text{ picoseconds}$$

Figure 4.13 provides a flowchart detailing the circuit optimization process. Twenty-six frequency points from 0.5 GHz to 10 GHz were used to obtain good agreement between measured S-parameters and simulated S-parameters,

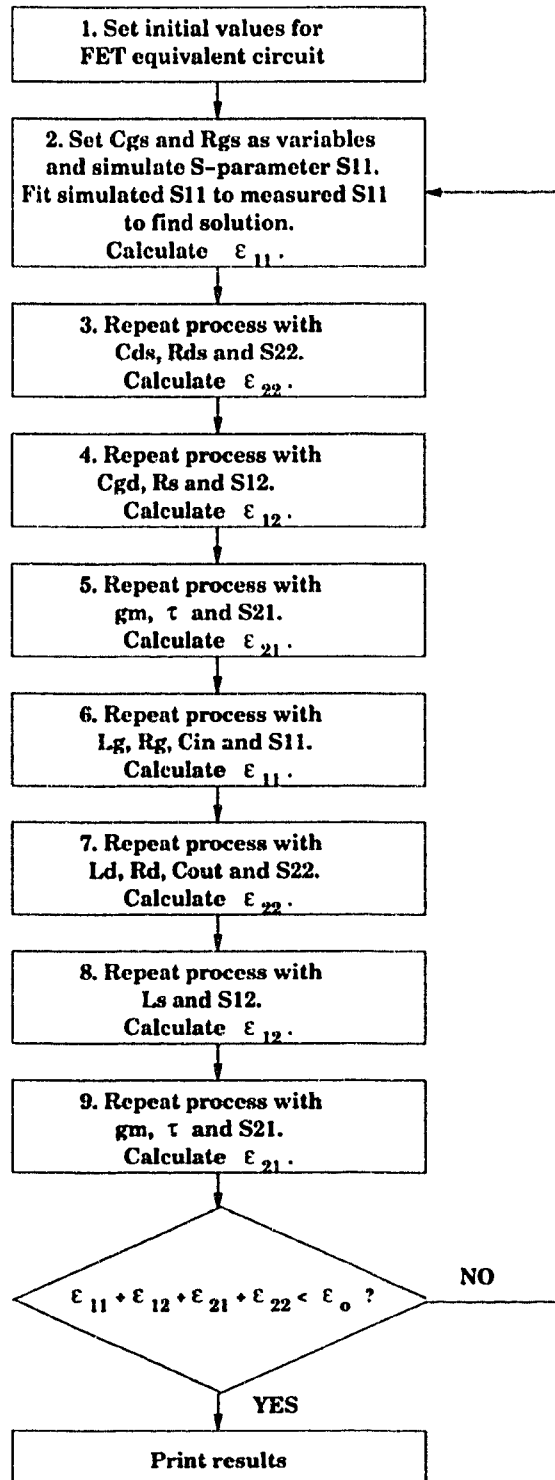


Figure 4.13: FET equivalent circuit optimization flowchart. ϵ_o is the desired value of the sum of all the error functions.

as shown in Figures 4.14 and 4.15. The S_{11} , S_{12} and S_{21} error functions were minimized to the order of 0.01 while the S_{22} error function was minimized to the order of 0.1, as shown in Table 4.2.

S-parameter	Value of ϵ After Iterations
S_{11}	$\epsilon = 0.011$
S_{12}	$\epsilon = 0.014$
S_{21}	$\epsilon = 0.021$
S_{22}	$\epsilon = 0.058$

Table 4.2: Discrepancy between measured and simulated S-parameters.

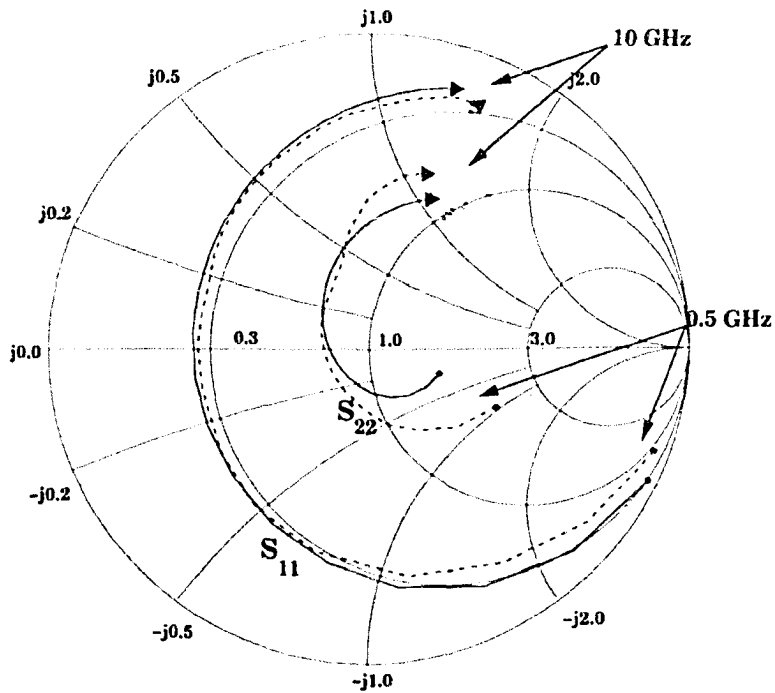


Figure 4.14: Smith Chart displaying measured reflection S-parameters (S_{11} and S_{22}) of ATF-34143 and simulated FET equivalent circuit reflection S-parameters from 0.5 GHz to 10 GHz. Measured values are shown by dotted lines and simulated values are shown by solid lines.

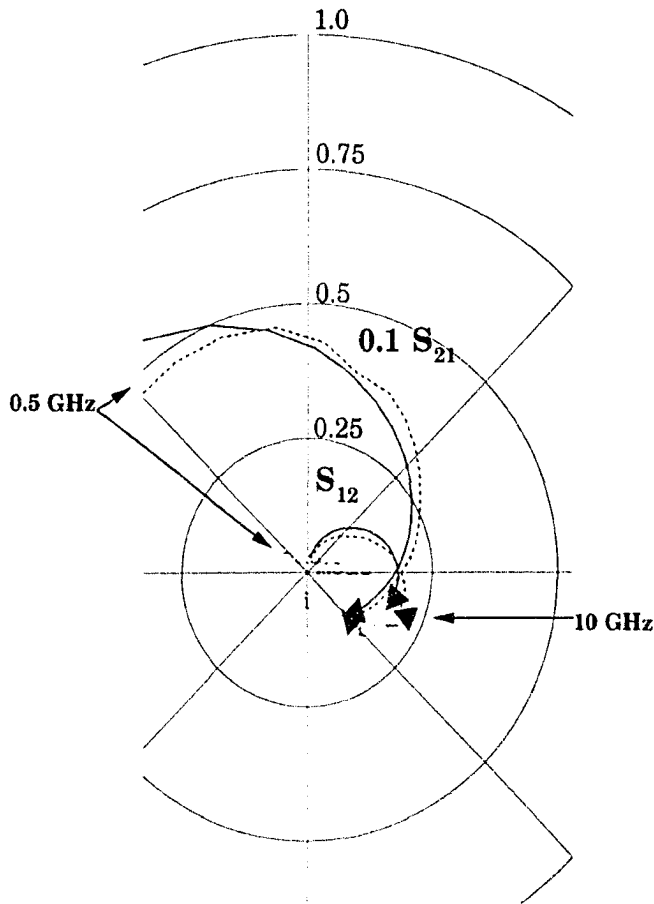


Figure 4.15: Polar plot displaying measured transmission S-parameters (S_{12} and S_{21}) of ATF-34143 and simulated FET equivalent circuit transmission S-parameters from 0.5 GHz to 10 GHz. Measured values are shown by dotted lines and simulated values are shown by solid lines. It should be noted that the S_{21} data values have been reduced to 10% in order to keep S_{12} data visible.

4.8 Obtaining Noise Parameters from the FET Equivalent Circuit

Recall Pospieszalski's equations for determining FET noise parameters from the FET equivalent circuit in Section 4.4. Aside from a FET equivalent circuit model, the equivalent noise temperatures of the intrinsic drain and gate resistances R_{ds} and R_{gs} are needed. Fortunately, Gupta *et al.* [13] showed

that equivalent gate temperature T_g can be set to the ambient temperature. In this case, we are working at room temperatures so $T_g \sim 300$ K. To estimate the drain equivalent temperature T_d , Pospieszalski's method requires one noise measurement at one frequency point.

4.8.1 Estimation of T_d

Although Pospieszalski's method requires only one noise measurement at one frequency point, many points were used for a better estimation of T_d . The Agilent N8973A noise figure meter has an upper frequency limit of 3 GHz, so a noise measurement $T_{measured}$ consisting of 100 frequency points from 0.5 GHz to 3 GHz was used (see Figure 4.16). The noise measurement setup involved placing a bias tee at the input and output of the ATF-34143 pHEMT mounted on a microstrip fixture so that the pHEMT could be biased at 3 V and 20 mA during measurement. To remove the effects of the bias tees and fixture, bias tee and fixture S_{21} parameters from 0.5 GHz to 3 GHz were entered into loss tables stored in the noise figure meter. During measurement, the N8973A noise meter automatically calibrates out the effects caused by lossy objects placed at the input and output of the device under test (DUT) by using the data stored in its loss tables.

Upon obtaining a noise measurement of the ATF-34143, known circuit element values were substituted into Equations 4.9 to 4.12 as well as setting $T_g = 300$ K, leaving T_d as the lone variable. Noise parameters obtained from Equations 4.9 to 4.12 were then substituted into the equation for determining noise temperature T (Equation 4.7 with $Z_g = R_g = 50 \Omega$). This represents the simulated noise temperature $T_{simulated}$ of the transistor. Again, the least squares method was used to determine the discrepancy between measured and simulated results:

$$\varepsilon = \sum_{k=1}^K \frac{1}{K} \left| \frac{T_{(measured)k} - T_{(simulated)k}}{T_{(measured)k}} \right|^2 \quad (4.15)$$

By using *Mathematica's FindMinimum* function, T_d was calculated to be 927 K, with ε being equivalent to 0.04. Although the noise measurement was repeatable with more than one transistor (displaying consistency in transistor performance), it should be noted that at lower frequencies (< 1 GHz), higher noise than expected was present. A possible cause of this is $1/f$ noise, which occurs at low frequencies.

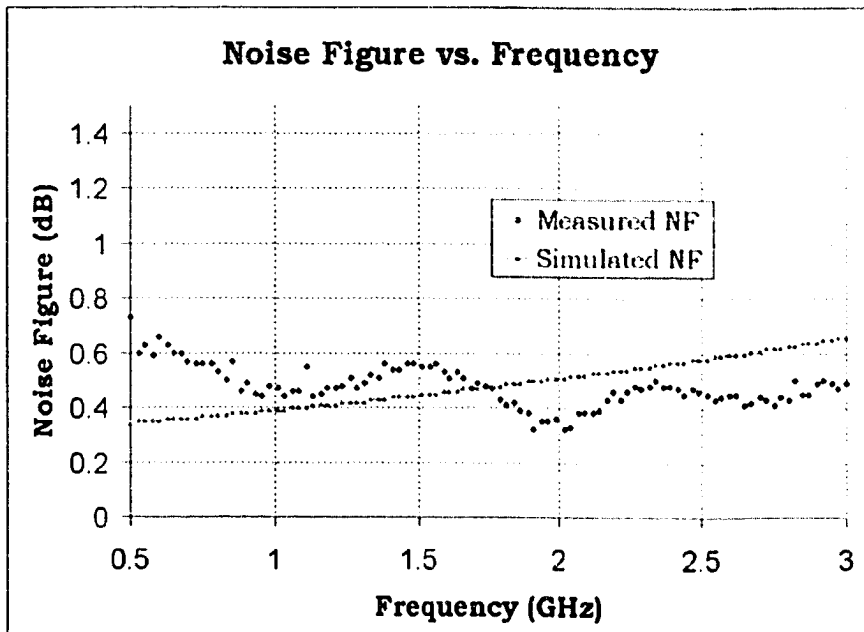


Figure 4.16: Measured and simulated noise figure from 0.5 GHz to 3 GHz used to estimate equivalent drain temperature T_d .

4.8.2 Intrinsic Noise Parameter Calculation

Using the FET equivalent circuit and calculated equivalent drain temperature T_d , Pospieszalski's equations (Equations 4.9 to 4.12) were used to calculate the noise parameters of the intrinsic FET:

$$T_{min} = 7.5\text{K or } NF_{min} = 0.11\text{dB}$$

$$Z_{opt} = 157\angle 65^\circ \text{ or } \Gamma_{opt} = 0.77\angle 32^\circ$$

$$R_n = 4.6\Omega$$

4.8.3 Total FET Equivalent Circuit Noise Parameter Calculation

Recall that Pospieszalski's model does not include extrinsic circuit elements. To account for extrinsics, *nodal* was used to simulate noise parameters of the total FET equivalent circuit model. *Nodal* has a noise model incorporated into its *MESFET* circuit element function, which can be altered to fit Pospieszalski's noise model. *Nodal*'s *MESFET* circuit element is modelled as shown in Figure 4.17.

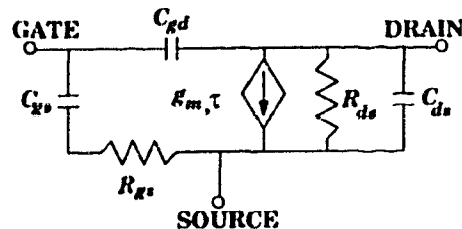


Figure 4.17: Nodal's MESFET model.

By default, the *MESFET* function uses the Pucel noise model, which has three frequency-independent noise coefficients P , R and C [40]. Also, R_{gs} has a temperature that can be set while R_{ds} does not. To alter the *MESFET* function's noise model so that it coincides with Pospieszalski's, all Pucel noise

parameters P , R and C were set to zero and R_{gs} was set at equivalent gate temperature T_g . To eliminate R_{ds} , it was set as an open circuit and an external resistor was added to represent the new R_{ds} whose temperature was set to the equivalent drain temperature T_d . Extrinsic parameters such as C_{in} , C_{out} , L_g , L_d , L_s , R_g , R_d and R_s were also added externally to complete the total FET equivalent circuit.

Using *nodal's NoiseParameters* function, the noise parameters of the total FET equivalent circuit were calculated:

$$T_{min} = 16\text{K or } NF_{min} = 0.23\text{dB}$$

$$Z_{opt} = 153\angle 47^\circ \text{ or } \Gamma_{opt} = 0.65\angle 28^\circ$$

$$R_n = 6.1\Omega$$

The effect of including extrinsics in the noise model is significant: T_{min} and R_n increase while the phase and magnitude of Z_{opt} are altered. Agilent specifications offer measured noise parameters from 2 GHz to 10 GHz. Noise parameters below 2 GHz are a result of extrapolation by Agilent. For present purposes, the most relevant set of noise parameters are the ones extrapolated to 1.5 GHz. A comparison between Agilent specifications, Pospieszalski's model and the *nodal* calculation noise parameters is displayed in Table 4.3.

Noise Parameter	Pospieszalski (1.42 GHz)	<i>nodal</i> (1.42 GHz)	Agilent (1.5 GHz)
NF_{min} (dB)	0.11	0.23	0.14
$ \Gamma_{opt} $	0.77	0.65	0.77
$\angle\Gamma_{opt}$	32°	28°	48°
$r_n = \frac{R_n}{50}$	0.09	0.12	0.11

Table 4.3: Comparison between specified and calculated noise parameters.

When plotted on the Smith Chart, Γ_{opt} values appear relatively close, displaying a consistency between the models and extrapolation:

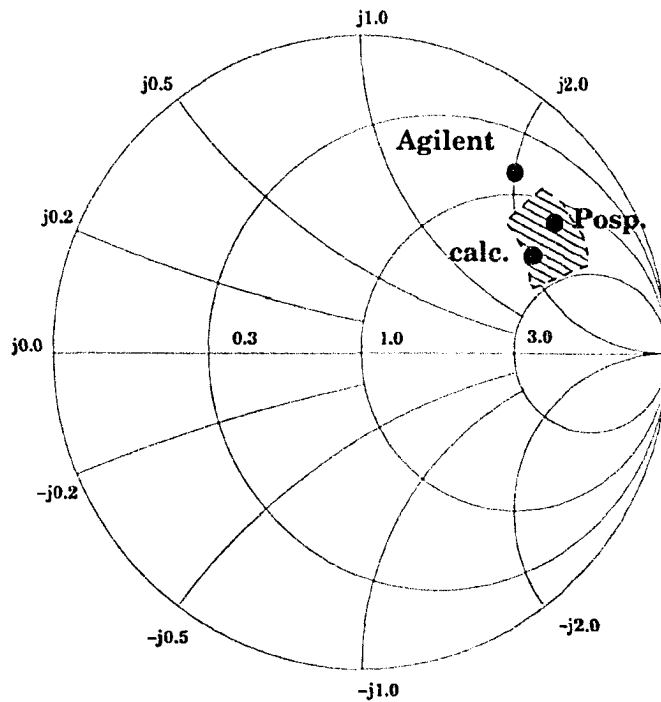


Figure 4.18: Calculated and specified Γ_{opt} values displayed on the Smith Chart. The shaded area represents the estimated accuracy of Γ_{opt} .

The Agilent specification sheet also gives an extrapolated value of $\Gamma_{opt} = 0.84\angle 31^\circ$ at 1 GHz, which can be used as a upper limit for the magnitude of Γ_{opt} . At frequencies below 9 GHz, the magnitude of Γ_{opt} decreases as frequency increases [6]. Taking the *nodal* calculated optimum reflection coefficient at 1.42

GHz and Agilent extrapolated values at 1 GHz and 1.5 GHz into account, an estimate of the optimum reflection coefficient at 1.42 GHz can be given with the following accuracy: $\Gamma_{opt} = (0.7 \pm 0.1)\angle(30^\circ \pm 10^\circ)$. According to Table 4.3, the accuracy of the normalized equivalent noise resistance can be given as $r_n = 0.1 \pm 0.05$. There is significant discrepancy between the *nodal* calculated minimum noise figure and the Pospieszalski calculated minimum noise figure due to the added noise from the extrinsics in the total FET equivalent model used in *nodal*. Judging from the *nodal* simulation, the minimum noise figure NF_{min} can be estimated to be in the 0.2 dB range, but it will be shown later in Chapter 5 that circuit losses add at least a few tenths of a dB to noise figure, and that the achievable NF_{min} is actually more on the order of 0.4 dB.

Chapter 5

Design of Low Noise Amplifiers (LNAs) With Coaxial Connectors and Probe LNAs for the Synthesis Telescope

This chapter consists of three main sections. The first covers concepts in LNA design which provide necessary background for discussing the two types of amplifiers built for this project. The two types of amplifiers are the LNA with coaxial connectors and the probe LNA, which has a waveguide probe directly integrated with the LNA circuit. The second section discusses LNA design with the Agilent ATF-34143 pHEMT and the last section discusses integrating the waveguide probe with the ATF-34143 — the Mark 1 probe LNA design.

Section 5.1 covers criteria that one must consider when designing an LNA. Aside from low noise figure, properties such as stability, gain and input return loss are also very important. Designing for low input return loss applies to the design of an LNA with coaxial connectors, which requires transforming

the standard 50Ω characteristic impedance of coaxial transmission line to a transistor's optimum impedance, Z_{opt} , for lowest noise. The input return loss of the probe LNA design cannot be directly measured because the input of the LNA circuit is integrated with a waveguide probe.

Although the initial goal of this project was to improve upon the design of the Mark 1 probe LNA, it was decided that an LNA with coaxial connectors should be designed and built as an intermediate step, as will be discussed in Section 5.2. Since the Synthesis radio telescope is already configured for LNAs with coaxial connectors, installation into the waveguide feeds for testing would be easier. As well, a design with coaxial connectors makes measurement and testing simple and straightforward. Characteristics of the probe LNA such as its noise figure are more challenging to measure because the waveguide probe at the input prevents direct connection to the LNA input with test instruments. Furthermore, installing probe LNAs into the waveguide feeds of the Synthesis telescope would require more effort than installing LNAs with coaxial connectors. For instance, removal of the original waveguide-to-coaxial transitions of the Synthesis Telescope feed antennas would be necessary to install probe LNAs. Thus work on the Mark 1 was reserved for the final stage of this project and is discussed in Section 5.3.

5.1 LNA Design Concepts

5.1.1 Impedance Matching for Lowest Noise

Two of the most important noise parameters of a transistor are the real and imaginary parts of the optimum impedance Z_{opt} , which is the impedance presented to the input of the transistor which is required to obtain its lowest noise performance. When designing an LNA with coaxial connectors, the most im-

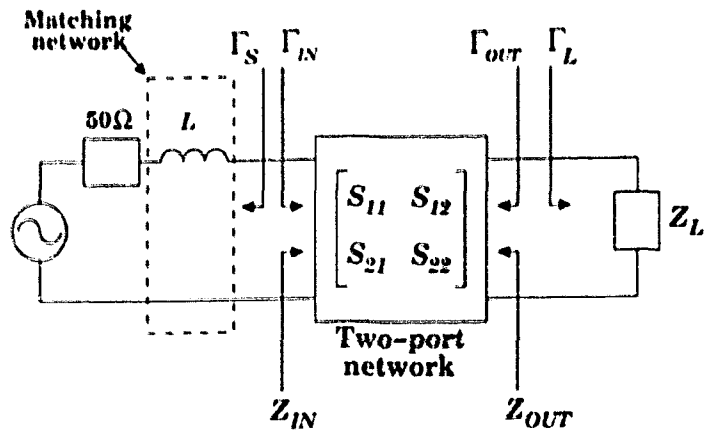
portant impedance matching consists of transforming the $50\ \Omega$ coaxial cable input to Z_{opt} by building a matching network. In an ideal world, the matching network is lossless (i.e. non-resistive) and constructed with ideal capacitors, inductors, or transmission lines. To add resistances would introduce additional noise. In the real world, inductors, capacitors and even the circuit board itself introduce small parasitic losses and add to the noise figure of the LNA. Therefore it is very important that the lowest loss components are selected. Also, parasitics are not only composed of resistances but of small inductances and capacitances as well. While insignificant at lower frequencies, these parasitics need to be accounted for as frequency increases. It must be ensured that the LNA frequency of operation is within the frequency range that the components are specifically designed for.

The mapping of resistances, reactances, admittances and susceptances on the Smith Chart has been discussed in Section 2.2.2. To create a matching network, a given input impedance is transformed into a desired output impedance by the use of circuit components. When added in series (parallel), resistors increase resistance (conductance), inductors add positive reactance (negative susceptance), and capacitors add negative reactance (positive susceptance). Adding a length of transmission line causes movement along a circle centered on the point on the Smith Chart corresponding to the transmission line's characteristic impedance.

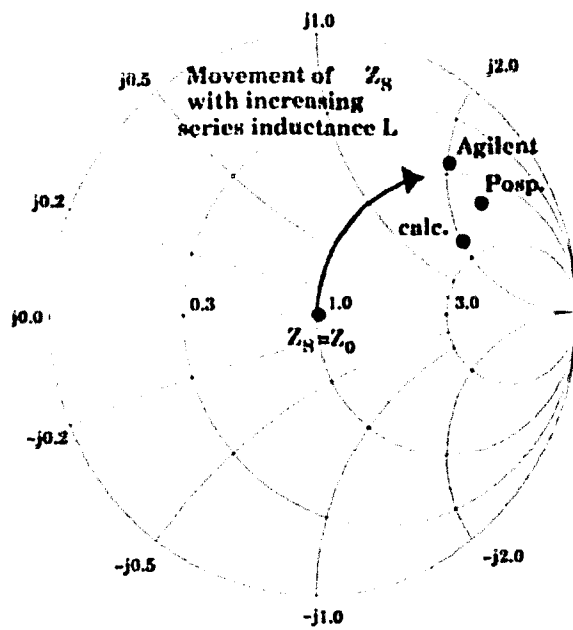
A matching network can be as simple as a series inductor that translates the impedance seen by the transistor from the center of the Smith Chart ($50\ \Omega$) along a constant resistance curve, making it closer to Z_{opt} as shown in Figure 5.1. However, one must consider the DC biasing of the transistor, where DC voltages are applied to the gate and drain to keep the transistor in the desired state of operation. For instance, to direct the DC voltage specifically to the

gate, a blocking capacitor at the input of the LNA is needed to keep the DC signal from leaking into the generator. A blocking capacitor acts as an open circuit at low frequencies and as a short circuit at high frequencies. To keep the RF signal from leaking into the biasing circuit, an RF choke is used (refer to Section 5.1.5 for further discussion on the biasing circuit used in this project). An RF choke is an inductance that acts as an open circuit at high frequencies and as a short circuit at low frequencies. For instance, the initial configuration at the input of the LNA design was composed of a 0.7 pF DC block, a 56 nH RF choke and a 35.5 nH series inductor. Refer to Figure 5.2 for the schematic of the initial input matching network design and its visual interpretation on the Smith Chart. To provide further isolation between the LNA circuit and the biasing circuit, RF bypass capacitors were added. An RF bypass capacitor acts like a short circuit at high frequencies. As well, a 50 Ω resistor was added after the RF choke to improve stability at lower frequencies. The stabilizing resistor forces Z_S to be closer to the center of the Smith Chart at lower frequencies.

The initial configuration of the input matching network design appears sufficient in getting Z_S closer to Z_{opt} . As will be discussed later in Section 5.2.4, however, the input matching network needs to be modelled more thoroughly during the design process. Not only do the values of inductors, capacitances and resistances need to be considered, but so do the widths and lengths of conducting traces of microstrip between the components. As well, the number of tuning elements can greatly complicate the building and testing of a working LNA. When dealing with fine-tuning the LNA in order to achieve lowest noise, it helps to rely on fewer tuning elements in the input matching network. A better matching network would be one composed of a large DC block and large RF choke. This way, there is good isolation between the LNA circuit

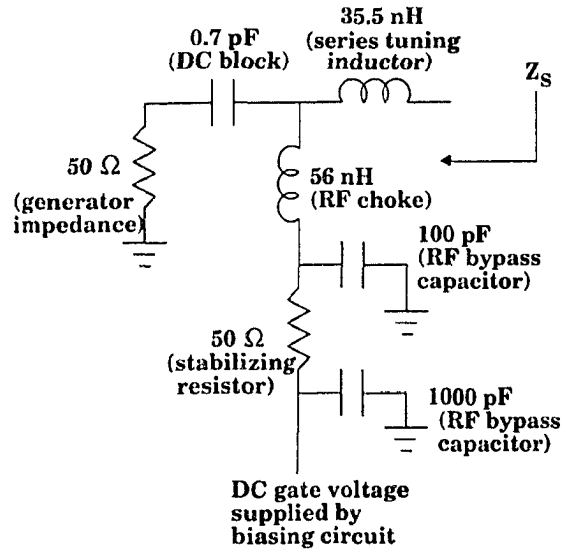


(a)

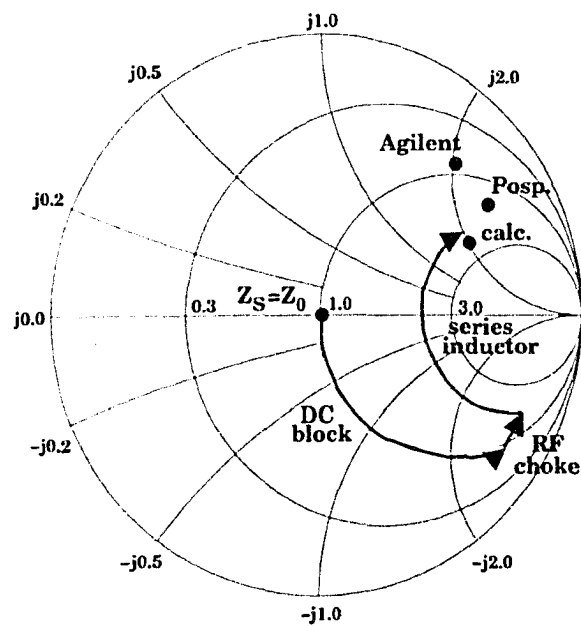


(b)

Figure 5.1: a) A matching network consisting of series inductor L . b) Movement of Z_S on Smith Chart with increasing L . Γ_{opt} values shown are from Table 4.3.



(a)



(b)

Figure 5.2: a) Initial configuration of the input matching network design for the LNA with coaxial connectors. b) Smith Chart interpretation of the input matching network design. The value of Z_0 for which the Smith Chart is drawn is 50 Ω .

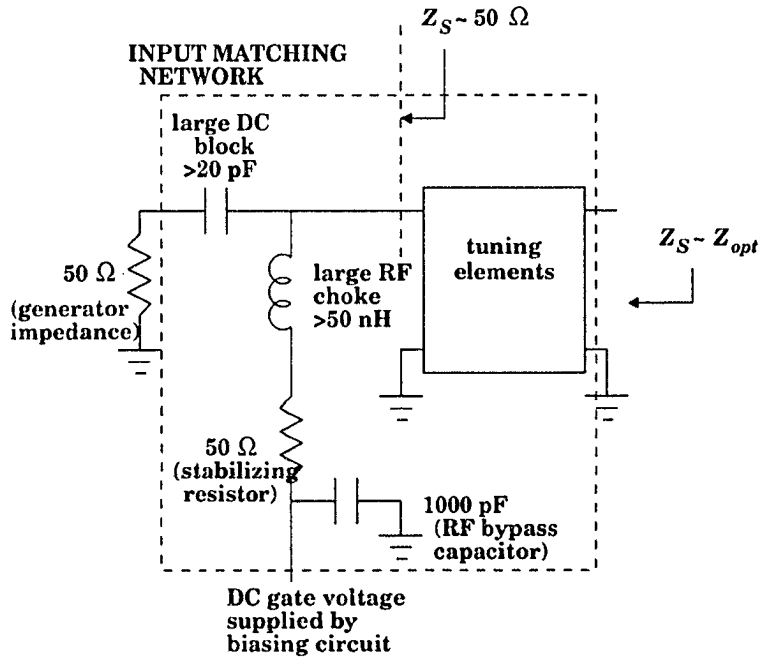


Figure 5.3: A better input matching network.

and the biasing circuit and Z_S remains close to the center of the Smith Chart until tuning elements are added. As well, restricting the number of bypass capacitors to just a single large capacitance placed before the biasing circuit greatly improves stability (refer to Section 5.2.3). Figure 5.3 summarizes a more practical and straightforward input matching network.

5.1.2 Stability

Aside from low noise figure and high gain, an LNA must be stable. When an amplifier is unconditionally stable, no oscillations will occur no matter what source and load reflection coefficients Γ_S and Γ_L are presented. Input and output reflection coefficients Γ_{IN} and Γ_{OUT} respectively depend on load and source reflection coefficients Γ_L and Γ_S as follows [7]:

$$\Gamma_{IN} = S_{11} + \frac{S_{12}S_{21}\Gamma_L}{1 - S_{22}\Gamma_L} \quad (5.1)$$

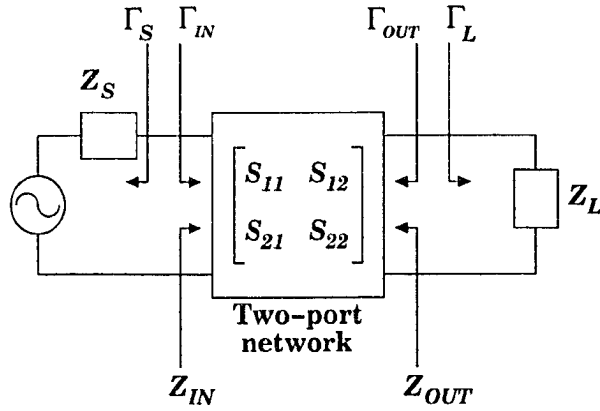


Figure 5.4: Two port network and associated reflection coefficients.

$$\Gamma_{OUT} = S_{22} + \frac{S_{12}S_{21}\Gamma_S}{1 - S_{11}\Gamma_S}. \quad (5.2)$$

where all reflection coefficients are as shown in Figure 5.4.

Oscillation occurs when there is positive feedback at the input or output of the amplifier, which is also represented as an input or output reflection coefficient with a magnitude greater than one ($|\Gamma_{IN}| > 1$ or $|\Gamma_{OUT}| > 1$).

A check for unconditional stability can be made when the S-parameters of an amplifier are known. Stability factor k is defined as the following [7]:

$$k = \frac{1 + |\Delta|^2 - |S_{11}|^2 - |S_{22}|^2}{2|S_{12}||S_{21}|} \quad (5.3)$$

where

$$\Delta = S_{11}S_{22} - S_{12}S_{21}. \quad (5.4)$$

For unconditional stability,

$$k > 1.$$

and

$$|\Delta| < 1$$

At 1.42 GHz, the ATF-34143 has the following measured S-parameters (refer to Chapter 3 for further detail about the technique used in S-parameter measurement):

$$S_{11} = 0.77\angle -67^\circ$$

$$S_{12} = 0.08\angle 52^\circ$$

$$S_{21} = 4.7\angle 118^\circ$$

$$S_{22} = 0.27\angle -64^\circ$$

Substituting the above S-parameters into Equations 5.3 and 5.4 results in a stability factor k of 0.48 and $|\Delta| = 0.32$, which means the ATF-34143 is not unconditionally stable and that there are possible values of Γ_S and/or Γ_L that will cause $|\Gamma_{OUT}|$ and/or $|\Gamma_{IN}|$ to be greater than 1. These values can be determined by investigating the areas of stability on the Smith Chart in the Γ_S -plane and Γ_L -plane.

Areas of stability on the Smith Chart can be determined with stability circles, circles where values of Γ_S and Γ_L respectively cause $|\Gamma_{OUT}|$ and $|\Gamma_{IN}|$ to be equal to 1. The Smith Chart itself encompasses an area in the Γ -plane where $|\Gamma| \leq 1$. Since the transistor is not unconditionally stable, there will be areas on the Smith Chart that overlap with areas of the stability circle in the Γ_S -plane and/or Γ_L -plane. If $|S_{11}| < 1$ and $|S_{22}| < 1$, the stable regions are the regions that contain $\Gamma_S = 0$ and $\Gamma_L = 0$ (the centers of each Smith Chart) and are bounded by the Smith Chart boundary and stability circle. The following

are the equations for the radius r_L and center C_L of the output stability circle where values of Γ_L cause $|\Gamma_{LN}|$ to be equal to 1 [7].

$$r_L = \left| \frac{S_{12}S_{21}}{|S_{22}|^2 - |\Delta|^2} \right|$$

$$C_L = \frac{(S_{22} - \Delta S_{11}^*)^*}{|S_{22}|^2 - |\Delta|^2}.$$

Similarly for the Γ_S -plane, the radius r_S and center C_S of the input stability circle are defined as follows [7]:

$$r_S = \left| \frac{S_{12}S_{21}}{|S_{11}|^2 - |\Delta|^2} \right|$$

$$C_S = \frac{(S_{11} - \Delta S_{22}^*)^*}{|S_{11}|^2 - |\Delta|^2}.$$

Figure 5.5 demonstrates how the overlap of the stability circles with the Smith Chart indicates unstable regions of the Smith Chart if both $|S_{11}|$ and $|S_{22}|$ are less than 1. When an amplifier is unconditionally stable, the stability circles lie completely outside the Smith Chart area.

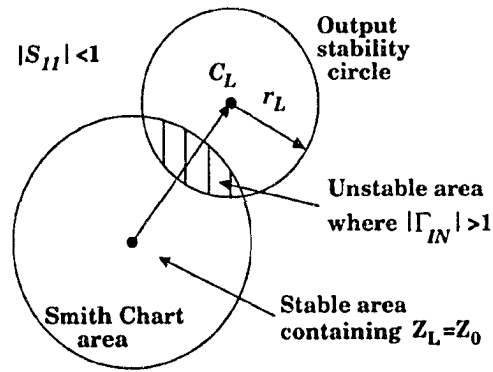
Using the S-parameters of the ATF-34143 at 1.42 GHz, its stability circles can be calculated and mapped out (see Figure 5.6) with radii and centers

$$r_L = 12.06$$

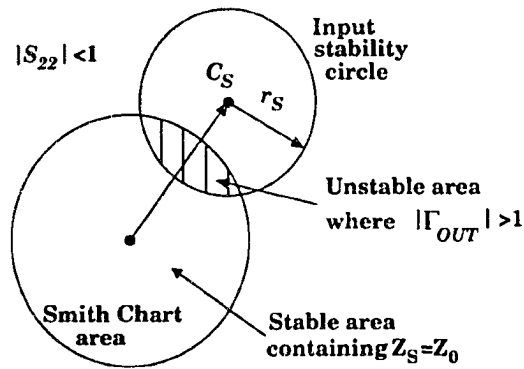
$$C_L = 11.5\angle -72.2^\circ$$

$$r_S = 0.77$$

$$C_S = 1.58\angle 73.5^\circ.$$

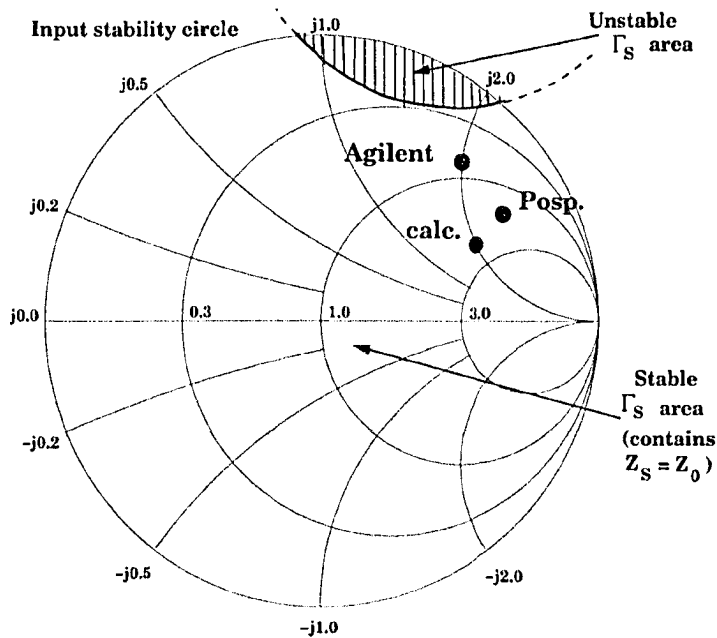


(a)

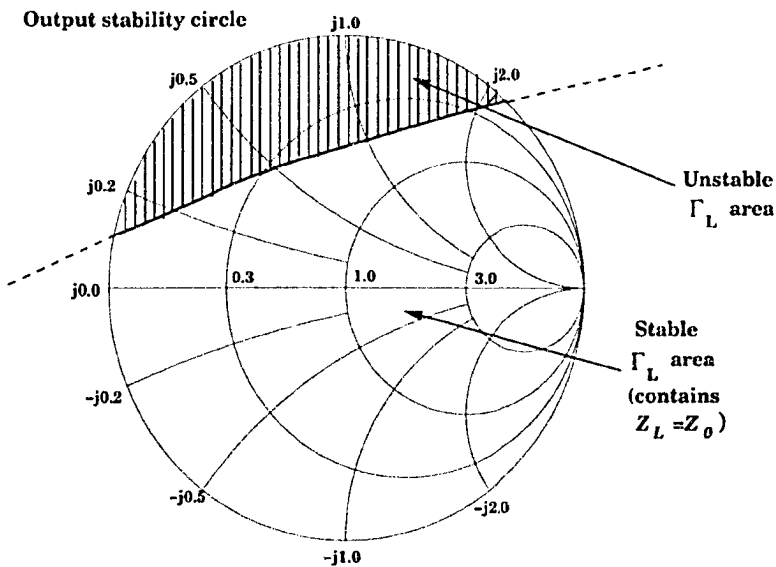


(b)

Figure 5.5: Stability circles and unstable regions in the Smith Chart. a) The output stability circle in the Γ_L -plane. b) The input stability circle in the Γ_S -plane.



(a)



(b)

Figure 5.6: Stability circles of the ATF-34143 at 1.42 GHz. a) The input stability circle. The values for Γ_{opt} are taken from Table 4.3. b) The output stability circle.

The area where values of Γ_S cause transistor noise to be lowest (calculated Γ_{opt} values) is stable and therefore designing an LNA for lowest noise is viable.

Additional measures to improve stability can be taken. Adding resistance to the drain of a transistor as well as a small shunt capacitance can provide stability at higher frequencies [42]. Extra inductance added in the source leads of a transistor also improves stability while improving input return loss (see Section 5.1.4).

5.1.3 Gain

As mentioned in Section 1.9, gain of at least 30 dB or greater is required for a Synthesis Telescope front-end LNA so that the noise of the subsequent stages will be sufficiently reduced by the gain of the first stage. Because the ATF-34143 is a potentially unstable transistor, the value for maximum stable gain should be used as a figure of merit. Maximum stable gain depends on the forward and reverse transmission S-parameters [7]:

$$G_{MSG} = \frac{|S_{21}|}{|S_{12}|}.$$

In the case of the ATF-34143, the maximum stable gain at 1.42 GHz is 17.7 dB. Therefore, an LNA requires at least two transistor stages for sufficient gain as a Synthesis Telescope front-end.

5.1.4 Input Return Loss

Input return loss indicates the mismatch between the input impedance of an amplifier and the characteristic impedance of the transmission line at its input by acting as a measure of the amount of power reflected back when an input signal is injected into the input of the amplifier through the transmission line.

The input return loss value can be expressed in terms of the measured S-parameter S_{11} :

$$\text{Input Return Loss} = -S_{11}(\text{dB}) = -20 \log |S_{11}|.$$

Similarly, output return loss is represented by S-parameter S_{22} :

$$\text{Output Return Loss} = -S_{22}(\text{dB}) = -20 \log |S_{22}|.$$

Input return loss is of more concern than output return loss, however, because too big a mismatch at the input of the LNA can lead to degradation in noise performance. During the course of this project, commercial amplifiers were purchased and measured with the N8973A noise meter to have excellent noise temperatures of under 20 K (< 0.3 dB). However, once the commercial amplifiers were installed on one of the Synthesis Telescope dishes for testing, system noise temperatures were considerably higher than anticipated, and some amplifiers were unstable when connected to the waveguide feed. These problems may be attributed to the extremely poor input return losses of the amplifiers: measured input return loss for the commercial amplifiers averaged only 0.5 dB, which is equivalent to 89% of the input power being reflected back from the input of the LNA.

When there is absolutely no mismatch between the input of the LNA and the transmission line, no reflections occur and the input return loss is infinite. Maximum power transfer from the source to the input of the LNA is achieved. In actuality there will always be some loss – even input return losses on the order of 5 dB (about 70% of the input power is absorbed by the input of the LNA) are acceptable. As previously mentioned in Section 4.1, maximum power transfer occurs when the impedance of the power source and the impedance of

the load are conjugates of each other. In general, the source impedance is equal to the standard value for coaxial transmission line characteristic impedance: 50Ω . Therefore maximizing transmission of signal from the source to the LNA input requires building an input matching network that transforms 50Ω to the conjugate of the input impedance of the transistor, Z_{in}^* . One cannot design for maximum power transfer and lowest noise simultaneously because generally $Z_{opt} \neq Z_{in}^*$ and designing for lowest noise involves building an input matching network that transforms the source impedance of 50Ω to $Z_S = Z_{opt}$ instead of $Z_S = Z_{in}^*$.

A way to improve the input return loss of an LNA while maintaining good noise performance consists of adding extra series inductance at the source terminal of the transistor. Inductance L_s at the source terminal provides feedback to the input impedance of the transistor by adding $\frac{g_m L_s}{C_{gs}}$ to the real part of the intrinsic circuit's Z_{in} and adding $(\omega L_s - \frac{1}{\omega C_{gs}})$ to the imaginary part of Z_{in} without changing Z_{opt} significantly [8]. On the Smith Chart, $Z_S = Z_{in}^*$ moves closer to $Z_S = Z_{opt}$ with increasing source inductance. Figure 5.7 demonstrates the effect of increasing source inductance on the input impedance of the NEC 34108 FET.

There is a limit to the amount of source inductance that can be added. Excessive source inductance can lead to LNA oscillations because of gain peaks at higher frequencies. For the ATF-34143, source inductances on the order of a few tenths of a nH to a few nH are sufficient [32].

5.1.5 DC Biasing

For this project, the S-parameters and resulting transistor noise model were obtained for the ATF-34143 biased with a drain voltage of 3 V and a drain current of 20 mA (recommended by Agilent [6]). In order to maintain these

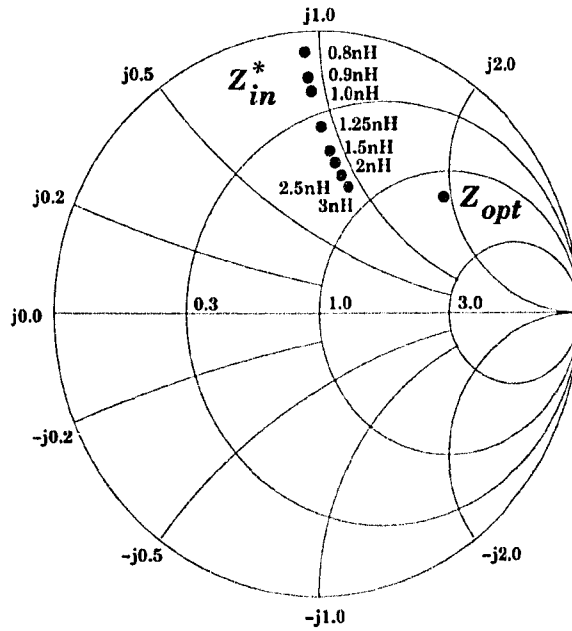


Figure 5.7: The dependency of Z_{in}^* on increasing values of source inductance L_s for the NEC 34018 FET [8].

biasing conditions during LNA operation, a biasing circuit was selected based on the design used in GaAs FET LNAs designed by Al Ward with modification instructions provided by Paul Wade [43]. The design is an active biasing circuit that sets the gate voltage at a value required to maintain the desired transistor drain voltage and current for each stage of the LNA. This is accomplished using the 2N2907 transistor as a feedback amplifier. Refer to Figure 5.8 for the active biasing circuit schematic.

Resistor R_4 sets the desired drain current while resistors R_5 and R_6 set the desired drain voltage. To calculate values for the resistors ($R_4= 40.2 \Omega$, $R_5= 412 \Omega$ and $R_6= 1000 \Omega$), the following equations are used [43].

$$R_5 = \frac{R_6(5 \text{ V})}{V_{drain} - (0.65 \text{ V})} - R_6$$

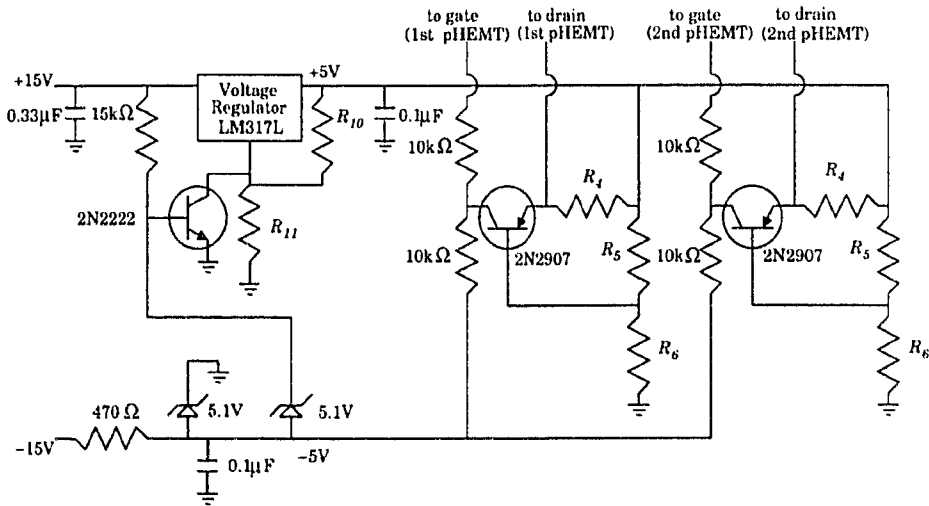


Figure 5.8: Biasing circuit schematic [43].

$$R_1 = \frac{(5 \text{ V}) - V_{\text{drain}}}{I_{\text{drain}}}$$

A National Semiconductor LM317L voltage regulator is used to convert the positive power supply voltage of 15 V to 5 V. When the LM317L is configured as shown in Figure 5.8, Equation 5.5 can be used to calculate values for R_{10} and R_{11} ($R_{10} = 221 \Omega$ and $R_{11} = 665 \Omega$) [44]:

$$V_{\text{output}} = 1.25 \left(1 + \frac{R_{11}}{R_{10}} \right) \quad (5.5)$$

The 2N2222 transistor connected to the voltage regulator is a safety shutdown feature of the biasing circuit. If negative voltage is lost, the 2N2222 transistor forces the voltage regulator to output its minimum value of 1.2 V, causing power dissipation in the LNA transistors to be low enough to prevent damage. The 2N2222 transistor detects loss of negative voltage through a 5.1 V Zener diode connected to its base.

Table 5.1 is a list of components used to construct the biasing circuit used for both the LNA design with coaxial connectors and the probe LNA design.

Component	Manufacturer	Model
Capacitors	AVX	X7R Dielectric (12065C)
Resistors	Panasonic	Precision Thick Film Resistors (0603)
2N2222 Transistors	Fairchild Semiconductor	MMBT2222A
2N2907 Transistors	Fairchild Semiconductor	MMBT2907A
Zener diodes	Diodes Inc.	SMAZ5V1
LM317 Voltage Regulators	National Semiconductor	LM317L (TO-92 package)
Circuit board	GIL Technologies	GML 1000

Table 5.1: List of components for the LNA biasing circuit.

The components were mounted on the same type of circuit board as the LNA — GIL Technologies GML 1000 high frequency laminate (refer to Section 5.2.5).

5.2 LNA Design With Coaxial Connectors

5.2.1 Initial LNA Configuration

To meet the 30 dB minimum gain requirement of a Synthesis Telescope front-end receiver, the LNA design with coaxial connectors consists of two stages of amplification using two ATF-34143 transistors. In the initial design, three matching networks were included to optimize the first stage for low noise and the second stage for a compromise between low noise and high gain. Located between the LNA input and the input of the first transistor, the input matching network transforms 50Ω to Z_{opt} as demonstrated in Figure 5.2. The resulting output impedance Z_{out1} of the first transistor, which is directly related to its output reflection coefficient Γ_{out1} , can be calculated with Equation 5.2.

Located between the output of the first transistor and the input of the second transistor, the interstage matching network presents the output impedance of the first transistor with its conjugate Z_{out1}^* in order to maximize power trans-

mission. The interstage matching network transforms Z_{out1} to an impedance Z_{opt} which is presented to the input of the second transistor for lower noise.

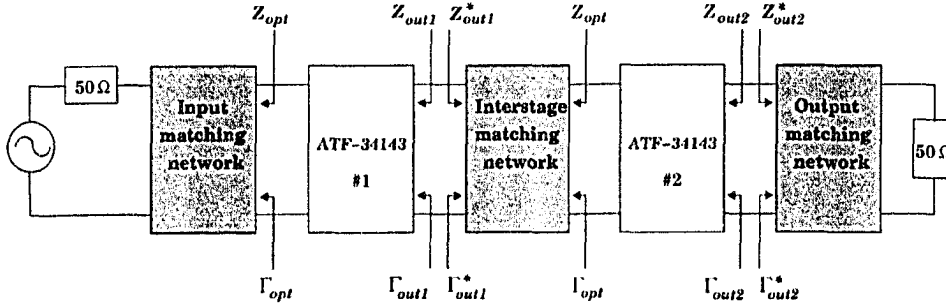


Figure 5.9: Matching networks for a two-stage LNA.

Finally, the output matching network transforms the output impedance of the second transistor Z_{out2} closer to the characteristic transmission line impedance 50Ω in order to minimize reflections when the output of the LNA is connected to a coaxial cable. A series resistance of 10Ω and a small shunt capacitance of 1 pF were added to the drain of the second transistor to improve stability at higher frequencies (see Section 5.1.2). Small lengths of inductive transmission line were added to the source leads to improve input return loss and stability (refer to Sections 5.1.2 and 5.1.4). The ATF-34143 is packaged so that there are two source leads. Specifically, approximately 1.6 nH of extra inductance was added to each lead. Each lead is grounded with a via that has an inductance of approximately 0.4 nH . The source leads are in parallel and the total source inductance of each transistor is approximately 1 nH . Transmission line inductances and via inductances were calculated with *nodal's Inductance* function.

Nodal was used to simulate the performance of the LNA and the resulting simulated noise figure was 0.3 dB (20 K). The 30 dB minimum gain requirement was satisfied, input and output return losses were on the order of 10 dB and the stability K factor was greater than 1 up to frequencies on the order of

10 GHz. However, when the LNA design was physically realized, the noise measurements were unsatisfactory, with noise figures on the order of 1 dB. There were also problems with oscillations. After much trial and error via replacement and shifting of components especially at the input of the first stage, a noise figure of 0.4 dB (30 K) was finally achieved.

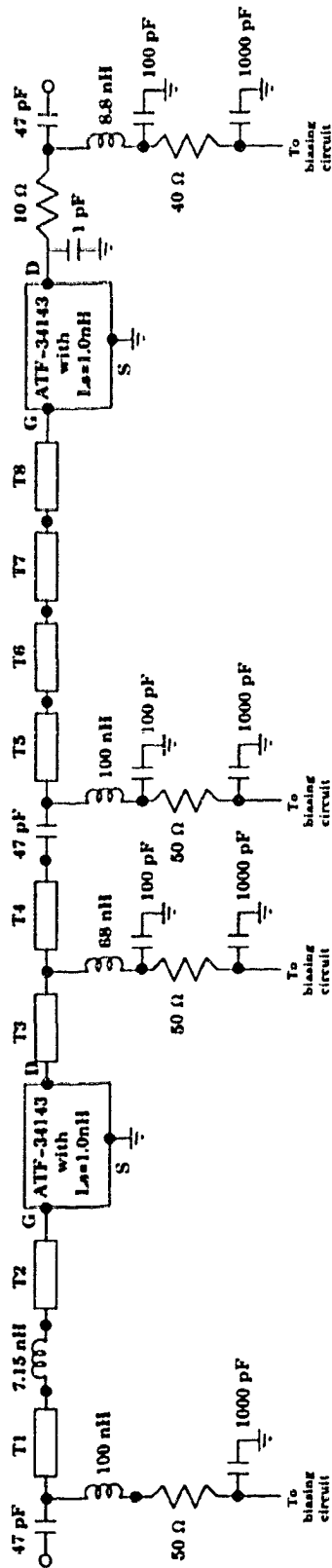
5.2.2 Final LNA Configuration

The final schematic of the LNA with coaxial connectors is shown in Figure 5.10. Note the pieces of transmission line in the schematic. During the process of fine-tuning the circuit in order to obtain low noise-figure, several components were removed from the circuit to simplify the circuit. After certain components were removed, all that remained were microstrip traces of their landing patterns. These microstrip traces are included in the final configuration schematic. In Figure 5.11, the impedance presented to the input of the first transistor by the input matching network is shown on the Smith Chart. The LNA circuit is shown in Figure 5.14.

During troubleshooting, the LNA circuit was reduced to only the components necessary for connection to the biasing circuit. These components included the DC blocks (located at the input, between the first stage and the second stage, and at the output), RF bypass capacitors and RF chokes. Further, the DC blocks and RF chokes were constrained to values that did not cause large shifts in impedance - in other words, they ceased to function as tuning elements. Finally, a series inductor was inserted at the input and its value varied until the lowest noise figure was achieved. A noise figure value of 0.4 dB was obtained with a series inductor of 7.15 nH. Other performance specifications of the coaxial LNA at 1.42 GHz are as follows:

- Gain: 30 dB

- Input return loss: 7 dB
- Output return loss: 10 dB



- T1 = microstrip line of width 0.050" and length 0.130"
- T2 = microstrip line of width 0.050" and length 0.130"
- T3 = microstrip line of width 0.025" and length 0.080"
- T4 = microstrip line of width 0.030" and length 0.045"
- T5 = microstrip line of width 0.025" and length 0.095"
- T6 = microstrip line of width 0.050" and length 0.150"
- T7 = microstrip line of width 0.050" and length 0.120"
- T8 = microstrip line of width 0.050" and length 0.130"

Figure 5.10: Schematic for the LNA with coaxial connectors.

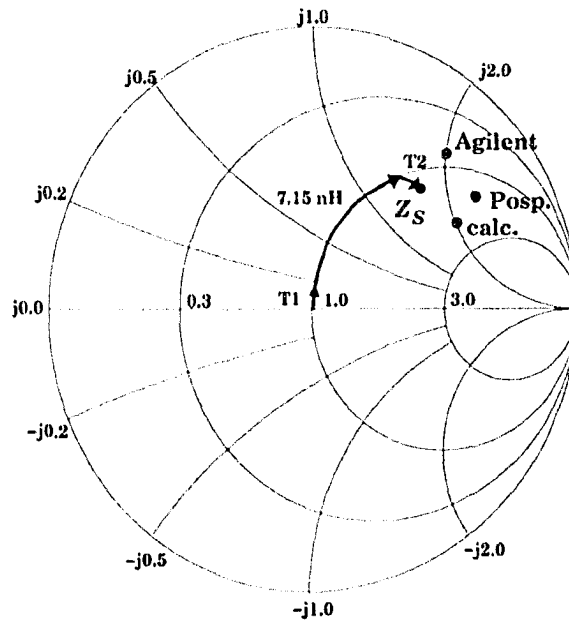


Figure 5.11: Impedance Z_S seen by the input of the first transistor in the LNA using the schematic in Figure 5.10. Using *nodal*, $Z_S = 63 + j83\Omega$. The other three values are Z_{opt} values taken from Table 4.3.

5.2.3 Dealing With Low Frequency Oscillations

Note that there is only one bypass capacitor in the input matching network unlike the initial configuration, where two bypass capacitors were used in the input matching network as shown in Figure 5.2. The initial configuration resulted in lower frequency oscillations (on the order of 100 MHz) that were eliminated with the removal of the 100 pF bypass capacitor in the input matching network. The removal of the 100 pF bypass capacitor allows the input of the transistor to see an impedance closer to the centre of the Smith Chart (50Ω) at lower frequencies, keeping the transistor stable (see Figure 5.12).

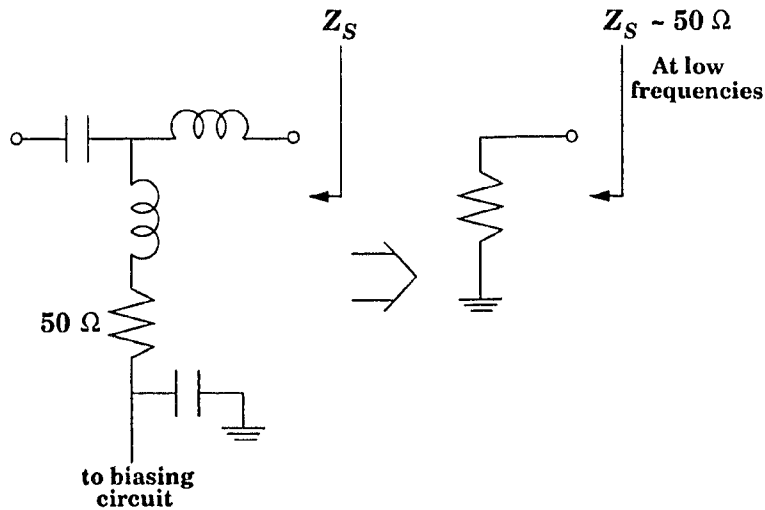
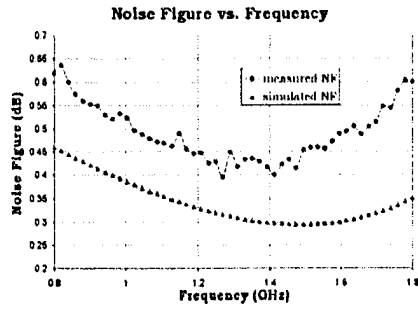


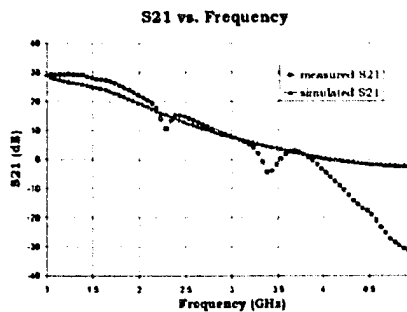
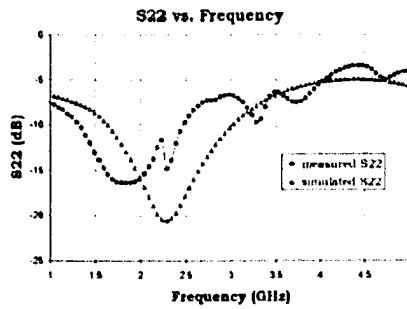
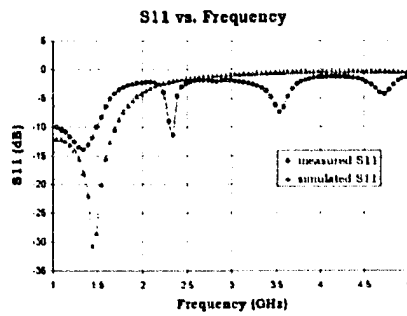
Figure 5.12: Input matching network with stabilizing resistor.

5.2.4 Better Circuit Simulation

Why didn't the initial configuration work despite the good simulation results for noise figure? The circuit model that was used in the initial simulation was too simple — especially at the input of the first transistor, on which LNA noise figure is most dependent. Extra traces of microstrip need to be included in the simulation schematic. The landing patterns that were used for the components were too large, although they are the landing patterns recommended in the component specification sheets. It was later discovered that the component models given on the specification sheets do not include landing pattern effects. It is up to the circuit designer to include these effects in circuit simulation. Figure 5.13 displays the simulated and measured results for the final LNA configuration. Although generally in good agreement, the simulated data is “smoother” and varies slightly from the measured data and this may be attributed to parasitics in the actual circuit that are not accounted for in the simulation circuit schematic.



(a)



(b)

Figure 5.13: a) Simulated and measured noise figure of the LNA with coaxial connectors. b) Simulated and measured input return loss of the LNA with coaxial connectors. c) Simulated and measured output return loss of the LNA with coaxial connectors. d) Simulated and measured gain of the LNA with coaxial connectors.

5.2.5 Low Loss Components

Note the difference of approximately 0.1 dB between the simulated and measured noise figure in Figure 5.13a. The figure of 0.1 dB is reasonable: At 2 GHz, Agilent suggests adding 0.20 dB to the theoretical minimum noise figure for its ATF-36077 pHEMT due to circuit losses [45]. Recall from Section 4.8.3 that the calculated minimum noise figure for the ATF-34143 was 0.23 dB. *Nodal* simulation of the LNA circuit noise figure results in 0.3 dB noise figure due to noise from additional resistors in the schematic, which leaves 0.1 dB that can be attributed to additional losses in the circuit components and circuit board.

The 0.1 dB disparity between the measured and simulated noise figure of the LNA would surely be higher if lower quality components were used. A major part of the LNA design process was the investigation of commercial high-quality components. For inductors and capacitors, Q factor is an indicator of loss, being the ratio of reactance to the equivalent series resistance (ESR) in the component at a given frequency. Ideally, an inductor or a capacitor would be lossless and have a Q factor of infinity. In the real world, the most one can do is find components with higher Q values.

$$Q = \frac{X}{ESR} \quad (5.6)$$

where

$$X = \omega L \text{ (inductor)}$$

$$X = \frac{1}{\omega C} \text{ (capacitor)}$$

Another important component property to consider is the self resonant frequency (SRF), the frequency at which the capacitive part and inductive part of the component become equal and cancel each other out (ie. $\omega L = \omega C$). X becomes zero and the component ceases to act like a capacitor or inductor. The operating frequency of a component should be below its SRF.

Air-core wire inductors such as those offered by Coilcraft offer minimum Q values on the order of 100 with very low maximum ESR values on the order of 0.001 Ω . Capacitors tend to have higher ESR values than inductors because they contain dielectric material that introduces additional losses. Initially, ultra-low ESR American Technical Ceramics (ATC) capacitors with average ESR values of approximately 0.1 Ω were used for the LNAs [46]. Later in the duration of this project, however, even lower ESR capacitors were offered by Dielectric Laboratories (DLI), having average values of 0.06 Ω at 2 GHz [47]. Replacing the ATC capacitors with the lower loss DLI capacitors lowered noise figure by approximately 0.05 dB. However, DLI did not offer ultra-low ESR capacitors with values as high as 1000 pF so ATC 100 B Series capacitors were kept as 1000 pF bypass capacitors.

The circuit board is composed of 0.030" thick GML 1000 substrate produced by GIL Technologies. GML 1000 offers a good compromise between low loss and cost, making it ideal material for building prototype circuits. At 1 GHz, GML 1000 has a loss of 0.029 dB/inch. This can be compared to the RO4003 low-loss substrate that was used for the S-parameter test fixtures (refer to Section 3.1), which is more expensive and has a loss at 1 GHz of 0.018 dB/inch [10].

Component	Manufacturer	Model	Loss
Resistors	Panasonic	Precision Thick Film Resistors (0603)	N/A
Capacitors	DLI	C06UL	ESR = 0.06 Ω at 2 GHz
1000 pF bypass capacitors	ATC	100 B	ESR = 0.1 Ω at 1 GHz
Inductors	Coilcraft	Midi, Mini and Micro Spring Air Core*	Maximum ESR values on the order of 0.001 Ω
Circuit board	GIL Technologies	GML 1000	0.029 dB/inch

*The RF choke at the drain of the first stage transistor is a 68 nH Coilcraft 0603CS inductor due to size restrictions in the original LNA circuit board design.

Table 5.2: Components used for the LNA with coaxial connectors.

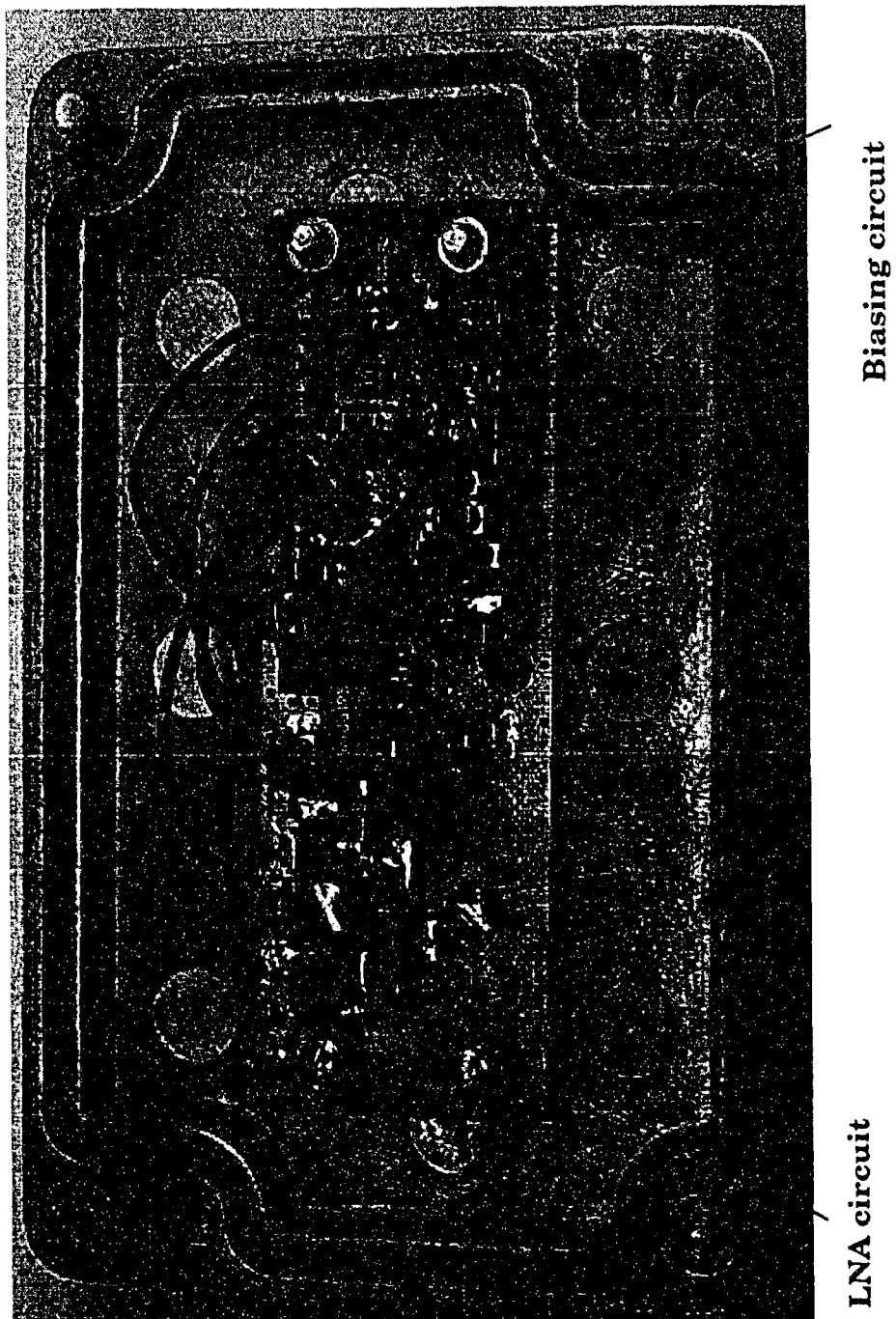


Figure 5.14: LNA with coaxial connectors.

5.3 Probe LNA Design - the Mark 1

The Mark 1 design is centered on the concept of a waveguide probe connected directly to the input of the ATF-34143 transistor. Coaxial connection losses are eliminated by removing the coaxial cable connection between antenna and LNA. Losses can be further reduced if the probe presents the optimum impedance Z_{opt} required by the transistor because fewer components are required for tuning input impedance of the transistor in order to obtain lowest noise.

The probe is a triangular microstrip trace which tapers down to the width of the gate lead of the transistor packaging. The dimensions of the probe were determined by Bruce Veidt, who used powerful electromagnetic simulation software called *Microstripes* to ensure that the probe would present an impedance close to Z_{opt} of the ATF-34143 at 1.42 GHz when placed in the waveguide feed. Using the probe design, Annie-Claude LaChapelle designed and constructed the Mark 1 - a single-stage LNA [28]. Further development is required: the Mark 1 provides gain of approximately 15 dB, which is not sufficient for a Synthesis Telescope front-end. Also, the bias lines of the Mark 1 could be better decoupled from the main LNA circuit.

To increase probe LNA gain, an attempt at a two-stage probe LNA was made - the Mark 2. Unfortunately, there were problems with oscillations and a low noise figure was not achieved. The original design of the Mark 1 was improved, however, by incorporating the power supply design used in the LNA with coaxial connectors (see Section 5.1.5) as well as replacing components with lower loss versions. The noise figure of the Mark 1 was reduced to the same performance as the LNA with coaxial connectors when placed in the test waveguide with a waveguide-to-coaxial transition. Further improvements can be made on the probe LNA design and are described at the end of this section.

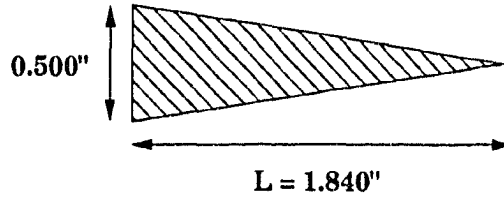


Figure 5.15: Dimensions of the probe for Mark 1 [28].

5.3.1 Measured Impedance of the Probe

The impedance of the waveguide probe was measured using Short-Open-Load-Thru (SOLT) Calibration. SOLT Calibration is similar to TRL Calibration as described in Section 3.1, with the exception of short, open and load ($50\ \Omega$) test fixtures being used for reference during measurements instead of reflect and line fixtures. Unlike the case of S-Parameter measurement, in this situation a $50\ \Omega$ load is not difficult to realize because we are working at a single frequency of 1.42 GHz as opposed to a wide band of 0.5 - 10 GHz. To simulate the waveguide feed in each Synthesis Telescope dish, the probe was placed in a piece of waveguide during measurements. The measured probe reflection coefficient Γ_{probe} was found to be $0.71\angle 63^\circ$ in the waveguide at 1.42 GHz. Figure 5.16 displays Γ_{probe} relative to Γ_{opt} values.

5.3.2 Mark 1 LNA Design

As stated previously, the waveguide probe is directly connected to the input of the ATF-34143 transistor. Additional components at the input of the transistor provide a connection to the power supply circuit and allow biasing of the transistor gate. The connection to the power supply circuit is composed of a thin piece of transmission line, a 15 nH chip inductor, a bypass capacitor and a stabilizing $91\ \Omega$ resistor (refer to Section 5.2.3) as shown in Figure 5.17.

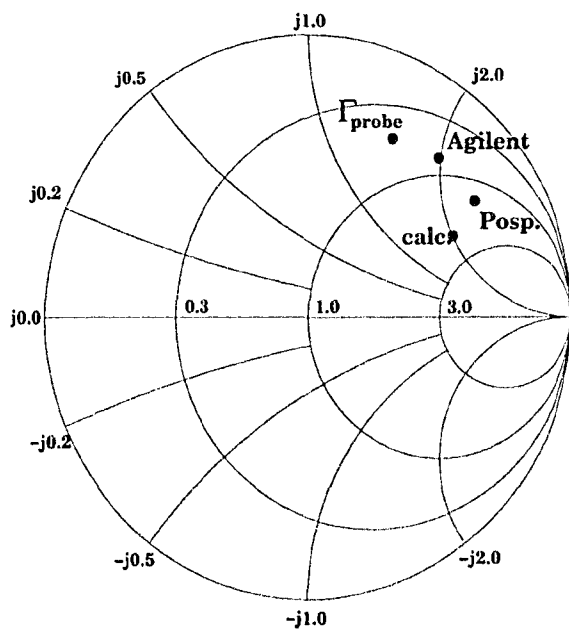
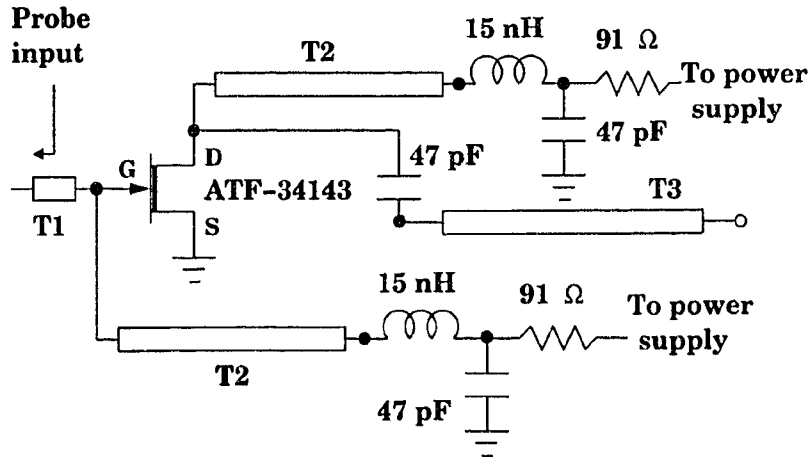


Figure 5.16: Input impedance of the probe inside the waveguide. The Smith Chart is normalized to 50Ω and the three other impedance values are Γ_{opt} values taken from Table 4.3.

The power supply connection at the drain of the transistor is of similar configuration. It should be noted that the schematic does not include the presence of ferrite beads at the power supply connections, which were removed to lower noise figure (see Section 5.3.4).

Knowing the impedance of the waveguide probe at 1.42 GHz and taking the additional components at the input into account, the impedance presented at the input of the transistor at 1.42 GHz can be calculated using *nodal*. Because there are no tuning elements in the input circuit, the resulting reflection coefficient presented at the input of the transistor Γ_S is still quite close to the probe impedance as is shown in Figure 5.18.



T1 = microstrip line of width 0.010" and length 0.050"
T2 = microstrip line of width 0.010" and length 0.350"
T3 = 50 Ω microstrip line LNA output

Figure 5.17: Mark 1 LNA schematic.

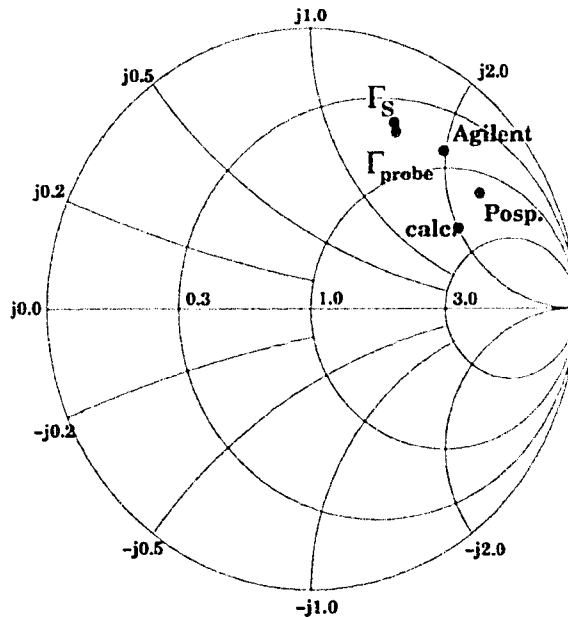


Figure 5.18: Impedance Γ_S presented to the input of the ATF- 34143 transistor in the Mark 1 LNA. The Smith Chart is normalized to 50 Ω. Γ_{probe} represents the measured impedance of the probe and the other three values are Γ_{opt} values taken from Table 4.3.

Length of Probe L	Reflection Coefficient of Probe
1.84"	0.71 \angle 63°
2.00"	0.70 \angle 40°
2.16"	0.72 \angle 27°

Table 5.3: Varying the impedance of the waveguide probe by changing the length of the probe.

5.3.3 Varying Probe Impedance and the Mark 2 Design

The impedance of the waveguide probe can be changed by varying the length of the probe L . Impedance measurements using SOLT calibration were performed on three different probe lengths. The results are displayed in Table 5.3.

As shown in Figure 5.19, the 2.16" probe length reflection coefficient is closest to the calculated Γ_{opt} of the ATF-34143. Therefore the 2.16" length was chosen for the Mark 2 design. The Mark 2 design is a 2-stage LNA. The design was meant to be simple with no tuning elements. Components were limited to large RF chokes, stabilizing resistors, DC bypass capacitors and large DC blocking capacitors. As was the case in the LNA design with coaxial connectors (refer to Section 5.2.4), however, the landing patterns for mounting components were too large. The lowest attainable noise figure was 0.9 dB (67 K) and oscillations were present despite attempts made to scrape off extra traces of microstrip.

5.3.4 Improvement of the Mark 1 and Noise Measurements

By removing ferrite beads used in the transistor gate and drain connections to the power supply circuit, the noise figure of Mark 1 was reduced. The power supply circuit itself was replaced with the one used for the LNA design with coaxial connectors (see Figure 5.8). As well, the 15 nH inductors, which were

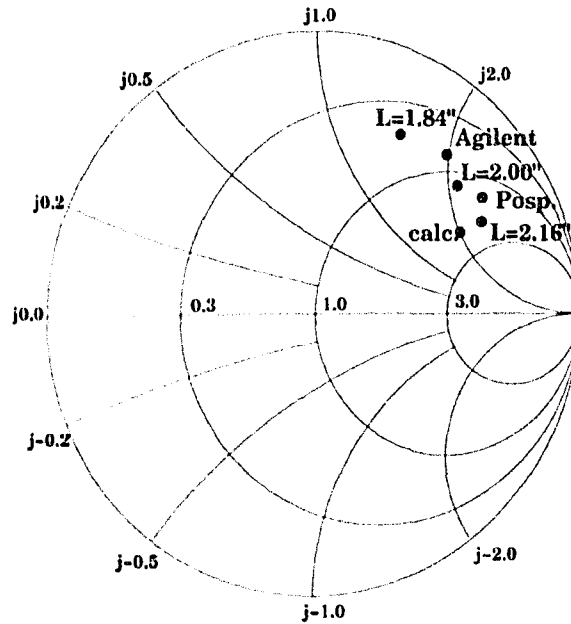
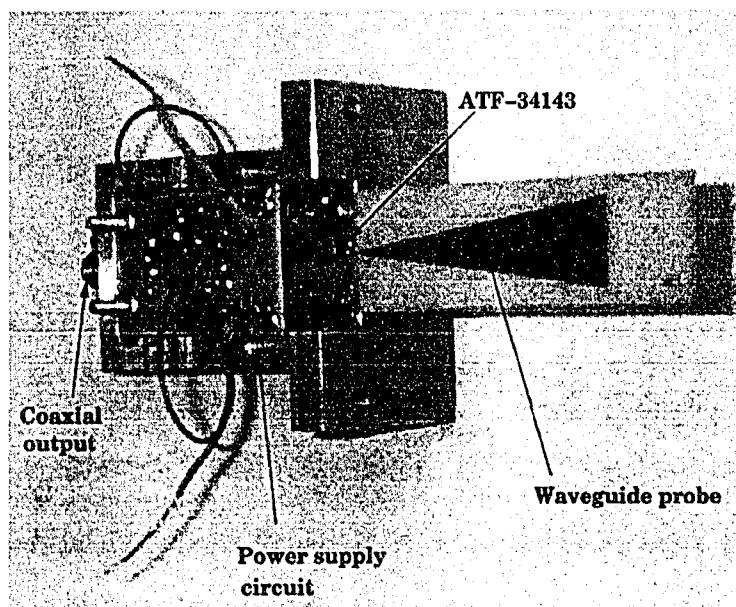


Figure 5.19: Measured impedances of different lengths of probes on the Smith Chart, which is normalized to 50Ω .

originally Panasonic surface mount inductors, were replaced with lower loss Coilcraft 0603HC surface mount inductors. The noise figure measurement of the Mark 1 in the waveguide was reduced to 0.55 dB (39 K), which is equivalent to that of the noise figure of the coaxial LNA when connected to a probe that is placed in the waveguide. It is already known that the LNA with coaxial connectors yields a noise figure of 0.4 dB (30 K) when its input and output see an impedance of 50Ω . Therefore the additional 0.15 dB (10 K) of noise when the LNA with coaxial connectors is placed in the waveguide can be attributed to losses in the waveguide and waveguide-to-coaxial transition (see Figure 1.2). The improved version of the Mark 1 can be seen in Figure 5.20.

The noise measurement setup with the waveguide is relatively simple. A piece of cylindrical waveguide approximately 2.5' long is equipped with two removable waveguide-to-coaxial transitions inserted at each end. The N8973A noise figure meter is connected to the waveguide-to-coaxial transition at one



(a)



(b)

Figure 5.20: a) Improved Mark 1 probe LNA. b) The Mark 1 with biasing circuit removed.

end of the waveguide, leaving a free waveguide-to-coaxial transition at the other end for measurement of the LNA with coaxial connectors. For measurement of a probe LNA, the free waveguide-to-coaxial transition is removed and the probe LNA is inserted in its place. Refer to Figures 5.21 and 5.22 for the noise measurement setup with the waveguide.

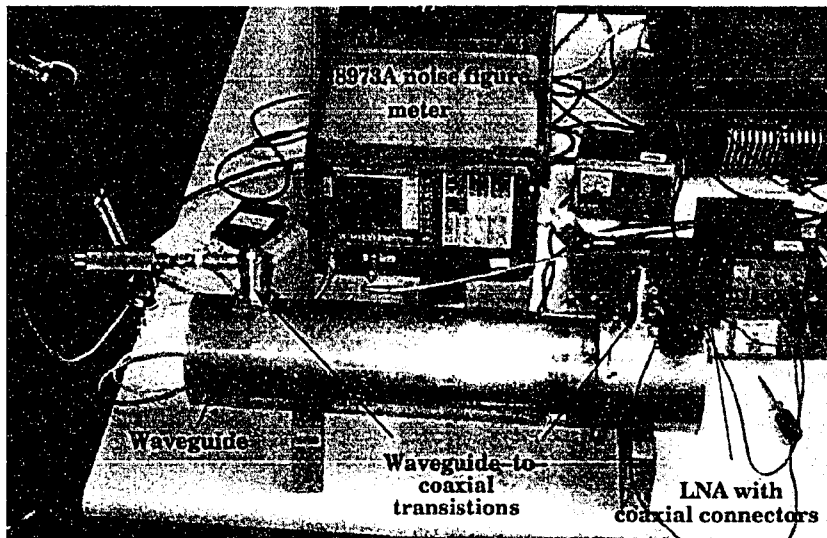


Figure 5.21: Noise measurement of LNA with coaxial connectors in waveguide.



Figure 5.22: Noise measurement of probe LNA in waveguide.

5.3.5 Suggested Further Improvements

Probe Impedance

As discussed in Section 5.3.3, the impedance of the probe antenna can be varied by changing the length of the probe. More investigation can be done to determine the ideal probe length for best noise performance.

Lower Loss Components and Better LNA Design

The newer Coilcraft 15nH inductors that replaced the original Panasonic 15nH higher loss inductors successfully reduced the noise figure of the Mark 1. Noise figure may be further reduced by using even lower loss inductors. The Coilcraft 0603HC 15nH inductors that are currently used have ceramic cores, which introduce greater losses than air cores. For instance, Coilcraft's Mini Spring air core 18.5 nH inductors each have a maximum resistance more than 20 times smaller than that of the 0603HC 15 nH ceramic inductors. Air core inductors are larger however and the LNA circuit board would need to be redesigned to allow for larger components. Ultra low loss capacitors such as those provided by ATC and DLI should also be used in RF bypassing and DC blocking.

To simplify troubleshooting, a low loss large RF choke could be placed as close to the input of the transistor as possible while minimizing excess microstrip traces. This would keep the impedance presented to the transistor input as close to the probe impedance as possible. As well, excess inductance could be added to the source leads of the transistor in order to increase stability and power transfer (refer to Section 5.1.4).

Newer Transistor Technology and Better Selection of Transistors

Inevitably, transistors with better noise performance have been developed since the start of this project. Indium phosphide (InP) HEMTs are an example, with

noise figures even lower than that of GaAs HEMTs. However, these devices are still primarily available in the research and development sector of industry, and are more expensive to obtain.

Commercial devices offer a noise figure of approximately 0.5 dB or 35 K noise temperature at 2 GHz. HEMTs made for higher frequencies such as the NE 325 (0.45 dB noise figure or 32 K noise temperature at 12 GHz [48]) and the ATF-36077 (0.5 dB noise figure or 35 K noise figure at 12 GHz [45]) are possibly worth investigating. I suspect that the transistor used in the 0.3 dB (20 K) commercial LNAs mentioned in Section 5.1.4 is the ATF-36077 pHEMT, judging from packaging and noise performance. However, as mentioned in Section 5.1.4, there were problems due to the extremely poor input return loss of the device. The datasheet of the NE 325 also specifies poor input return loss as well as low gain at frequencies closer to 1.42 GHz, which could pose design problems [48]. Nevertheless, when selecting a transistor, the theoretical noise figure should be at least 0.2 dB lower than the desired noise figure of the LNA, in order to allow for circuit losses as described in Section 5.2.5.

Chapter 6

Conclusion

As part of an effort to double the sensitivity of the Synthesis Telescope at 1420 MHz, this project aimed to reduce receiver front-end noise temperatures from a mean value of 35 K to 20 K. Currently, the receiver front-ends of the Synthesis Telescope are LNAs with a mean noise temperature of 35 K and gain of 40 dB. Initially, this project was geared towards a probe LNA design with the Agilent ATF-34143 pHEMT that would have a noise figure of 20 K and a gain of at least 30 dB. There were three main goals:

- Obtaining the correct S-parameters of the Agilent ATF-34143 pHEMT over a wide frequency range
- Calculating the noise parameters of the ATF-34143 at 1.42 GHz
- Improving the Mark I probe LNA design

An intermediate goal was later added to this project after the S-parameters and noise parameters of the ATF-34143 were obtained:

- Designing a LNA with coaxial connectors using ATF-34143 transistors

LNAs with coaxial connectors would provide more immediate results because they are easier to install in the Synthesis Telescope dishes, which are already

configured with coaxial connectors. Installing probe LNAs in the dishes would require significant alteration of the waveguide feeds, including removal of the waveguide-to-coaxial transitions. Also, as will be discussed shortly, this project ended with the probe LNA design still requiring further development.

Using Thru-Line-Reflect (TRL) calibration and low-loss test fixtures, S-parameters of the ATF-34143 were successfully measured from 0.5 to 10 GHz. The S-parameters were used to obtain a circuit model of the ATF-34143 transistor. Noise parameters of the ATF-34143 were obtained with *nodal* circuit simulation software using Pospieszalski's method for the intrinsic circuit in the transistor circuit model.

Knowledge of the noise parameters of the ATF-34143 at 1.42 GHz permitted design of an LNA with coaxial connectors. The noise figure of the LNA is 0.4 dB or 30 K, a 5 K improvement over the LNAs currently in operation in the feeds of the Synthesis Telescope. The gain of the LNA is 30 dB, reducing the noise contribution from the next stage to a few hundredths of a Kelvin (see Section 1.7), which is sufficient for a Synthesis Telescope front-end. Along with Teresia Ng's proposed antenna design improvements that can lower system noise temperature by 6 K (see Section 1.6), the LNAs can be incorporated to lower the system noise temperature by 11 K. This would bring the radio telescope system noise temperature at 1.42 GHz from 60 K down to 49 K.

The probe LNA design requires further development. Currently, the probe LNA design is a one-stage LNA with the same noise performance as the LNA with coaxial connectors when placed in a waveguide. The gain, however, is only 15 dB because there is only one stage of amplification. There is much potential for even better noise performance than the LNA design with coaxial connectors because of the elimination of sources of loss: fewer components are used at the input of the transistor and there is no coaxial connection between the LNA

and the antenna. Suggestions for improvement include adjusting the probe impedance, adding external source inductance, using lower loss components and simplifying the design for troubleshooting purposes by minimizing excess microstrip traces at the input of the transistor. If possible, a transistor with better noise performance (preferably at least 0.2 dB lower than the desired LNA noise figure) and comparable input return loss and gain may be selected. A second stage may be added in order to meet the gain requirement of a Synthesis Telescope front-end.

Bibliography

- [1] University of Calgary. CGPS public information site. URL:
<http://www.ras.ucalgary.ca/CGPS>.
- [2] National Research Council of Canada. NRC website about DRAO. URL:
http://www.hia-ihh.nrc-cnrc.gc.ca/drao/index_e.html.
- [3] Dominion Radio Astrophysical Observatory. DRAO website. URL:
<http://www.drao.nrc.ca>.
- [4] T.L. Landecker, P. E. Dewdney, T. A. Burgess, A. D. Gray, L. A. Higgs, A. P. Hoffmann, G. J. Hovey, D. R. Karpa, J. D. Lacey, N. Prowse, C. R. Purton, R. S. Roger, A. G. Willis, W. Wyslouzil, D. Routledge and J. F. Vaneldik, "The Synthesis Telescope at the Dominion Radio Astrophysical Observatory," *Astronomy and Astrophysics Suppl.*, vol. 145, pp. 509-524, Sept. 2000.
- [5] Teresia Ng, "Studies of Noise and Polarization Performance of the Antennas of the DRAO Synthesis Telescope." M.Sc. Thesis, University of Alberta, 2003.
- [6] Agilent Technologies, "Low Noise Pseudomorphic HEMT in a Surface Mount Plastic Package." ATF-34143 pHEMT Specification Sheet.

- [7] Guillermo Gonzalez, *Microwave Transistor Amplifiers*. Prentice Hall, Upper Saddle River, New Jersey, 2nd ed., 1997.
- [8] Dale D. Henkes, "LNA Design Uses Series Feedback to Achieve Simultaneous Low Input VSWR and Low Noise," *Applied Microwave and Wireless*, p. 26, Oct. 1998.
- [9] Agilent Technologies, "In-fixture Microstrip Device Measurements Using TRL* Calibration." Product Note PN 8720-2.
- [10] Rogers Corporation, "RO 4000 Series High Frequency Circuit Material." Specification Sheet RO 1.4000.
- [11] SouthWest Microwave. Southwest Microwave Catalog, Arizona, 2003.
- [12] Marian W. Pospieszalski, "Modeling of Noise Parameters of MESFET's and MODFET's and Their Frequency and Temperature Dependence," *IEEE Transactions on Microwave Theory and Techniques*, vol. 37, pp. 1340-1350, Sept. 1989.
- [13] Madhu S. Gupta and Paul T. Greiling, "Microwave Noise Characterization of GaAs MESFET's: Determination of Extrinsic Noise Parameters," *IEEE Transactions on Microwave Theory and Techniques*, vol. 36, pp. 745-751, Apr. 1988.
- [14] Agilent Technologies, "Fundamentals of RF and Microwave Noise Figure Measurements." Application Note AN 57-1.
- [15] W. Brockerhoff, H. Meschede, W. Prost, K. Heime, G. Weimann and W. Schlapp, "RF Measurements and Characterization of Heterostructure Field-Effect Transistors at Low Temperatures," *IEEE Transactions on Microwave Theory and Techniques*, vol. 37, pp. 1380-1388, Sept. 1989.

- [16] G. Dambrine, A. Cappy, F. Heliodore and E. Playez, "A New Method for Determining the FET Small-Signal Equivalent Circuit," *IEEE Transactions on Microwave Theory and Techniques*, vol. 36, pp. 1151–1159, July 1988.
- [17] J. Costa, M. Miller, M. Golio and G. Norris, "Fast, Accurate, On-Wafer Extraction of Parasitic Resistances and Inductances in GaAs MESFETs and HEMTs," *IEEE MTT-S Digest*, 1992.
- [18] A. R. Taylor, S. J. Gibson, M. Peracaula, P. G. Martin, T. L. Landecker, C. M. Bruut, P. E. Dewdney, S. M. Dougherty, A. D. Gray, L. A. Higgs, C. R. Kerton, L. B. G. Knee, R. Kothes, C. R. Purton, B. Uyaniker, B. J. Wallace, A. G. Willis and D. Durant, "The Canadian Galactic Plane Survey," *Astronomical Journal*, vol. 125, pp. 3145–3164, 2003.
- [19] L. B. G. Knee, "The Canadian Galactic Plane Survey," *Revista Mexicana de Astronomia y Astrofisica (Serie de Conferencias)*, vol. 15, p. 301, 2003.
- [20] John D. Kraus, *Radio Astronomy*. Powell, OH: Cygnus Quasar Books, 2nd ed., 1986.
- [21] G.L. Verschuur and K.I. Kellerman, *Galactic and Extragalactic Radio Astronomy*. Springer-Verlag, Berlin, 1974.
- [22] Arecibo Observatory. Arecibo Observatory website. URL: <http://www.naic.edu/>.
- [23] J. L. Pawsey and R.N. Bracewell, *Radio Astronomy*. Oxford at the Clarendon Press, 1955.
- [24] Tom Landecker and Bruce Veidt, "New Low-Noise Amplifiers for the Synthesis Telescope," report, DRAO, Nov. 2001.

- [25] MIT Haystack Observatory. Undergraduate Research Educational Initiative website. URL: <http://web.haystack.mit.edu/urei/index.html>.
- [26] J. Bautista, R. Clauss, S. Petty and J. Shell, "DSN Low Noise Amplifiers in the New Millenium," *TMOD Technology and Science Program News*, Jan. 2001.
- [27] J. L. Casse, E. E. M. Woestenburg and J. J. Visser, "Multifrequency Cryogenically Cooled Front-End Receivers for the Westerbork Synthesis Radio Telescope," *IEEE Transactions on Microwave Theory and Techniques*, vol. 30, Feb. 1982.
- [28] Annie-Claude Lachapelle, "Note for Low Noise Amplifier," report, DRAO, 2000.
- [29] Bruce Veidt. personal communication.
- [30] K. Chang, R. York, P. Hall and T. Itoh, "Active Integrated Antennas." *IEEE Transactions on Microwave Theory and Techniques*, vol. 50, pp. 937-944, Mar. 2002.
- [31] Adel S. Sedra and K. C. Smith, *Microelectronic Circuits*. Oxford University Press, New York, New York, 4th ed., 1998.
- [32] Agilent Technologies, "High Intercept Low Noise Amplifiers for 1500 MHz through 2500 MHz Using the ATF-34143 Low Noise PHEMT." Application Note AN 1175.
- [33] Wolfram Research, "The History of Mathematica." URL: <http://www.wolfram.com/company/history/>.

- [34] F. Bilotti, A. Toscano and L. Vegni, "Tapered Stripline Embedded in Inhomogeneous Media as Microwave Matching Line," *IEEE Transactions on Microwave Theory and Techniques*, vol. 49, pp. 970-978, May 2001.
- [35] Rogers Corporation, "A Low Cost Laminate for Wireless Applications," *Microwave Journal*, vol. 39, Sept. 1996.
- [36] Pavel Bretchko and Reinhold Ludwig, *RF Circuit Design*. Prentice Hall, Upper Saddle River, New Jersey, 2000.
- [37] Rogers Corporation. Impedance calculator download site. URL: http://www.rogerscorporation.com/mwu/mwi_java/mwiform.htm.
- [38] Agilent Technologies, "In-Fixture Measurements Using Vector Network Analyzers." Application Note AN 1287-9.
- [39] Raoul Pettai, *Noise in Receiving Systems*. John Wiley & Sons, New York, 1984.
- [40] R. A. Pucel, H. A. Haus and H. Statz, "Signal and Noise Properties of GaAs Microwave FET," *Advances in Electronics and Electron Physics*, vol. 38, 1975.
- [41] Wolfram Research. URL: <http://documents.wolfram.com/v5/Built-inFunctions/AdvancedDocumentation/Optimization/>.
- [42] Agilent Technologies, "Low Noise Amplifiers for 900 MHz using the Agilent ATF-34143 Low Noise PHEMT." Application Note AN 1190.
- [43] Paul Wade, "Understanding the WB5LUA GaAs FET Bias Circuit." URL: <http://www.w1ghz.org/10g/bias.htm>.
- [44] National Semiconductor, "LM317L 3-Terminal Adjustable Regulator." Specification sheet, Sept. 2004.

- [45] Agilent Technologies, "2-18 GHz Ultra Low Noise Pseudomorphic HEMT." ATF-36077 pHEMT Specification Sheet.
- [46] American Technical Ceramics, "ATC 600S Series Ultra-Low ESR, High Q NPO RF & Microwave Capacitors." Specification Sheet.
- [47] Dielectric Labs Incorporated, "DLI Introduces New Ultra-Low ESR Microwave MLCs," *Microwave Product Digest*, Oct. 2003.
- [48] NEC Electronics Corporation, "C to Ka Band Super Low Noise Amplifier N-Channel HJFET Chip." Specification Sheet.